NOVEL HYBRID ORGANIC/INORGANIC, SINGLE-SITED CATALYSTS AND SUPPORTS FOR FINE CHEMICAL AND PHARMACEUTICAL INTERMEDIATE SYNTHESIS

A Thesis
Presented to
The Academic Faculty

by

Christopher Stephen Gill

In Partial Fulfillment
of the Requirements for the Degree
Doctor of Philosophy in the
School of Chemical & Biomolecular Engineering

Georgia Institute of Technology
May 2009

NOVEL HYBRID ORGANIC/INORGANIC, SINGLE-SITED CATALYSTS AND SUPPORTS FOR FINE CHEMICAL AND PHARMACEUTICAL INTERMEDIATE SYNTHESIS

Approved by:

Dr. Christopher Jones, Advisor
School of Chemical & Biomolecular Engineering
Georgia Institute of Technology

Dr. Marcus Weck
Department of Chemistry
New York University

Dr. Pradeep Agrawal
School of Chemical & Biomolecular Engineering
Georgia Institute of Technology

Dr. Amyn Teja
School of Chemical & Biomolecular Engineering
Georgia Institute of Technology

Dr. John Zhang
School of Chemistry & Biochemistry
Georgia Institute of Technology

Date Approved: January 21, 2009

To my parents: David and Karin Gill

Thanks for everything!

ACKNOWLEDGEMENTS

First and foremost, I wish to thank my advisor, Dr. Chris Jones, for his acceptance of me into the research group and guidance along the journey. His patience and quiet motivation have been greatly appreciated, thus allowing me to develop the skills and critical mindset to undertake new scientific challenges. I also wish to thank Dr. Marcus Weck and his research group for their additional guidance and chemistry expertise. Furthermore, I thank my co-workers for making the lab an enjoyable place to work. I thank my predecessors Joe Nguyen, John Richardson, Rebecca Hicks, and Jason Hicks, and Krishnan Venkattasubbiah for their mentorship, advice, teaching, intellectual stimulation, and friendship. I also thank Jeff Drese, Eric Ping, and Wei Long, and I hope they have benefited from my collected knowledge from the senior students they never met.

I also wish to thank my parents, David and Karin Gill, who have guided and advised me my entire life. I am especially thankful for instilling in me the values that I hold dear: integrity, self-responsibility, confidence, leadership, compassion, and love. I am truly grateful for the special importance they placed on education and self-learning my entire life. These virtues have allowed me to excel in my academic and personal lives. I have no doubt they will further benefit me in my personal and professional lives for the rest of my life. I am truly blessed to have such caring parents.

Last, but certainly not least, I wish to thank my fiancée, Brooke Mullis. Who knew a chance meeting while she was working as an undergraduate researcher in the Jones lab would blossom into such a wonderful relationship? Brooke's love, friendship,

and respect has always kept my spirits high and motivated me to work harder. This past year and a half has been difficult without Brooke nearby, but our relationship thrived, becoming stronger with the distance and time. I am grateful for her patience and understanding, and I cannot wait until we begin our married lives together.

TABLE OF CONTENTS

LIST OF TABLES

LIST OF FIGURES

LIST OF SCHEMES

LIST OF SYMBOLS AND ABBREVIATIONS

ATRP	atom transfer radical polymerization
BET	Brunauer-Emmet-Teller
CP-MAS	cross-polarization magic angle spinning
DSC	differential scanning calorimetry
ee	enantiomeric excess
EA	elemental analysis
EPI	epichlorohydrin
FID	flame ionization detector
FT	Fourier transform
GC	gas chromatography
GPC	gel permeation chromatography
HKR	hydrolytic kinetic resolution
IR	infrared spectroscopy
MCM	Mobil Corporation material
MNP	magnetic nanoparticles
MPB	magnetic polymer brush
NMR	nuclear magnetic resonance
PBC	polymer brush catalyst
PS	poly(styrene)
SiMNP	silica coated magnetic nanoparticles
SBA-15	Santa Barbara mesoporous silica material #15
SEM	scanning electron microscopy

TEOS	tetraethylorthosilicate ($Si(OCH_3)_4$)
TOF	turnover frequency
TEM	transmission electron microscopy
TMS	trimethoxysilane ($SiH(OCH_3)_3$)
TGA	thermogravimetric analysis
XRD	X-ray diffraction

SUMMARY

The study of catalysis is a fundamental aspect of chemical engineering, as its implications affect all chemical transformations. Traditionally, catalysis has been subdivided into two areas: homogeneous and heterogeneous catalysis. Homogeneous catalysis refers to single-sited catalysts that exist in the same phase as the reaction media. These catalysts tend to be highly active and selective but often difficult to recover and reuse. In contrast, heterogeneous catalysts are typically multi-sited catalysts that exist in a different phase from the reaction media. These catalysts tend to be less active and selective than their homogeneous counterparts. However, the vast majority of industrial scale catalysts are heterogeneous because they can be easily separated, making them easily implemented in continuous processes, allowing for efficient, large scale operations.

Due to the limitations of traditional homogeneous and heterogeneous catalysts, researchers have increasingly investigated hybrid catalysts that incorporate aspects of homogeneous and heterogeneous catalysis. This is accomplished via immobilization of homogeneous catalyst analogues onto solid-phase supports, thereby preserving the activity and selectivity of homogeneous catalysts while allowing for facile recovery and reuse from the insoluble, heterogeneous support. This thesis focuses on development of one subset of these hybrid catalysts, covalently immobilized homogeneous catalyst analogues on solid, insoluble supports.

A variety of systems is presented here including organic and organometallic catalysts immobilized on organic and inorganic supports. Five cases are included. The first discusses utilization of supported acid and base catalysts for use in one-pot cascade

reactions. The second example illustrates use of silica-coated magnetic nanoparticle supported acid catalysts for organic transformations. The third case presents novel polymer brush supported Cobalt-salen catalysts for the enantioselective, hydrolytic kinetic resolution of epoxides. A fourth case presents novel, magnetic polymer brush supported organic and organometallic catalysts for organic transformations. The fifth example illustrates polymer and silica supported ruthenium-salen catalysts for the asymmetric cyclopropanation of olefins. In each case, the catalysts are compared to other existing catalysts, and advantages/disadvantages of these hybrid catalysts are illustrated. The overall goal of this thesis work is to develop novel supports and immobilization techniques to advance the field of hybrid organic/inorganic catalysts for the production of fine chemical and pharmaceutical intermediates.

PREFACE

The work contained herein was written either with intent to publish in scientific journals, in submission currently, or already published. Modifications have been applied to make the chapters coherent with the required thesis formatting. This dissertation is arranged as such: Chapter 1 introduces general catalysis concepts and provides background into the subsequent catalytic reactions. Chapters 2 – 6 discuss individual projects written for publication. Chapter 7 summarizes the dissertation and offers suggestions for future investigations based on this work.

CHAPTER 1

INTRODUCTION

1.1 Immobilized catalysts: A marriage of homogeneous and heterogeneous catalysis

The study of catalysis is a fundamental aspect of chemical engineering, as its implications affect all chemical transformations. Before any industrial process can be designed, the catalytic implications of any process must be thoroughly examined. Fundamental properties such as kinetics, diffusion, activation energies, activity, selectivity, deactivation, etc. must be understood, as they have profound influences on the overall design. At the heart of all these processes is the catalyst itself. Should a process use a homogeneous or heterogeneous catalyst? This simple question in itself has major ramifications on reactor design and subsequent purification steps. Because catalysts are so ubiquitously important to a process, even minor changes to the catalyst can have tremendous consequences on an overall process. Consequently, researchers in industry and academia alike are constantly searching for new catalysts and methods to improve the performance of existing catalysts.

Traditionally, the study of catalysis has been divided into two areas: homogeneous and heterogeneous catalysis. This distinction denotes in which phase the catalyst resides. Homogeneous catalysts refer to those existing in the same phase as the reaction media. Commonly, this will apply to either liquid or soluble, solid catalysts in a liquid solution. Mineral acids and bases are examples of homogeneous catalysts that are used extensively in industry. In contrast, heterogeneous catalysts reside in a different phase as the reaction media. These are most commonly solid catalysts in liquid or gas streams. An everyday example may be found in the catalytic converters of gasoline powered automobiles. Platinum alloys convert pollutants in the exhaust to more benign compounds, drastically reducing emissions of harmful pollutants into the environment.

Because homogeneous and heterogeneous catalysts each have their own advantages and disadvantages, it is important understand basic concepts of each and where they are best applied.

As previously mentioned, homogeneous catalysts exist in the same phase as the reaction media. These catalysts are generally single-sited, meaning they have a single, specific site for which the catalysis occurs. Because of advanced synthesis and characterization techniques, these catalysts can be custom designed to be highly active and selective for a given reaction. The ultimate example of selectivity in catalysis has been provided by nature over millions of years of evolution in the form of cellular enzymes. Enzymes have evolved extremely high specificities to reactants consumed and products formed within a cell even in the presence of all other cellular chemistries. Although synthetic, non-biologic catalysts rarely replicate the selectivity and specificity of enzymatic biocatalysts, enzymes serve as inspiration for which novel, homogeneous catalysts are designed.[1]

Despite the tremendous advantages of high activity and selectivity possessed by homogeneous catalysts, their use in industry has been hampered by difficult separation from the product stream. Recycling of these catalysts can be of economic and environmental importance, especially in the case of expensive and/or toxic transitional metal catalysts.[2] In the pharmaceuticals industry, where some chiral chemicals can only be synthesized using homogeneous organometallic catalysts, removal of the metals to ppm levels is of vital importance for product purity as mandated by the United States Food and Drug Administration.[3] In other cases, the catalyst is never recovered, either because the catalyst is extremely active and only minute concentrations are required (as is the case with olefin polymerization catalysts) or it is simply cheaper to use the catalyst once rather than to separate and recover it (as can be the case with mineral acid/base catalysts).

In contrast to homogeneous catalysts, heterogeneous catalysts are multi-sited catalysts that exist in a different phase from the reaction media. Multi-sited catalysts may have several different chemical environments on the surface of the material that promote activity. These catalysts tend to be ill-defined, less active, and less selective than homogeneous catalysts due to imprecise synthetic methods and less advanced characterization techniques. Furthermore, the broad application of heterogeneous catalysts is restricted by the nature of the surface active sites and the types of reactions they can promote.[4] However, the vast majority of industrial scale catalysts are heterogeneous because they can be easily reused in continuous processes. Packed-bed or slurry reactors allow for efficient reuse of the catalyst in large-scale, high throughput operations. Heterogeneous catalysts are also amenable to reuse in smaller scale, batch-type reactions via recovery by filtration or centrifugation.

Due to the limitations of traditional homogeneous and heterogeneous catalysts, researchers have increasingly investigated hybrid catalysts that incorporate aspects of homogeneous and heterogeneous catalysis (Figure 1.1).[2, 4-10] This is accomplished via immobilization of homogeneous catalysts onto solid-phase supports, thereby preserving the high activity and selectivity of the catalyst while allowing for its facile recovery and reuse due to the insoluble, solid support. This thesis will focus on development of one subset of these hybrid catalysts, covalently immobilized homogeneous catalyst analogues on solid supports.

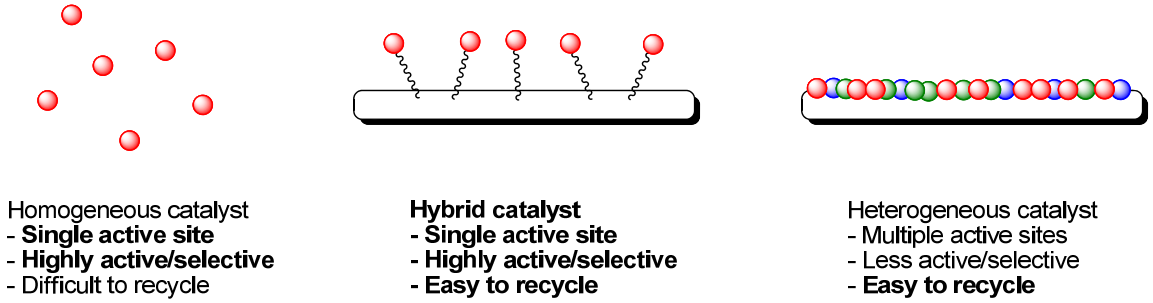

Figure 1.1. Cartoon depicting the three distinct types of catalysts.

1.2 Immobilization methods for hybrid catalysts

A number of methods may be used to immobilize catalysts to form hybrid materials (Figure 1.2).[6] The specific reaction conditions may dictate which method is best suited for the particular circumstance.

1.2.1 Immobilized catalysts: Adsorption

The simplest method of immobilizing homogeneous catalysts on solid supports involves adsorption of the homogeneous catalyst onto a solid support.[6] This type of catalyst is created by first synthesizing the solid support and then contacting it with the catalyst. The catalyst can be weakly bound via physisorption or more strongly bound via electrostatic interactions or metal coordination. In all cases, there is no covalent linkage between the support and the catalyst. As such, these materials are prone to leaching and may be relegated to mild reaction conditions.

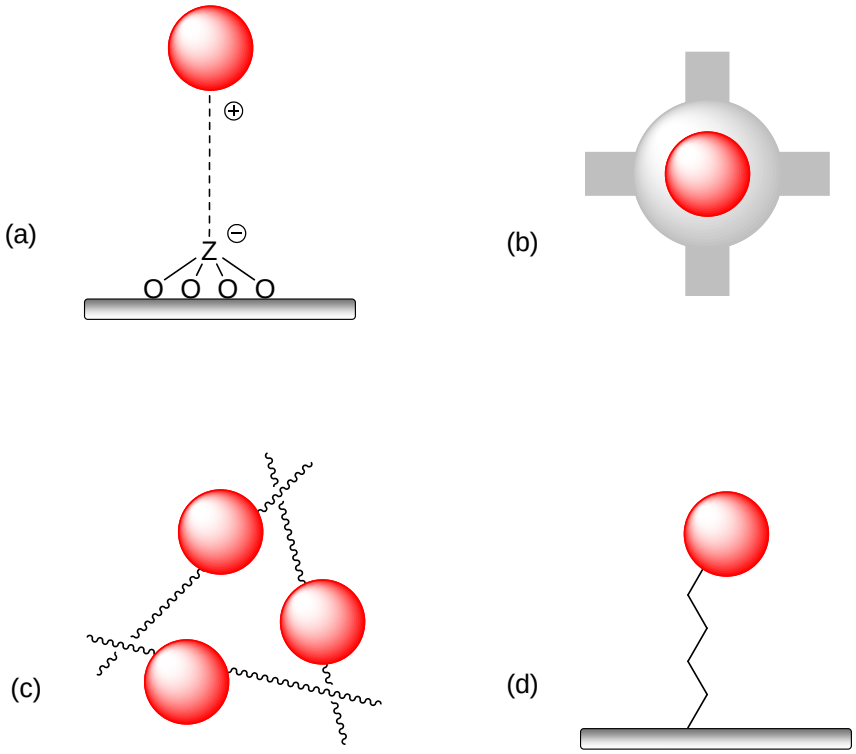

Figure 1.2. Immobilization methods for hybrid catalysts: (a) adsorption, (b) encapsulation, (c) direct incorporation, and (d) covalent grafting.

1.2.2 Immobilized catalysts: Encapsulation

A second immobilization method involves encapsulation of the catalyst and requires no bonding between the catalyst and support.[6] Two types of encapsulated catalysts commonly appear. The first involves synthesis of the support material with the catalyst present in the reaction mixture. Two examples include sol-gel and polymeric materials. In either case, the polymerizable unit (commonly alkoxysilanes or sodium silicates with sol-gels or olefins or other polymerizable monomers in the case of polymers) and catalyst are mixed together in one-pot while the solid support forms. In this case, catalyst selection is limited to those that can survive the support synthesis conditions. These materials may also be prone to leaching as the sol-gel or polymer may be subject to swelling in certain solvents. The active catalyst may diffuse out of the swollen solid support, reducing its recyclability and leading to product contamination.

This swelling can also be problematic in fixed volume reactors, leading to increased pressure differentials across the reactor.

A second type of encapsulated catalyst utilizes a ship-in-the-bottle synthesis.[6] A rigid, microporous support is synthesized first, generally zeolites or MCM[11] type materials. The solid support is then impregnated with catalyst precursors by diffusion into the porous network. The catalyst is then "assembled" from reaction of the precursors within the network. If the catalyst is larger than the pore channels, it cannot diffuse out of the support, and is entrapped within the solid matrix. While these materials do allow for simple recycle of a truly homogeneous catalyst, these materials also present disadvantages. These include decreased activities due to slow molecular diffusion of reactants and products into and out of the porous solid and difficult characterization of the catalyst, as these materials tend to have low catalyst loadings.[6]

1.2.3 Immobilized catalysts: Direct Incorporation

The third common type of hybrid catalyst incorporates the active catalyst directly into the support framework. These can be polymeric[12] or silica based.[13, 14] Like sol-gel or polymer encapsulated materials, the catalyst and polymerizable monomers are combined together in the support synthesis. However, in this case, the catalyst contains a polymerizable unit as well. When the support forms, the catalyst site is directly incorporated into the solid structure. The resulting catalyst can be more stable than the previous two types due to the covalent linkage to the support. In addition, ordered materials can be created through use of structure directing agents during the synthesis, as is the case with pre-modified mesoporous silicas.[13, 14] Non-ordered directly incorporated catalysts such as sol-gel silicas or polymers can subject to solvent swelling/shrinkage. However, they are less prone to leaching due to the covalent linkage to the support, unlike encapsulated or adsorbed catalysts where no covalent bonding is present. This type

of directly incorporated catalyst will be illustrated in Chapter 6 as polymer resin supported Ru-salen catalysts.

1.2.4 Immobilized catalysts: Covalent grafting

The fourth and most common type of hybrid catalyst utilizes covalent grafting to immobilize single-sited catalysts on insoluble, solid supports.[5, 15] In this technique, the solid support is synthesized first, and the surface is subsequently modified with chemical functional groups. Using this method, the catalyst may be immobilized in one step or in a step-by-step fashion as commonly utilized in solid phase synthesis.[10] This method has been investigated extensively due to the variety of chemistries that can be performed. Since the catalyst and support are synthesized in different steps, the catalyst choice is not limited by the reaction conditions of the solid support synthesis. In addition, the solid support and small molecule modifiers can be thoroughly characterized prior to immobilization. This becomes important because characterization of the completed solid supported catalyst can be hindered by low catalyst loadings. The covalent nature of the bonding between the support and the catalyst can generate a more stable catalyst and may prevent leaching. Due to these positive attributes, the majority of this thesis work will focus on this covalent grafting method to generate immobilized catalysts. A range or organic and organometallic catalysts are prepared, characterized, and tested in each of the chapters.

1.3 Catalyst Support Materials

As previously mentioned, covalent grafting of homogeneous catalyst analogues on insoluble, solid supports offers numerous possibilities in terms of flexibility for a wide range or synthesis and/or reaction conditions. Consequently, a discussion on the various support materials that may be used is presented here. Although post-grafting techniques are possible on organic polymeric supports (such as Wang resins), this introduction will

primarily focus on inorganic supports due to their increased thermal, chemical, and mechanical stability. These insoluble solid supports are generally inorganic oxides. The most common supports include porous aluminas and silicas. For any support to be useful in a post-synthesis covalent grafting application, the surface must bear reactive surface species capable of subsequent chemical modification. For inorganic oxides, these modifications are achieved by reaction with surface hydroxyl groups. The most common method of chemically modifying the inorganic oxide surface involves co-condensation of alkoxysilanes with the surface hydroxyl groups (Figure 1.3). This reaction generally uses methoxy or ethoxy silanes as C_3 or higher alkoxy groups tend to be less reactive due to their increased bulkiness. This reaction forms a covalent Si-O-Si bond between the solid support and functional group. The functional group on the alkoxysilane can be any number of chemically reactive species. Common commercially available examples include amines, alcohols, carbonyls, halogens, thiols, olefins, etc. Additionally, alkoxysilanes can be custom synthesized from reaction of terminal olefins with trialkoxysilane ($SiH(OR_3)$ where R = Me or Et). Custom silane synthesis examples are presented in Chapter 4 and in the future work discussion in Chapter 7.

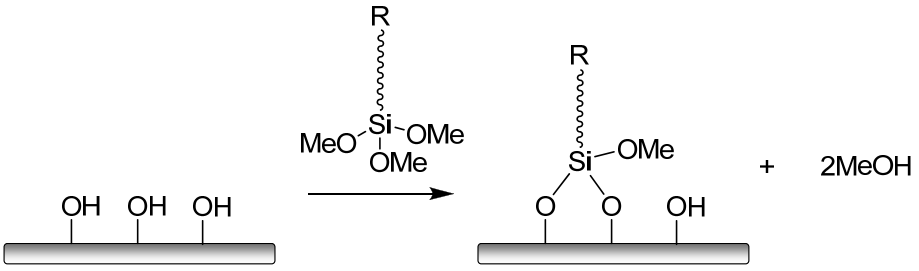

Figure 1.3. Surface modification of inorganic oxides with methoxysilanes.

Furthermore, reaction of alkoxysilanes with solid supports can result in the condensation of one, two, or three surface hydroxyl groups (Figure 1.4). Additionally, if water is present during the reaction, it can hydrolyze the alkoxy groups of the silane, forming hydroxyl groups. These hydroxyl groups can react with other alkoxysilanes, thus grafting off of the surface forming multi-layers of functional groups instead of directly to

the surface, forming monolayer coverage of functional groups. Depending on the user's desire for a material with higher loading and less uniform surface coverage or a material with lower loading and a more well-defined monolayer coverage will dictate whether to include water in the grafting procedure. Should a monolayer coverage be desired, the inorganic oxide must be pre-dried under high temperature and vacuum to remove all water, as these materials tend to be highly hygroscopic.

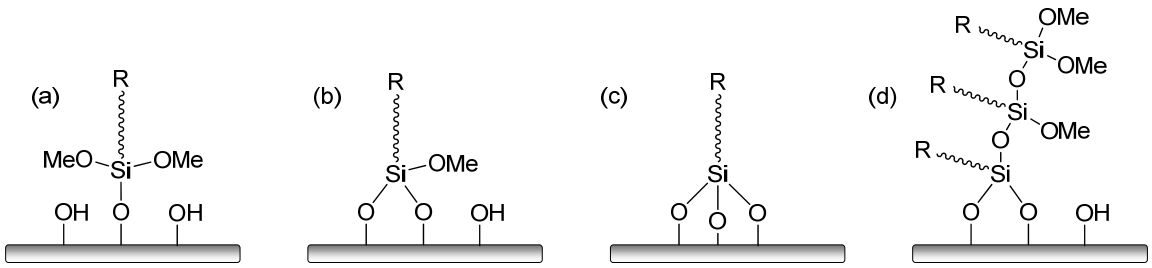

Figure 1.4. Reaction of trimethoxysilanes with (a) one, (b) two, or (c) three surface hydroxyl groups. (d) Reaction of methoxysilanes with solid supports in the presence of water.

The variety of insoluble catalyst supports is as extensive as the options with which to modify them. Supports used in this work include porous and nonporous silicas, polymer brushes, and iron oxide magnetic nanoparticles with each having their own individual advantages and disadvantages.

1.3.1 Mesoporous SBA-15 silica

SBA-15 is one member of a family of mesoporous silicas that make ideal candidates for catalyst supports by covalent grafting.[4, 7, 9, 16] It is an ordered, amorphous silica material first created by Zhao and Stucky in 1998, in an effort to increase the material's thermal stability via increased wall thickness relative to MCM type materials.[17] (SBA-15 denoting the university of origin: Santa Barbara mesoporous silica material number 15). Structurally, the material consists of unidirectional, hexagonally arranged pores between 35 and 150 Å in diameter. The pore walls consist of amorphous silica terminating in silanol or siloxane bridge groups at the surface. Due to the highly porous

nature of the material, surface areas in excess of 800 m^2/g can be achieved. This material makes a promising catalyst support due to its high surface area for chemical modifications, thermal and structural stability, well defined and characterized nature, and chemical inertness to most reaction conditions.[4]

SBA-15 is synthesized in a template process (Figure 1.5).[17] In acidic, aqueous solution, a structure directing agent (triblock copolymer of poly(ethylene oxide)-poly(propylene oxide)-poly(ethylene oxide)) is dissolved to form micelles. These block copolymers self-assemble to form unidirectional, cylindrical micelles in hexagonal arrays. Tetraethylorthosilicate (TEOS) is added to the solution, which polymerizes around the organic micelles forming the pore walls of the material. Finally, after filtration and washing, the material is calcined to combust the organic structure directing agent, leaving the mesoporous SBA-15 silica. The SBA-15 can now be reacted with alkoxysilanes to covalently graft surface functional groups as seen in Figure 1.3. SBA-15 was utilized in Chapters 3 and 4 as a catalyst support for sulfonic acids and Co-salen catalysts, respectively.

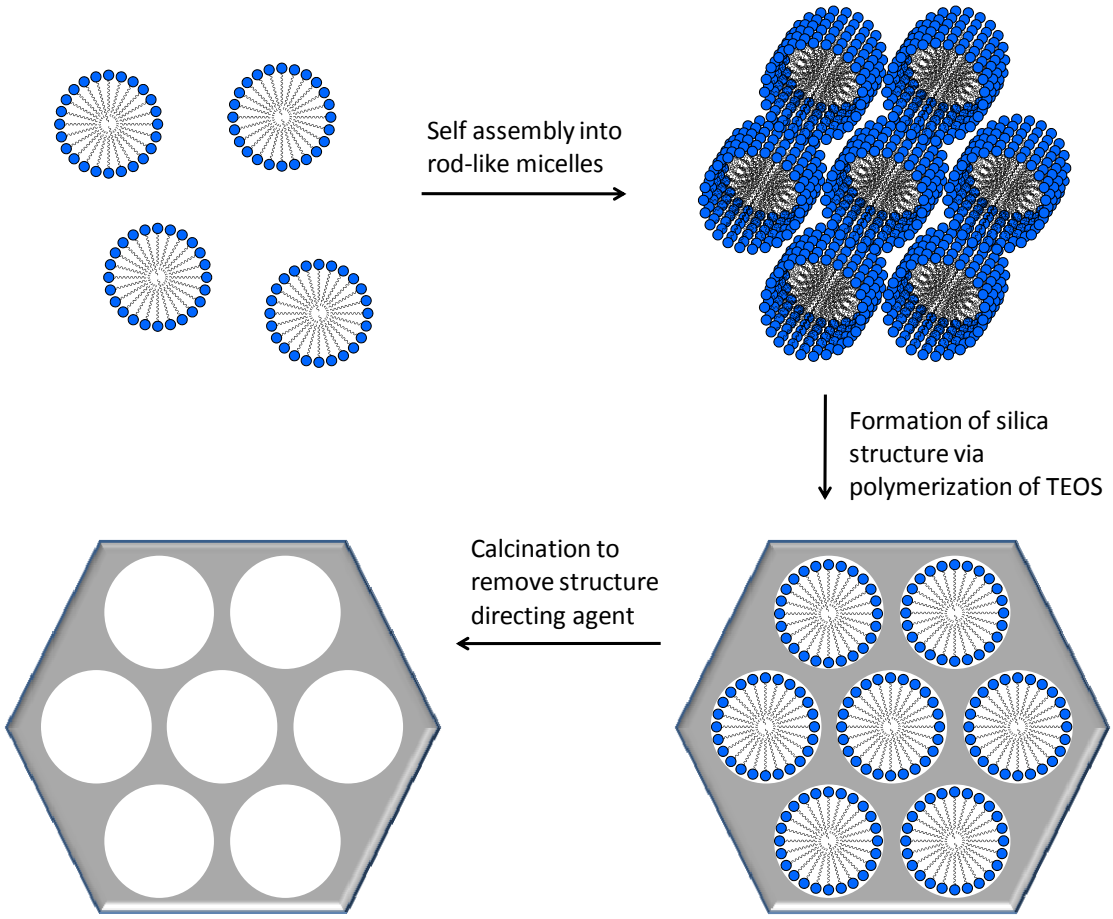

Figure 1.5. Synthesis of SBA-15 mesoporous silica.

1.3.2 Magnetic nanoparticles

Magnetic nanoparticles (MNPs) are another solid, insoluble catalyst support utilized in this thesis work. Unlike amorphous silica supports, these MNPs are crystalline in nature. MNPs are commonly composed of iron oxides often arranged in spinel crystallite structures of the formula AB_2O_4, where A = Co, Fe, Ni, or Mn and B = Fe (Figure 1.6). MNPs can be synthesized from thermo-chemical or by co-precipitation methods, with the latter being more common and less expensive.[18] In the co-precipitation synthesis, iron(III) and metal(II) salts are dissolved in solution. The nanoparticles are precipitated by the addition of base forming the AB_2O_4 spinel crystallite and stabilized with surfactants. These particles can then be surface modified with desired functional

groups to make them suitable for catalyst immobilization and dispersible in organic or aqueous solution.

It is these nanoscale crystallites that give the nanoparticles a unique characteristic: superparamagnetism. There are a number of different types of magnetism for multi-domain magnetic materials. However, once the particle size drops below a critical diameter (generally about 10 nm), these single crystallite particles possess only one domain. When the thermal energy is sufficient to reverse the direction of magnetization of the entire crystallite, the random changes result in no net magnetic moment. However, when these particles are placed in the presence of a magnetic field, the domains are aligned with the magnetic field, creating a net magnetic moment (Figure 1.7). Once the external magnetic field is removed, thermal fluctuations again randomize the magnetic moments of the particles, again resulting in zero net magnetic moment.[18]

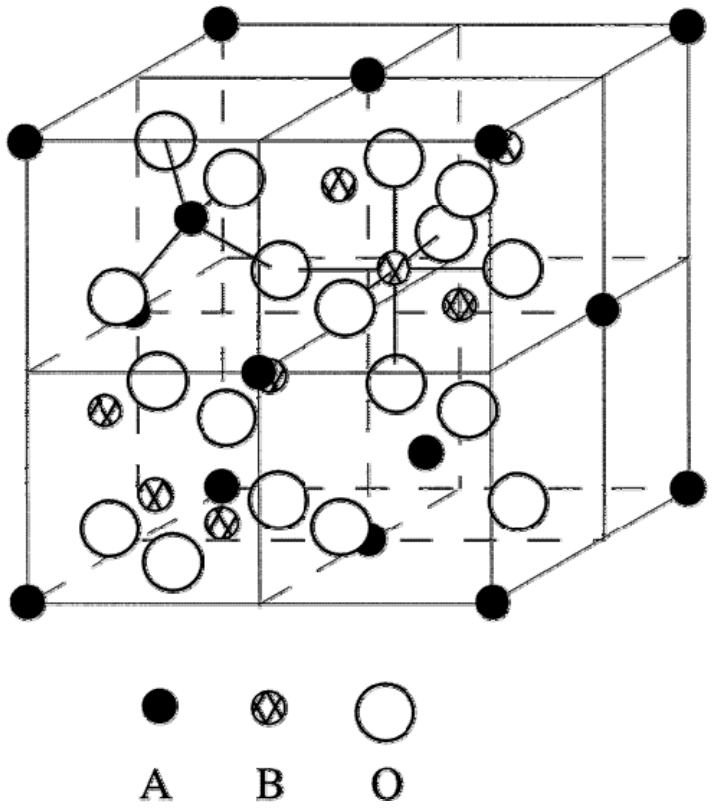

Figure 1.6. Crystalline structure of spinels of the formula AB_2O_4.

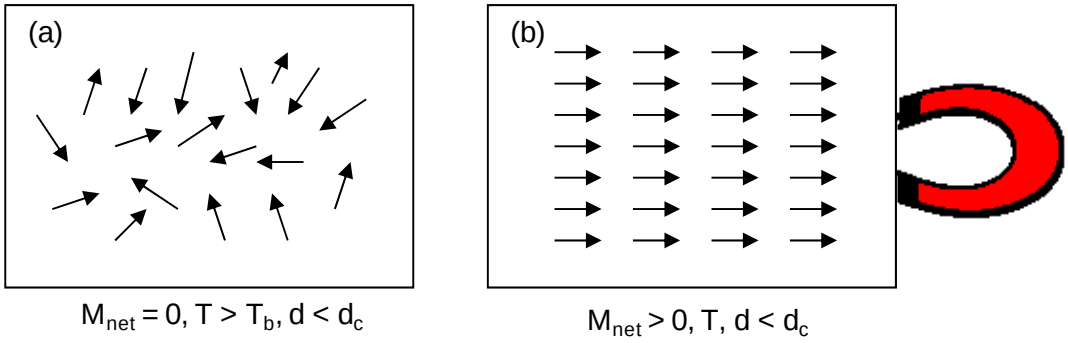

Figure 1.7. Superparamagnetic single domain crystallites in the (a) absence and (b) presence of an external magnetic field.

It is this phenomenon of reversible on/off magnetism that makes these superparamagnetic nanoparticles interesting candidates for catalyst supports. Because MNPs exhibit no net magnetic moment by themselves, they can be dispersed into reaction media. Immobilized catalysts on the MNPs can promote reactions in solution, and upon completion, the MNPs and supported catalyst can be easily recovered with an external magnet. In addition to the novel magnetic recovery method, MNPs also possess other positive attributes. They exhibit high surface areas (above 200 m^2/g) resulting from the small particle diameters.[19] As the diameter of any particle decreases, the surface area per unit mass increases on the order of $1/D_{particle}$. Because MNPs possess only external surface area, reactions are generally not diffusion limited, unlike porous catalyst supports or in solid-phase synthesis resins which can suffer from internal diffusion limitations.[20] The particles are also thermally and chemically stable under some conditions. Furthermore, the particles possess hydroxyl groups on the surface, for which further modifications via silane chemistry are possible. A recent review highlights a number of MNP supported catalysts that have appeared prior to 2006.[19] Since then, additional examples of MNP supported organic[21-25] and organometallic[26-29] catalysts have been published. MNP supported catalysts and their unique recovery method are illustrated in Chapters 2, 3, and 5.

1.3.3 Polymer brush catalyst supports

Polymer brush catalysts (PBCs) are a very recent innovation in the field of hybrid organic/inorganic supported catalysts. They combine the covalent grafting and direct incorporation immobilization methods to create this novel architecture. These materials are highly flexible in terms of organic content and catalyst concentration along the polymer (by adjusting the styrene to styryl-modified catalyst ratio). Additionally, it is possible to create homopolymers, random copolymers, and block copolymers simply by modifying the synthesis procedures. These materials are unique in that they mimic soluble, polymer supported catalysts and yet are easily recoverable through centrifugation or via magnetic separation. Furthermore, the very nature of the material creates high, local catalyst concentrations, which can be especially important in reactions necessitating cooperative catalysis as seen in Chapters 4 and 5.

PBCs are synthesized beginning with immobilization of atom transfer radical polymerization (ATRP) initiators to the surface of insoluble supports by covalent grafting (Figure 1.8). Modified styryl monomers can then be polymerized, or copolymerized with styrene, from the surface forming the polymer brushes. Further chemical modification may be then performed to generate active PBCs, depending on the specific chemistries involved. Few reports of polymer brush supported catalysts currently exist, indicating there is much room for scientific investigation in this new field of hybrid organic/inorganic supported catalysts. Three examples of PBCs appear in this thesis work. Silica supported Co-salen PBCs are utilized in the hydrolytic kinetic resolution of epoxides in Chapter 4, and magnetic polymer brush catalysts (MPBCs) containing Co-salen and piperazine catalysts are illustrated in Chapter 5.

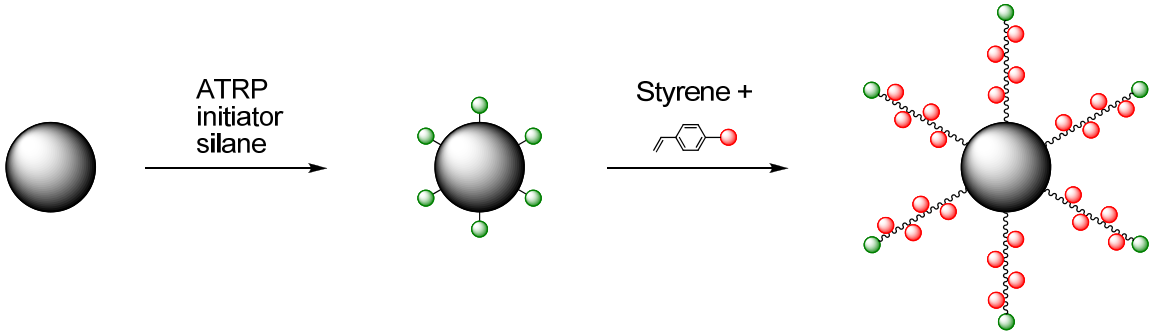

Figure 1.8. Cartoon representation of polymer brush catalyst synthesis.

1.4 Catalyst systems investigated in this work

A variety of organic transformations were investigated in this thesis work. The following pages provide a brief introduction to these supported catalysts: acid/base catalysis, Co-salen catalysts for the hydrolytic kinetic resolution of epoxides, and Ru-salen catalysts for the asymmetric cyclopropanation of olefins.

1.4.1 Supported acid/base catalysis

Acid and base catalysts are probably the most ubiquitous catalysts available to the modern chemist and chemical engineer. Liquid mineral acids and bases are used in industry, but they do present environmental and economic drawbacks. These catalysts cannot be easily recovered, and in most cases, the waste streams must be neutralized and treated with other waste water. This process can be inefficient and costly. As a result, many solid acids and bases have been developed to circumvent these problems. Solid acids and bases have several advantages over liquid acids and bases. They are non-corrosive to piping, easily separated, recyclable, environmentally benign. As such, they have found widespread use in industry. A recent survey of publically disclosed information quoted use of 180 different types of solid acid and base catalysts in 127 different industrial processes.[30]

The most common solid acids are zeolites and other inorganic oxides due to their widespread use in the petroleum refining industry in isomerization, alkylation, and catalytic cracking processes.[30] Because these materials are inorganic and crystalline, they have high thermal and mechanical stability, making them especially suited for high temperature and pressure operations. These materials are limited by their small pore diameters, especially zeolites, as bulky compounds have difficulty accessing internal active sites.

Other solid acids have been developed that do not suffer these problems. Prominent among these are acidic ion-exchange polymer resins. These non-crystalline, copolymer resins are generally composed of styrene, divinylbenzene (cross-linking agent), and vinylbenzenesulfonic acid monomers. These macroporous resins can be synthesized with average pore diameters of 300 Å or greater, making them suitable for use with large and small compounds. Because they are organic and non-crystalline in nature, these polymer resins are less thermally and chemically stable than zeolites and are prone to swelling/shrinking in various solvents. However, they are suitable for use in aqueous media, unlike most other solid acids.[30]

Chapters 2 and 3 make use of supported sulfonic acids for organic transformations. Chapter 2 uses MNP supported bases in conjunction with acidic polymer resin catalysts to promote acid and base catalyzed cascade reactions in one-pot (Figure 1.9). The novelty in this chapter is the ability to have acid and base catalysts together without self-quenching and the ability to recover the catalysts individually post-reaction via magnetic separation. Chapter 3 expands upon the use of magnetic nanoparticles as catalyst supports, but illustrates synthetic methods for four different supported sulfonic acids (Figure 1.10).

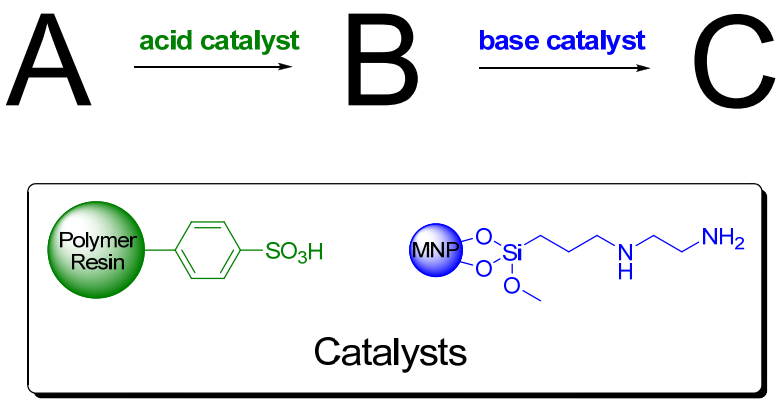

Figure 1.9. Solid acid and base catalysts promoting one-pot cascade reactions.

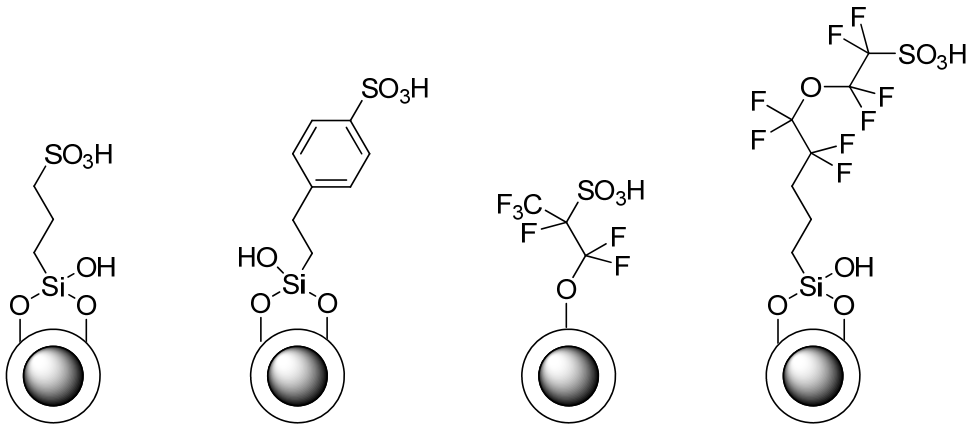

Figure 1.10. Four novel sulfonic acid catalysts supported on silica coated magnetic nanoparticles.

Solid bases have also received interest over the years, albeit to a lesser degree than solid acids.[30-33] However, they do find widespread application in industry for a variety of organic transformations: Michael additions, transesterifications, aldol additions, hydrogenations, aminations, Knoevenagel condensations, alkylations, etc. The most common solid bases include zeolites, supported alkali metals, alkaline oxides, and hydrotalcites. Due to the porous nature of these materials, they can suffer from diffusion limitations, and size restrictions of products and reactants (in the case of zeolites). They also tend to be strongly basic and can suffer from lower selectivities than those of weaker organic bases.[32] These weaker, organic bases may consist of supported amines on polymer resins. As mentioned previously, polymer resin supported catalysts are less

thermally and chemically stable and also prone to swelling in solvents. However, they are highly tunable in terms of the basicity and selectivity based on the choice of amine for each application. Chapters 2 and 5 illustrate use of supported amine bases. Polymer resin supported diamines catalyzed the Knoevenagel reaction of benzaldehyde and malononitrile for Chapter 2 (Figure 1.9). Chapter 5 demonstrates a piperazine based MPB catalyst for the same reaction (Figure 1.11).

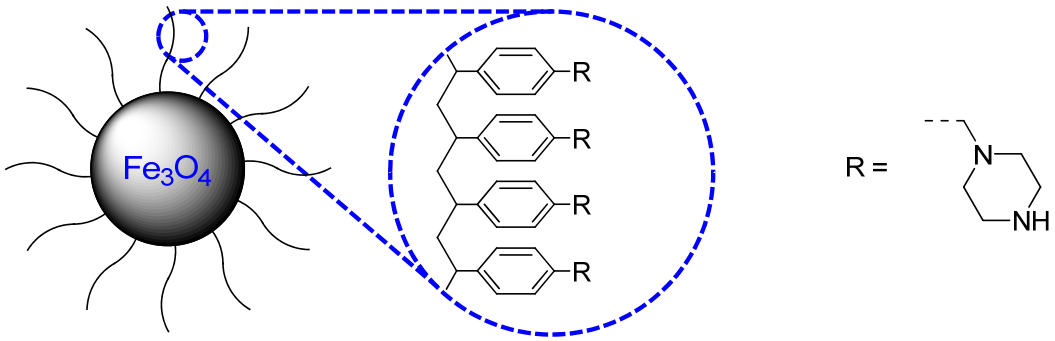

Figure 1.11. Piperazine modified magnetic polymer brush catalyst.

1.4.2 Supported metal-salen catalysts

The acronym “salen” stands for the Schiff base ligand (N,N’-bis(salicylaldehydo)ethylenediamine). The first salen-type ligand and copper complex were synthesized by Combes in 1889, and although the meaning of the term “salen” has changed since its introduction, it is currently accepted as describing a group of [O, N, N, O] tetradentate ligands with the structures shown in Figure 1.12.[34]

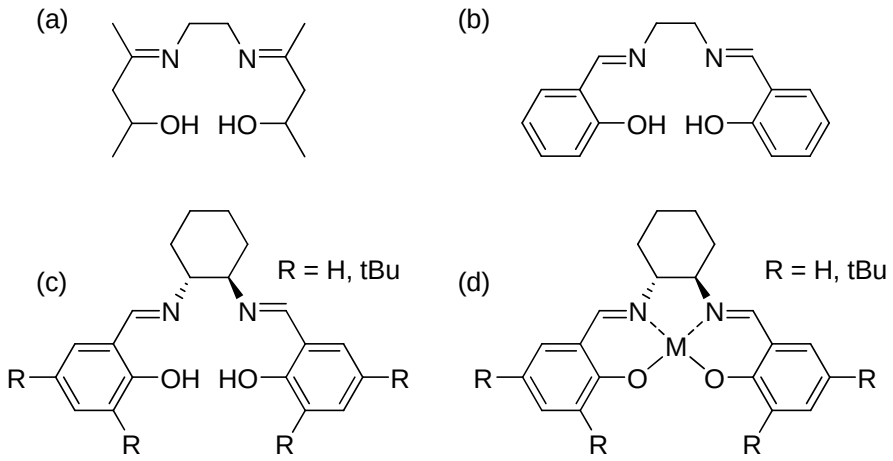

Figure 1.12. Salen structures: (a) Combes's first salen ligand, (b) generally accepted salen structure, (c) chiral salen, and (d) chiral salen metal complex.

In 2003, Jacobsen highlighted the utility of chiral salen catalysts by coining them "privileged" catalysts because of their extremely high enantioselectivities observed in broad range of reactions.[35] Such asymmetric transformations include epoxidations, hydrolytic kinetic resolution of epoxides, hetero Diels-Alder reactions, cyclopropanations, aziridations, and others (Figure 1.13). These asymmetric reactions are vitally important to the pharmaceuticals industry as inexpensive methods to synthesize chiral building blocks needed for drugs. Impressively, these reactions could all be catalyzed by the same salen ligand by substituting various transition metals into the complex including cobalt, manganese, chromium, aluminum, and ruthenium. The importance of a broader class of chiral catalysts was previously evidenced by the 2001 Chemistry Nobel Prize awarded to Knowles and Noyori for their work in enantioselective hydrogenation catalysis and Sharpless for enantioselective oxidation catalysis.[36]

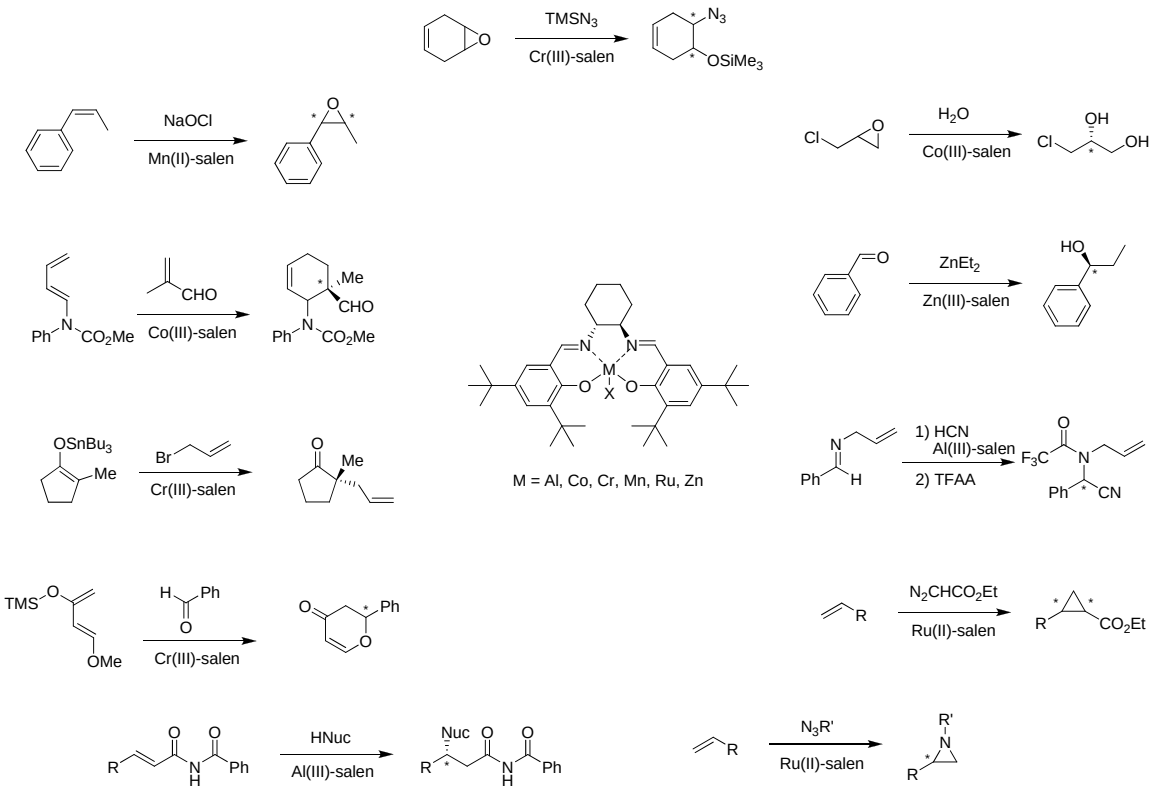

Figure 1.13. A sampling of enantioselective reactions catalyzed by metal-salen complexes.

As the utility and versatility of chiral salen catalysts has evolved in recent years, many researchers have turned their investigation to their immobilization on solid supports: soluble and insoluble polymers, siloxanes, zeolites, and silicas.[37] When supported on polymers, functionalized salen ligands are generally copolymerized with other monomers. Immobilization methods on non-polymeric supports can be generally categorized as electrostatic interactions, encapsulation, metal coordination, or covalent grafting (Figure 1.14). Three recent reviews on immobilized asymmetric catalysts by Song,[9] Hutchings,[6] and Li[38] cover these examples extensively. Such immobilized chiral catalysts, represent promising technology to meet growing pharmaceutical and agro-chemical demand for enantiopure chemicals.

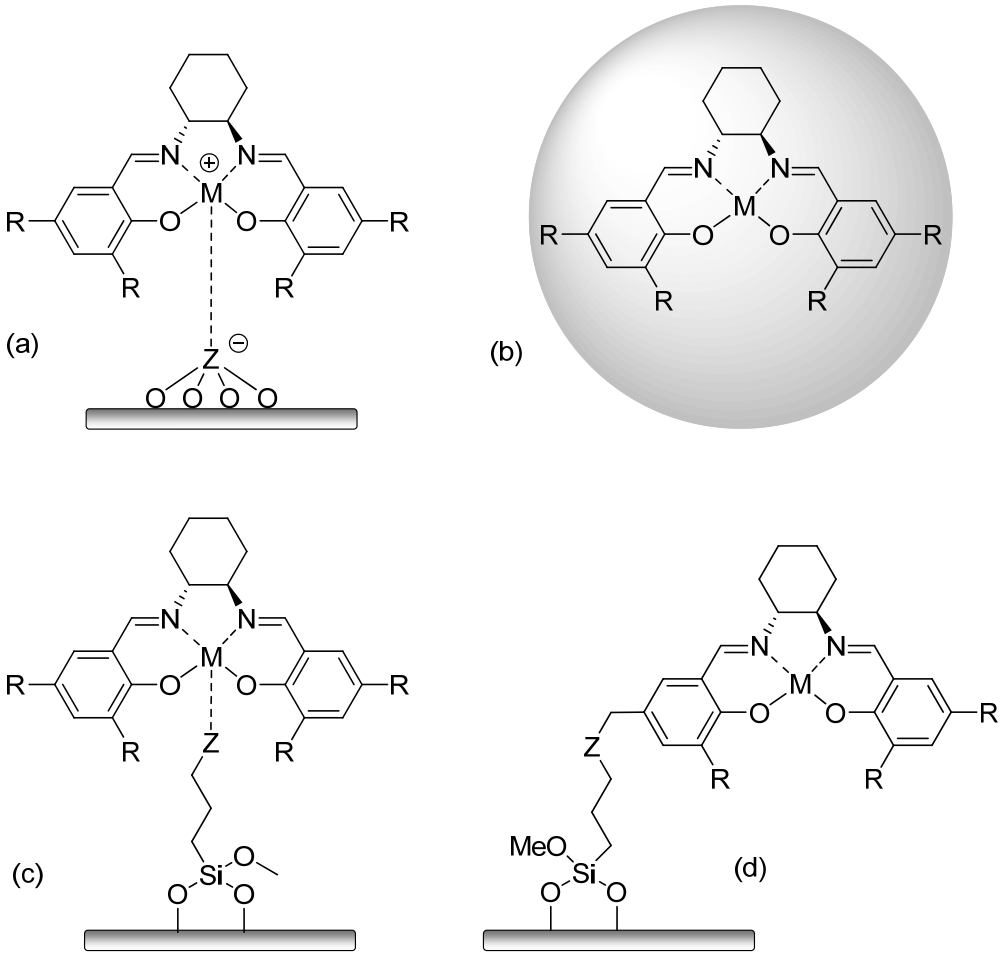

Figure 1.14. General salen immobilization methods: (a) electrostatic interactions with surface, (b) encapsulation, (c) metal coordination, and (d) covalent grafting.

1.4.2.1 Supported Co-salen catalysts

Following Jacobsen's discovery of the hydrolytic kinetic resolution of epoxides by homogeneous Co-salen complexes (Figure 1.15),[39] researchers have investigated methods of supporting these catalysts on solid supports for their recovery and reuse. Experimental evidence has indicated the reaction mechanism follows a bimetallic pathway, indicating the rate-limiting transition state of the reaction involves two Co-salen catalysts in close proximity of each other.[40] Consequently, supported Co-salen catalysts have been designed specifically to promote these site-site interactions and have in some cases exceeded the activity of the homogeneous catalyst![41-45] Chapters 4 and 5 make use

of polymer brush supported Co-salen catalysts to promote these site-site interactions for the HKR of epichlorohydrin. Chapter 4 discusses the effects of the linker between the salen ligand and the polymer backbone on activity and selectivity. It also presents investigations on possible catalyst deactivation pathways, an area of practical important that rarely receives mention. Chapter 5 discusses use of magnetic polymer brush supported Co-salen catalysts as an alternative method for recovery and reuse of these expensive catalysts.

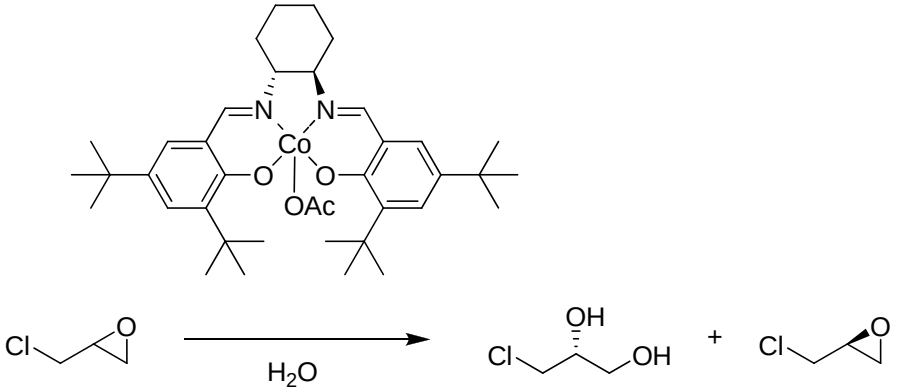

Figure 1.15. Cobalt(III)-salen catalyzed hydrolytic kinetic resolution of epichlorohydrin.

1.4.2.2 Supported Ru-salen catalysts

Like the hydrolytic kinetic resolution of epoxides, asymmetric synthesis of chiral cyclopropyl chemicals is of particular importance to the pharmaceutical and agro-chemical industries as an alternative method of procuring these important chiral building blocks used in the preparation of drugs and pesticides.[46-48] Ruthenium-salen catalysts have been shown to promote asymmetric cyclopropanation (Figure 1.16) and aziridation reactions of terminal olefins in high activity and selectivity. These two reactions are closely related and operate via the addition of a carbene or nitrene across the terminal olefin, respectively. Due to the potential hazards of working azides and aziridines, most of the published work has focused on Ru-salen catalyzed cyclopropanation reactions. Despite the high activity and selectivity of homogeneous Ru-salen catalysts, [49-51] no

reports of supported Ru-salen cyclopropanation or aziridation catalysts existed prior to this thesis work.

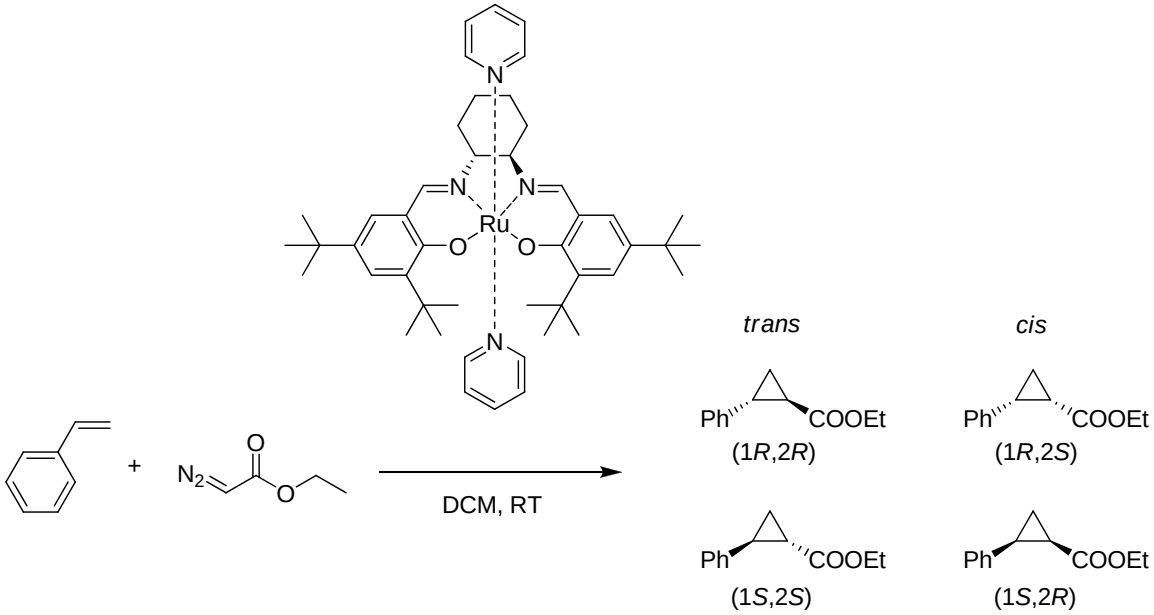

Figure 1.16. Ru-salen catalyzed cyclopropanation of styrene.

Chapter 6 delves into the unexplored field of supported Ru-salen catalysts for asymmetric cyclopropanation of olefins. Since this is an unexplored field, new insights into successful methods of supporting salen ligands and metallation procedures are investigated. Both polymer and SBA-15 supported catalysts were developed and demonstrated high activities and selectivities, approaching that of the homogeneous catalyst. Additionally, the supported Ru-salen catalysts were compared again other leading supported cyclopropanation catalysts and found to be among the most active and selective.

1.5 Thesis Goals

The overall theme to this thesis work is the development of novel hybrid organic/inorganic catalysts and catalyst supports for the synthesis of chemicals relevant to the fine chemical and pharmaceutical industries. Within this broad theme are several specific goals for the advancement of the field of supported catalysis. These include (1)

identification of novel catalyst supports and architectures for supported hybrid organic/inorganic catalysts, (2) understanding the effects of the covalent linker on catalytic performance, (3) intelligent design of supported catalysts based on mechanistic knowledge, and (4) demonstration of novel techniques of supporting homogeneous catalysts. The following chapters present five investigations highlighting a variety of supported organic and organometallic catalysts in support of these goals. This thesis concludes with a summary of how these investigations shed light into above mentioned four goals. Additional suggestions are included for future studies that build upon this thesis work and further advance the field of supported catalysis.

1.6 References

1. Breslow, R., *Science* **1982**, 218, 532.
2. Cole-Hamilton, D.J., *Science* **2003**, 299, 1702.
3. Thayer, A., *Chemical & Engineering News* **2005**, 83, 55.
4. Wight, A.P. and Davis, M.E., *Chem. Rev.* **2002**, 102, 3589.
5. Corma, A. and Garcia, H., *Adv. Synth. Catal.* **2006**, 348, 1391.
6. McMorn, P. and Hutchings, G.J., *Chem. Soc. Rev.* **2004**, 33, 108.
7. Thomas, J.M. and Raja, R., *J. Orgmet. Chem.* **2004**, 689, 4110.
8. Benaglia, M., Puglisi, A., and Cozzi, F., *Chem. Rev.* **2003**, 103, 3401.
9. Song, C.E. and Lee, S.G., *Chem. Rev.* **2002**, 102, 3495.
10. Clapham, B., Reger, T.S., and Janda, K.D., *Tetrahedron* **2001**, 57, 4637.
11. Beck, J.S., Vartuli, J.C., Roth, W.J., Leonowicz, M.E., Kresge, C.T., Schmitt, K.D., Chu, C.T.W., Olson, D.H., Sheppard, E.W., McCullen, S.B., Higgins, J.B., and Schlenker, J.L., *J. Am. Chem. Soc.* **1992**, 114, 10834.
12. Mastrorilli, P. and Nobile, C.F., *Coord. Chem. Rev.* **2004**, 248, 377.
13. Hoffmann, F., Cornelius, M., Morell, J., and Froba, M., *Angew. Chem. Int. Ed.* **2006**, 45, 3216.
14. Burkett, S.L., Sims, S.D., and Mann, S., *Chem. Commun.* **1996**, 1367.
15. Leadbeater, N.E. and Marco, M., *Chem. Rev.* **2002**, 102, 3217.
16. De Vos, D.E., Dams, M., Sels, B.F., and Jacobs, P.A., *Chem. Rev.* **2002**, 102, 3615.
17. Zhao, D.Y., Huo, Q.S., Feng, J.L., Chmelka, B.F., and Stucky, G.D., *J. Am. Chem. Soc.* **1998**, 120, 6024.
18. Latham, A.H. and Williams, M.E., *Accounts of Chemical Research* **2008**, 41, 411.
19. Fan, J. and Gao, Y., *Journal of Experimental Nanoscience* **2006**, 1, 457.
20. Vaino, A.R. and Janda, K.D., *Journal of Combinatorial Chemistry* **2000**, 2, 579.
21. Gill, C.S., Price, B.A., and Jones, C.W., *Journal of Catalysis* **2007**, 251, 145.

22. Luo, S.Z., Zheng, X.X., Xu, H., Mi, X.L., Zhang, L., and Cheng, J.P., *Adv. Synth. Catal.* **2007**, 349, 2431.
23. O' Dalaigh, C., Corr, S.A., Gun'ko, Y., and Connon, S.J., *Angew. Chem. Int. Ed.* **2007**, 46, 4329.
24. Phan, N.T.S., Gill, C.S., Nguyen, J.V., Zhang, Z.J., and Jones, C.W., *Angew. Chem. Int. Ed.* **2006**, 45, 2209.
25. Phan, N.T.S. and Jones, C.W., *Journal of Molecular Catalysis a-Chemical* **2006**, 253, 123.
26. Abu-Reziq, R., Alper, H., Wang, D.S., and Post, M.L., *J. Am. Chem. Soc.* **2006**, 128, 5279.
27. Ding, S.J., Xing, Y.C., Radosz, M., and Shen, Y.Q., *Macromolecules* **2006**, 39, 6399.
28. Duanmu, C., Saha, I., Zheng, Y., Goodson, B.M., and Gao, Y., *Chemistry of Materials* **2006**, 18, 5973.
29. Lv, G.H., Mai, W.P., Jin, R., and Gao, L.X., *Synlett* **2008**, 1418.
30. Tanabe, K. and Holderich, W.F., *App. Catal A: Gen.* **1999**, 181, 399.
31. Hattori, H., *Chem. Rev.* **1995**, 95, 537.
32. Ono, Y. and Baba, T. *Selective reactions over solid base catalysts*. 1997.
33. Farina, V., Reeves, J.T., Senanayake, C.H., and Song, J.H.J., *Chem. Rev.* **2006**, 106, 2734.
34. Cozzi, P.G., *Chem. Soc. Rev.* **2004**, 33, 410.
35. Yoon, T.P. and Jacobsen, E.N., *Science* **2003**, 299, 1691.
36. Nobel_lectures, *Angew. Chem. Int. Ed.* **2002**, 41, 998.
37. Canali, L. and Sherrington, D.C., *Chem. Soc. Rev.* **1999**, 28, 85.
38. Li, C., *Cat. Rev.* **2004**, 46, 419
39. Tokunaga, M., Larrow, J.F., Kakiuchi, F., and Jacobsen, E.N., *Science* **1997**, 277, 936.
40. Nielsen, L.P.C., Stevenson, C.P., Blackmond, D.G., and Jacobsen, E.N., *J. Am. Chem. Soc.* **2004**, 126, 1360.
41. Annis, D.A. and Jacobsen, E.N., *J. Am. Chem. Soc.* **1999**, 121, 4147.
42. Breinbauer, R. and Jacobsen, E.N., *Angew. Chem. Int. Ed.* **2000**, 39, 3604.
43. Zheng, X.L., Jones, C.W., and Weck, M., *Chemistry-a European Journal* **2006**, 12, 576.
44. Zheng, X.L., Jones, C.W., and Weck, M., *J. Am. Chem. Soc.* **2007**, 129, 1105.
45. Zheng, X.L., Jones, C.W., and Weck, M., *Adv. Synth. Catal.* **2008**, 350, 255.
46. Donaldson, W.A., *Tetrahedron* **2001**, 57, 8589.
47. Lopez, O., Fernandez-Bolanos, J.G., and Gil, M.V., *Green Chemistry* **2005**, 7, 431.
48. Salaun, J., *Chem. Rev.* **1989**, 89, 1247.
49. Miller, J.A., Gross, B.A., Zhuravel, M.A., Jin, W.C., and Nguyen, S.T., *Angew. Chem. Int. Ed.* **2005**, 44, 3885.
50. Miller, J.A., Hennessy, E.J., Marshall, W.J., Scialdone, M.A., and Nguyen, S.T., *J. Org. Chem.* **2003**, 68, 7884.
51. Miller, J.A., Jin, W.C., and Nguyen, S.T., *Angew. Chem. Int. Ed.* **2002**, 41, 2953.

CHAPTER 2

EXPANDING THE UTILITY OF ONE-POT MULTISTEP REACTION NETWORKS THROUGH COMPARTMENTATION AND RECOVERY OF THE CATALYST[†]

2.1 Introduction

Solid acid and base catalysts have found widespread use in industry due to their aforementioned advantages over homogeneous acids and bases. These solid catalysts can also be used in one-pot acid/base cascade reactions. Because solid-solid interactions are highly unfavorable, solid acids and bases can survive the other's presence without self-quenching. However, these solid catalysts are generally only recoverable as mixtures. This chapter discusses use of novel magnetic nanoparticle supported catalysts to address the issue of recovery and separation of individual acid and base catalysts.

Living systems combine the use of highly specific catalysts coupled with compartmentation in different regions of the cell to control multistep reaction networks, which are used to synthesize the complex organic molecules that cells need to survive.[1] Although there has been significant progress in mimicking nature's reaction cascade strategy over the past decades, the manipulation of sequential reactions using multiple catalysts in a single vessel is still relatively rare. Over the years, non-natural systems based on single- or multienzyme-mediated reaction sequences have been demonstrated, mimicking some aspects of nature s synthetic strategy.[2-7] Nonetheless, the vast majority of chemical syntheses are still conducted using the traditional paradigm of single catalytic reactions with homogeneous or heterogeneous chemical catalysts,

---

[†] Previously published work: N.T.S. Phan, C.S. Gill, J.V. Nguyen, Z.J. Zhang, C.W.Jones, *Angew. Chemie. Int. Ed.* **2006**, 45, 2209-2212.

followed by costly catalyst and/or product purification steps.[8-10] Controlling one-pot, multistep reactions using traditional homogeneous catalysts is difficult, since interactions between soluble catalysts may lead to deactivation. Many examples of complex reaction sequences or cascades do not use multiple catalysts, whereas in other cases combinations of homogeneous, heterogeneous, or enzyme catalysts in one pot were used to direct sequential reactions.[2-7, 11-27] These cases represent carefully constructed systems that were optimized for one specific sequence. In cases of multiple heterogeneous catalysts, the catalyst mixture can be recovered, but the individual components could not be separated.[28-33] In such cases, standard workup procedures after the reaction most likely result in the used catalysts simply becoming a component of the reaction waste. A critical aspect of living systems that thus far has not been effectively applied is the use of multiple combinations of catalysts sequentially.

An approach to achieve this within the chemical catalysis paradigm is to develop the ability to separate the multiple catalysts used in one-pot, multi-reaction cascades in essentially pure form, allowing reuse of the recovered catalysts in numerous other catalytic reactions, potentially in a combinatorial manner. Herein, we demonstrate this approach using a combination of catalysts recovered by magnetic,[34-42] gravimetric, and membrane methods,[43-46] allowing excellent control of multistep reactions with recovery of each individual catalyst. In particular, the use of magnetically separable catalysts allows the creation of a variety of versatile catalysts that can be easily recovered without the need for specialized equipment. Furthermore, the recovered catalysts can be reused in different, subsequent multistep one-pot reactions. This is an unprecedented level of control over multistep, one-pot catalytic reactions. This concept was demonstrated by combining base catalysts that are magnetically recoverable with acid catalysts that are recovered gravimetrically (Figure 2.1).

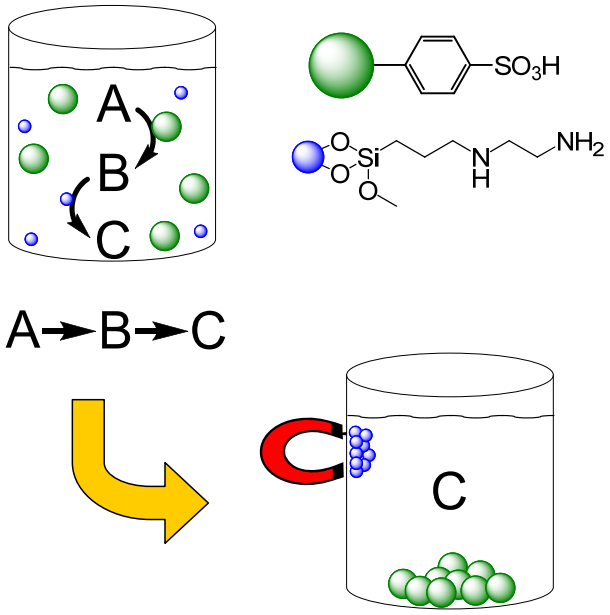

Figure 2.1 – Individually recoverable acid and base catalysts for one-pot cascade reactions.

2.2 Experimental Procedures

2.2.1 Chemicals

Cobalt (II) chloride (Alfa Aesar, anhydrous, 99.5%), iron (II) chloride (Alfa Aesar, anhydrous, 99.5%), acetone (Acros, 99%), ammonium hydroxide (Fisher, 29% v/v aqueous solution), benzaldehyde (Aldrich, anhydrous, 99%), benzaldehyde dimethylacetal (Acros, 99%), ethanol (Fisher, 99%), hexanes (Fisher, 99%), malononitrile (Acros, 99%), methylamine (Alfa Aesar, 40% w/w aqueous solution), nitromethane (Acros, 99%), platinum 0.5% on alumina (Alfa Aesar), *N*-propylethylenediamine (Acros, 99%), sodium dodecyl sulfate (Acros, 85%), tetrahydrofuran (THF) (Fisher, 99%), toluene (Acros, 99%), *p*-toluenesulfonic acid (Aldrich, monohydrate, 98%), *N*-[3-(trimethoxysilyl)propyl]ethylenediamine (Acros, 99%), trimethylsilyl cyanide (Acros, 98%), and xylene (Acros, 99%) were used as

received. Molecularporous membrane (Biotech RC) was purchased from Spectrumlabs. Amberlyst cation exchange resin (Aldrich, 16-50 mesh) was washed with copious amounts of THF and toluene, and dried under vacuum overnight at room temperature. Deionized water was purged with nitrogen overnight prior to use.

2.2.2 Instrumentation

A Fischer Scientific FS60H was used to sonicate samples. Nitrogen physisorption measurements were conducted using a Micromeritics ASAP 2010 system. Samples were pretreated by heating under vacuum at 150^{o}C overnight. A Netzsch Thermoanalyzer STA 409 was used for simultaneous thermal analysis combining thermogravimetric analysis (TGA) and differential scanning calorimetry (DSC) with a heating rate of 10^{o}C/min in air. X-ray powder diffraction (XRD) patterns were recorded using Cu-Kα radiation source on a Scintag X1 powder diffractometer. Scanning electron microscopy (SEM) images were captured using a Hitachi S800 field emission gun. Transmission electron microscopy studies were performed using a JEOL 100CX II Transmission Electron Microscope (TEM) at 100 kV and 100,000 magnification. The nanoparticles were dispersed on holey carbon grids for TEM observation. Elemental analyses were performed by Desert Analytics Lab (Tucson, AZ, USA) with ICP-MS. Gas chromatographic (GC) analyses were performed using a Shimadzu GC 14-A equipped with a flame ionization detector (FID) and an HP-5 column (length = 30 m, inner diameter = 0.25 mm, and film thickness = 0.25 μm). The temperature program for GC analysis heated samples from 50 to 140^{o}C at 30^{o}C/min, from 140 to 300^{o}C at 40^{o}C/min, and held at 300^{o}C for 2 min. Inlet and detector temperatures were set constant at 330^{o}C. Xylene was used as an internal standard to calculate reaction conversion. GC-MS

analyses were performed using a Hewlett Packard GC-MS 5890 with a DB-5 column (length = 30 m, inner diameter = 0.25 mm, and film thickness = 0.25 μm). The temperature program heated samples from 30 to 300°C at 15°C/min and held at 300°C for 5 min.

2.2.3 Catalyst synthesis

2.2.3.1 Synthesis of magnetic nanoparticles

Cobalt spinel ferrite ($CoFe_2O_4$) nanoparticles were synthesized following a microemulsion method.[47] Cobalt (II) chloride (0.9 g, 6.9 mmol) and iron (II) chloride (1.9 g, 14.9 mmol) were mixed in an aqueous solution (500 ml). An aqueous surfactant solution of sodium dodecyl sulfate (SDS) (12.9 g, 38.3 mmol) in deionized water (500 ml) was added, and the mixture was stirred at room temperature for 30 min to form a mixed micellar solution of $Co(DS)_2$ and $Fe(DS)_2$. The mixture was then heated to 55-65°C. A solution of methylamine (300 ml, 40% w/w aqueous solution) in deionized water (700 ml) was heated to the same temperature and rapidly added to the surfactant mixture. Black nanoparticles were precipitated. After the reaction mixture was stirred vigorously for 3 h, the nanoparticles were isolated by centrifugation and washed with copious amounts of deionized water, ethanol, and hexanes by magnetic decantation. The final product was dried in air at 50°C overnight to yield superparamagnetic cobalt spinel ferrite nanoparticles (1.7 g).

2.2.3.2 Amino-functionalized magnetic nanoparticles

The magnetic nanoparticles were functionalized with *N*-[3-(trimethoxysilyl)propyl]ethylenediamine according to a slightly modified reported

procedure.[48] $CoFe_2O_4$ nanoparticles (1.1 g) were dispersed in a mixture of ethanol and water (150 ml, 1:1 by volume). The suspension was sonicated for 30 min at room temperature. Ammonium hydroxide (15 ml, 29% v/v aqueous solution) was added, and the mixture was stirred vigorously at 60°C for 24 h under an argon atmosphere. The nanoparticles were washed with copious amounts of deionized water, ethanol, and hexanes via magnetic decantation. The resulting product was redispersed in a mixture of ethanol and water (150 ml, 1:1 by volume), and sonicated for 30 min at room temperature. *N*-[3-(trimethoxysilyl)propyl]ethylenediamine (1g) was then added, and the solution was heated at 60°C with vigorous stirring for 24 h under an argon atmosphere. The final product was washed with copious amounts of deionized water, ethanol, and hexanes by magnetic decantation, and dried under vacuum at room temperature overnight to yield amino-functionalized magnetic nanoparticles (1.1 g).

2.2.4 Catalytic studies

2.2.4.1 One-pot Deacetalization-Knoevenagel reaction

Basic magnetic nanoparticles (8 mg), cation exchange resin (50 mg), toluene (4 ml), benzaldehyde dimethylacetal (15.2 mg, 0.1 mmol), malononitrile (13.8 mg, 0.2 mmol), and xylene (10.6 mg, 0.1 mmol) were placed into a 10 mL glass vessel. The mixture was stirred at room temperature under an argon atmosphere. Reaction conversion was monitored by withdrawing aliquots from the reaction mixture at different time intervals, quenching with acetone, filtering through a short silica gel pad, analyzing by GC with reference to xylene, and further confirming by GC-MS. The nanoparticles were magnetically separated from the resin catalyst, dried under vacuum overnight at room

temperature, and reused with a new solid catalyst, Pt/Al_2O_3, in a second one-pot reaction. The separated resin catalyst was stored for further use.

2.2.4.2 One-pot Knoevenagel-Hydrogenation reaction

A mixture of the basic magnetic nanoparticles recovered from the first one-pot reaction, benzaldehyde (10.6 mg, 0.1 mmol), malononitrile (13.8 mg, 0.2 mmol), and xylene (10.6 mg, 0.1 mmol) in toluene (4 ml) was added to a 10 mL glass vessel and stirred at room temperature for 1 h under an argon atmosphere. The reaction was monitored by GC and GC-MS as previously described. Quantitative conversion was achieved. Platinum catalyst (0.5% Pt on Al_2O_3, 100 mg) was then added, and the whole mixture was transferred to a stainless steel Parr autoclave. The autoclave was purged with hydrogen, pressurized to 800 psi, and then reduced to 100 psi. After this procedure was repeated five times, the autoclave was pressurized with hydrogen to 1000 psi and stirred at 500 rpm at room temperature for 24 h. Reaction conversion was monitored by GC and GC-MS. The magnetic nanoparticles were magnetically separated from the platinum catalyst and reused in a third one-pot reaction. An experiment was carried out as well with 1000 psi hydrogen pressure from time zero as well.

2.2.4.3 One-pot Deacetalization-Knoevenagel-hydrogenation reaction

Basic magnetic nanoparticles (50 mg), cation exchange resin (300 mg), toluene (40 ml), benzaldehyde dimethylacetal (91 mg, 0.6 mmol), malononitrile (79 mg, 1.2 mmol), and xylene (64 mg, 0.6 mmol) were added to a stainless steel Parr autoclave. Platinum catalyst (0.5% Pt on Al_2O_3, 600 mg) was ground into fine powder, enclosed in a molecularporous membrane, and the membrane was then suspended from the top of the autoclave. The mixture was stirred at room temperature for 1 h. The reaction was

monitored by GC and GC-MS. Quantitative conversion was achieved. The autoclave was then purged with hydrogen as described above, pressurized with hydrogen to 1000 psi, and stirred at 500 rpm at room temperature for 48 h. Reaction conversion was monitored by GC and GC-MS. The membrane-enclosed, platinum catalyst was separated from the reaction mixture. The magnetic nanoparticles were separated from the resin catalyst by magnetic decantation. In a parallel experiment, quantitative conversion was achieved within 24 h when the platinum catalyst was not isolated from the other catalysts by the molecularporous membrane.

2.2.4.4 One-pot Deacetalization-Nitroaldol reaction

The one-pot deacetalization-nitroaldol reaction was carried out using the magnetic base catalyst recovered from the second one-pot reaction and the acid resin catalyst separated from the first one-pot reaction. The recovered catalysts, benzaldehyde dimethylacetal (15.2 mg, 0.1 mmol), and xylene (10.6 mg, 0.1 mmol) as internal standard in nitromethane (4 ml) were placed into a 10 mL glass vessel. The mixture was heated at 100^{o}C under an argon atmosphere with constant stirring for 20 h. Reaction conversion was monitored by GC and GC-MS.

2.2.4.5 One-pot Deacetalization-Aldol reaction

The one-pot Deacetalization-Aldol reaction was carried out using the magnetic base catalyst recovered from the second one-pot reaction and the acid resin catalyst separated from the first one-pot reaction. The recovered catalysts, benzaldehyde dimethylacetal (15.2 mg, 0.1 mmol), and xylene (10.6 mg, 0.1 mmol) as internal standard in acetone (4 ml) were placed into a 10 mL glass vessel. The resulting mixture was

heated at 50^{o}C under an argon atmosphere with constant stirring for 20 h. Reaction conversion was monitored by GC and GC-MS.

2.2.5 Catalyst separation

Separation of catalysts was achieved by sonicating the reaction vessel after applying an external permanent magnet to one side of the vessel. After quantitative conversion of the first one-pot reaction was achieved, an external magnetic field was applied on the outer surface of the glass reaction vessel containing the magnetic nanoparticles and the resin catalyst. The system was sonicated at room temperature to facilitate the separation of one catalyst from the other. The non-magnetic resin catalyst together with the reaction solution was removed from the reaction vessel by decantation while the external magnet held the basic nanoparticles stationary inside the vessel (Figure 2.2). The suspension of the non-magnetic resin catalyst in reaction solution was transferred to a new vessel, and the resin catalyst was separated under gravity. The separated resin catalyst was then added to toluene, sonicated to remove any physisorbed magnetic nanoparticles, and separated by magnetic decantation. It should be noted that a small amount of the magnetic nanoparticles adhered to the surface of the resin catalyst during the course of the reaction. However, these particles could be removed from the resin catalyst by sonication. Any nanoparticles collected were combined with the magnetic nanoparticles remaining in the reaction vessel. The magnetic base catalyst was also redispersed in toluene, sonicated, and recovered by magnetic separation to improve its purity. Elemental analyses of iron on the separated resin catalyst and sulfur on the recovered magnetic nanoparticles were performed with reference to the corresponding

fresh catalysts. Catalysts from the one-pot Knoevenagel-hydrogenation reaction were also recovered using the procedure described above.

Figure 2.2 – Facile separation of magnetic nanoparticles (black powder, left side) from non-magnetic polymer resin (bottom).

2.3 Results

2.3.1 Catalyst characterization

Transmission electron microscopy (TEM) was performed on the resulting amine functionalized $CoFe_2O_4$ magnetic nanoparticles, indicating the MNP consisted of primary particles of 6-8 nm that formed aggregates of 40 nm diameter (Figure 2.3) The XRD patterns were consistent with the characteristic pattern for spinel ferrites (Figure 2.4).[47] Nitrogen physisorption measurements reported BET surface areas of 200 m^2/g and no

measurable mesoporosity. Thermogravimetric analysis (TGA) showed that 0.3 mmol/g of the diamine was immobilized on the ferrite nanoparticles. SEM images portrayed an average polymer resin diameter of 600 μm (Figure 2.5).

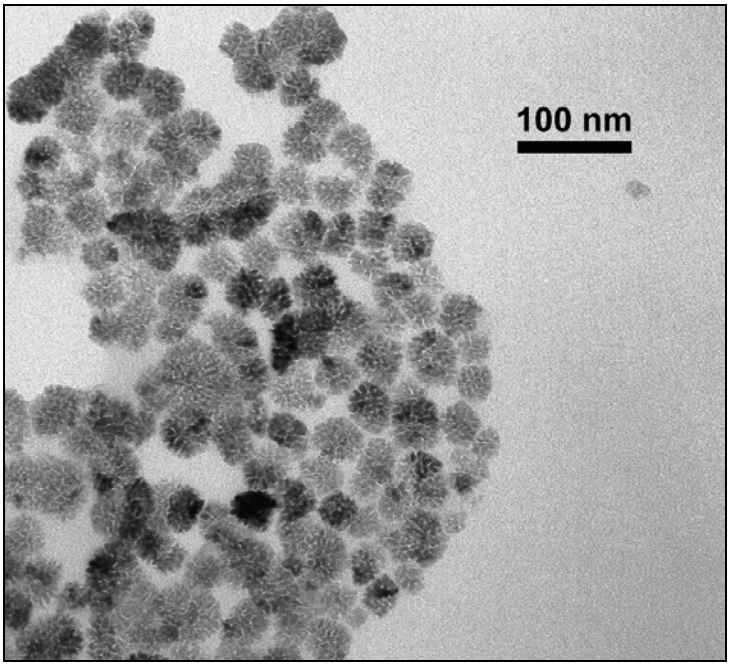

Figure 2.3 - TEM micrograph of the amino-functionalized magnetic nanoparticle catalyst

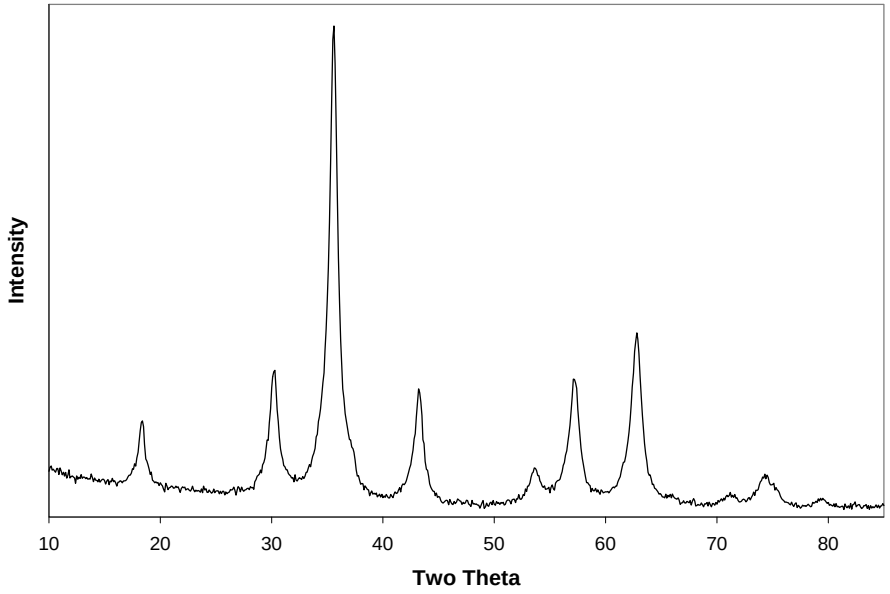

Figure 2.4 - X-ray powder diffractogram of the magnetic nanoparticle catalyst

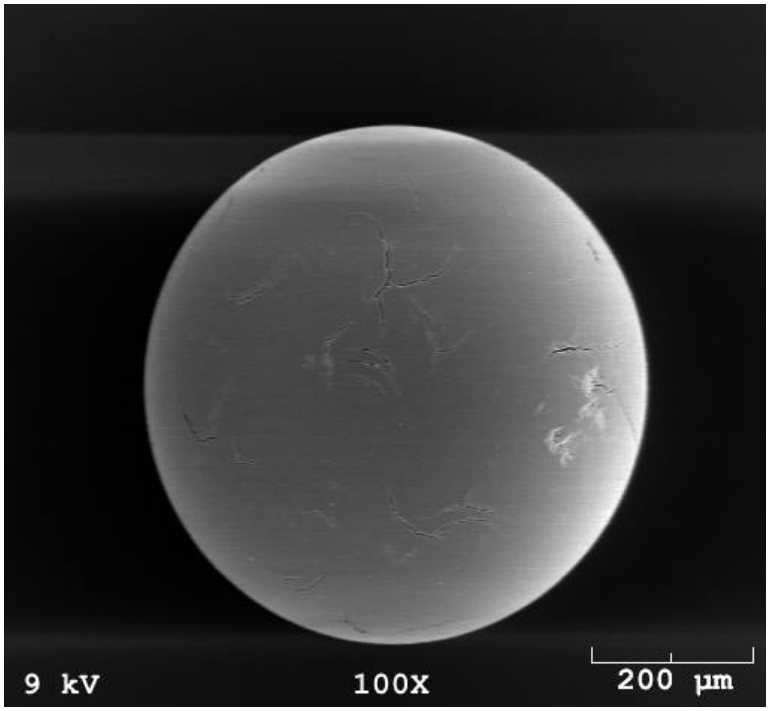

Figure 2.5 - SEM micrograph of the sulfonic acid-functionalized resin catalyst.

2.3.2 Catalytic studies

Complete conversion of **1** into **2** and **2** into **3** (Figure 2.6, blue box) was observed in just 30 minutes, with average turnover frequencies (TOF) of 3 h^{-1} for the acid resin catalyst and 75 h^{-1} for the basic magnetic catalyst. After reaction, the catalysts were separated by sonicating the reaction vessel and affixing a small permanent magnet externally to one wall of the vessel. The nonmagnetic resin catalyst was removed from the reaction vessel by decantation while the magnetic nanoparticle base catalyst was held stationary in the vessel by the magnet. Each catalyst was recovered in essentially pure form, as indicated by elemental analysis of the recovered catalysts. The amount of sulfur, an elemental tag for the resin catalyst, detected in the magnetic nanoparticle catalyst before and after reaction was essentially identical (0.07%S in the magnetic base catalysts

before reaction and 0.05%S after reaction). The same is true of the amount of iron, an elemental tag for the magnetic catalyst, in the resin catalyst before and after reaction (0.01%Fe in the acid resin catalyst before reaction and 0.03% Fe after reaction).

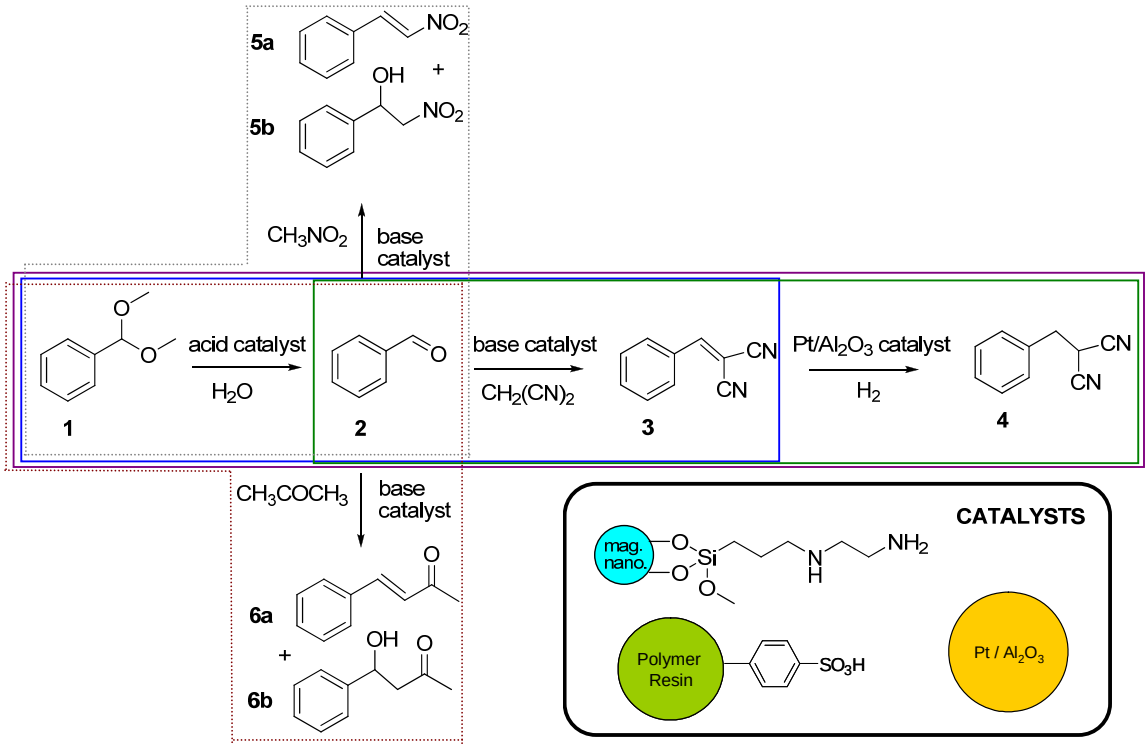

Figure 2.6 – Catalytic one-pot reaction networks.

Reuse of the separated catalysts in the same reaction gave the same results with the same kinetic profile, indicating that no noticeable deactivation of the catalyst occurred upon combination of the two opposing catalysts (Figure 2.7). The data for the first and second runs for the conversion of **1**-**2**-**3** match each other quite well, except for what appears to be a slight incubation period in the conversion of **2** to **3** in the first run. Since this reaction was run in a two step, one-pot sequence, there is some delay in the conversion of **2** to **3**, as it is being made in situ. In contrast, the second set of data for the conversion of **2** to **3** come from the one pot reaction of **2**-**3**-**4**. In this case, **2** is present at

the outset and there is therefore no delay in its conversion. The second set of data for the conversion of **1** to **2** comes from the single reaction **1-2** using the acid resin catalyst recovered from the one pot reaction of **1-2-3**.

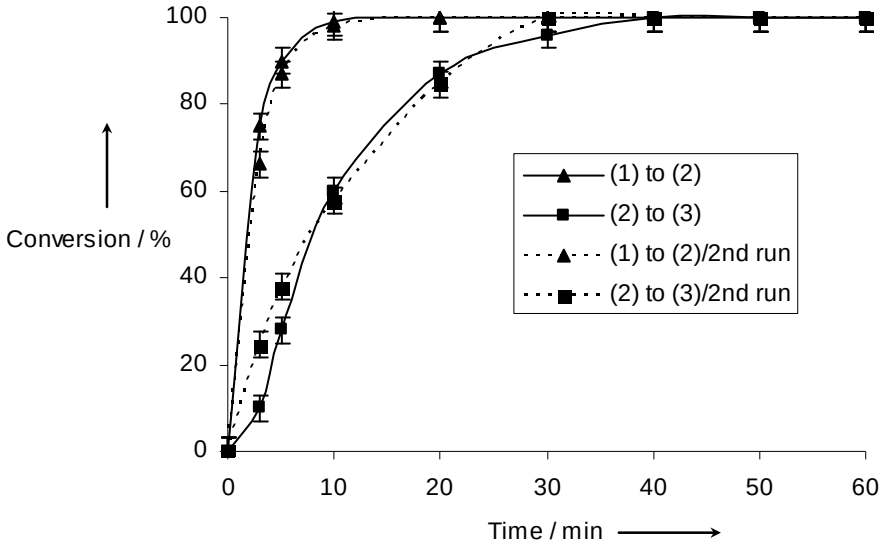

Figure 2.7 - One-pot sequential reactions with acidic polymer resin and basic magnetic nanoparticle catalysts. Triangles and squares represent kinetic data for the reactions of **1** to **2** and **2** to **3**, respectively. Broken lines show kinetic data for reactions with recycled catalysts.

Note also that each catalyst on its own was unable to promote the conversion of 1 into 3, indicating that the tandem action of two catalysts was required to complete the sequence, as is often seen in biological systems (Table 2.1). These data, when combined with the results of elemental analysis, show that the catalysts can be recovered in pure form and that they can be subsequently reused without loss of performance. This is the first example of a multistep, one-pot reaction in which the catalysts can be recovered in pure form and used in later manipulations.

Table 2.1 - Results of catalytic reaction sequences carried out in a single reaction vessel with multiple opposing catalysts.

Blue Sequence 1 - 2 - 3		
Catalyst	**1** to **2**	**2** to **3**
Solid acid & solid base	100%	100%
Solid acid	100%	0%
Solid base	0%	0%
Solid acid & homogeneous base	0%	0%
Solid base & homogeneous acid	0%	0%
Homogeneous acid & base	0%	0%
Green Sequence 2 – 3 - 4		
Solid base &	**2** to **3**	**3** to **4**
Pt/Al_2O_3	100%	100%
Violet Sequence 1 - 2 - 3 - 4		
Solid acid, solid	**1** to **3**	**3** to **4**
base & Pt/Al_2O_3	100%	78% [100%]
Gray Sequence 1 – 2 – 5a 5b		
Solid acid &	**1** to **2**	**2** to **5a 5b**
solid base	100%	100% [4:1
Red Sequence 1 – 2 – 6a 6b		
Solid acid &	**1** to **2**	**2** to **6a 6b**
solid base	100%	82% [26:1

To show the versatility of this method, the recovered magnetic nanoparticle catalyst was then effectively used in a second multistep, one-pot reaction (Figure 2.6, green box) in conjunction with a new solid catalyst, Pt/Al2O3. This tandem Knoevenagel–hydrogenation reaction was carried out in one pot with all reagents and catalysts added at time zero. The reaction was started at atmospheric pressure, and after a period of time the pressure of the reaction was increased to 1000 psig H_2 to facilitate

completion of the second reaction. In this case, **2** was converted into **3** using the basic catalyst and **3** was hydrogenated to **4** by the supported platinum, with both reactions going to completion. Similar results were also obtained when the one-pot reaction was pressurized to 1000 psig H_2 at time zero and maintained at this pressure throughout the course of the reaction (Table 2.1). As before, the individual catalysts were recovered through the magnetic separation process described above. The reaction sequence was then extended to three steps, again with catalyst recovery, with conversion of **1** into **4** (Figure 2.6, violet box) by adding the base catalysts supported on magnetic nanoparticles and the polymeric acid catalyst into the vessel along with the platinum catalyst enclosed in a membrane. In this case, all components were added to the reactor at time zero and the reaction was started at 1 atm total pressure. After 60 minutes, the hydrogen pressure was increased to 1000 psig to carry out the final step of the reaction. The overall yield of the final product **4** was 78% (Table 2.1); 100% yield of **4** was obtained in the absence of a membrane. This result indicated that some transport effects were slowing the final reaction when the membrane was used. Stepwise control over the reaction sequence and the ability to continually reuse the original catalysts in multiple reactions was demonstrated by the conversion of **1** to **2** to **5a** and **5b** (Figure 2.6, gray box) using the same acid and base catalysts. By adding the magnetic nanoparticles used in the first two reaction sequences (**1**→**2**→**3** and **2**→**3**→**4**) and the acidic resin used in the first reaction sequence (**1**→**2**→**3**) to new reagents in a single vessel, the synthesis of **5a** and **5b** was achieved with complete conversion of **1** into **5a** and **5b**. Note that this sequence represents the third use of a single sample of magnetic catalyst and the second use of a

single sample of the acid catalyst. Similarly, products **6a** and **6b** were prepared in another one-pot reaction (Figure 2.6, red box) with excellent results.

2.4 Conclusions

In summary, we have shown that excellent control of a reaction sequence using chemical catalysts can be achieved by 1) using combinations of a few versatile catalysts that can be used in a variety of reactions, with recovery of the catalyst in pure form after the reaction; 2) compartmentation of catalytic sites to allow for use of catalysts that would self-quench in homogeneous media; and 3) regulation of the reaction pathway by manipulating the reaction conditions, including control of the catalysts and reagents that are present. The combination of magnetically and gravimetrically recoverable catalysts allowed the first successful application of opposing catalysts to multistep, one-pot catalytic reactions including the ability to steer the direction of the reaction at each step, all with recovery of each individual catalyst after use. The successful use of the recovered catalysts in combination with other catalysts in subsequent, unrelated reactions showed the versatility of this approach.[49, 50] A library of magnetically and gravimetrically recoverable catalysts could thus be generated and used in a variety of one-pot multistep catalytic reactions, and this methodology may be further expanded almost without limit through other means of catalyst separation, such as membrane encapsulation.[51, 52]

2.5 Acknowledgements

The US DOE Office of Basic Energy Sciences is acknowledged for financial support through Catalysis Science Contract No. DE-FG02-03ER15459. DuPont is also thanked for a Young Professor Award.

2.6 References

1. Ovadi, J. and Srere, P.A., *International Review of Cytology - a Survey of Cell Biology, Vol 192* **2000**, 192, 255.
2. Bruggink, A., Schoevaart, R., and Kieboom, T., *Org. Process Res. Dev.* **2003**, 7, 622.
3. Schoevaart, R., van Rantwijk, F., and Sheldon, R.A., *J. Org. Chem.* **2000**, 65, 6940.
4. Srere, P.A., Mattiass.B, and Mosbach, K., *Proc. Natl. Acad. Sci. U. S. A.* **1973**, 70, 2534.
5. Mayer, S.F., Kroutil, W., and Kurt, F., *Chem. Soc. Rev.* **2001**, 30, 332.
6. Schoevaart, R., van Rantwijk, F., and Sheldon, R.A., *Chem. Commun.* **1999**, 2465.
7. Nakajima, N., Tanizawa, K., Tanaka, H., and Soda, K., *J. Biotechnol.* **1988**, 8, 243.
8. Baxendale, I.R., Ley, S.V., and Piutti, C., *Angew. Chem. Int. Ed.* **2002**, 41, 2194.
9. Storer, R.I., Takemoto, T., Jackson, P.S., and Ley, S.V., *Angew. Chem. Int. Ed.* **2003**, 42, 2521.
10. Ley, S.V., Baxendale, I.R., Brusotti, G., Caldarelli, M., Massi, A., and Nesi, M., *Farmaco* **2002**, 57, 321.
11. Wasilke, J.C., Obrey, S.J., Baker, R.T., and Bazan, G.C., *Chem. Rev.* **2005**, 105, 1001.
12. Tietze, L.F. and Beifuss, U., *Angew. Chem. Int. Ed.* **1993**, 32, 131.
13. Tietze, L.F., *Chem. Rev.* **1996**, 96, 115.
14. McCarroll, A.J. and Walton, J.C., *J. Chem. Soc.-Perkin Trans. 1* **2001**, 3215.
15. Parsons, P.J., Penkett, C.S., and Shell, A.J., *Chem. Rev.* **1996**, 96, 195.
16. Nicolaou, K.C., Montagnon, T., and Snyder, S.A., *Chem. Commun.* **2003**, 551.
17. Gorobets, E.V., Miftakhov, M.S., and Valeev, F.A., *Russ. Chem. Rev.* **2000**, 69, 1001.
18. Lee, J.M., Na, Y., Han, H., and Chang, S., *Chem. Soc. Rev.* **2004**, 33, 302.
19. Burk, M.J., Lee, J.R., and Martinez, J.P., *J. Am. Chem. Soc.* **1994**, 116, 10847.
20. Denmark, S.E. and Thorarensen, A., *Chem. Rev.* **1996**, 96, 137.
21. Makkee, M., Kieboom, A.P.G., and Vanbekkum, H., *J. Chem. Soc.-Chem. Commun.* **1980**, 930.
22. Makkee, M., Kieboom, A.P.G., and Vanbekkum, H., *Carbohydr. Res.* **1985**, 138, 237.
23. Schoevaart, R. and Kieboom, T., *Tetrahedron Lett.* **2002**, 43, 3399.
24. Schoevaart, R. and Kieboom, T., *Top. Catal.* **2004**, 27, 3.
25. Posner, G.H., *Chem. Rev.* **1986**, 86, 831.
26. Larsson, A.L.E., Persson, B.A., and Backvall, J.E., *Angew. Chem. Int. Ed.* **1997**, 36, 1211.
27. Persson, B.A., Larsson, A.L.E., Le Ray, M., and Backvall, J.E., *J. Am. Chem. Soc.* **1999**, 121, 1645.
28. Gelman, F., Blum, J., and Avnir, D., *J. Am. Chem. Soc.* **2000**, 122, 11999.
29. Gelman, F., Blum, J., and Avnir, D., *Angew. Chem. Int. Ed.* **2001**, 40, 3647.

30. Gelman, F., Blum, J., and Avnir, D., *J. Am. Chem. Soc.* **2002**, 124, 14460.
31. Gelman, F., Blum, J., and Avnir, D., *New J. Chem.* **2003**, 27, 205.
32. Gelman, F., Blum, J., Schumann, H., and Avnir, D., *J. Sol-Gel Sci. Technol.* **2003**, 26, 43.
33. Motokura, K., Fujita, N., Mori, K., Mizugaki, T., Ebitani, K., and Kaneda, K., *J. Am. Chem. Soc.* **2005**, 127, 9674.
34. Teunissen, W., Bol, A.A., and Geus, J.W., *Catal. Today* **1999**, 48, 329.
35. Whitesides, G.M., Kazlauskas, R.J., and Josephson, L., *Trends in Biotech.* **1983**, 1, 144.
36. Hill, C.L., Lamotte, A., Althoff, W., Brunie, J.C., and Whitesides, G.M., *J. Catal.* **1976**, 43, 53.
37. Gao, X., Yu, K.M.K., Tam, K.Y., and Tsang, S.C., *Chem. Commun.* **2003**, 2998.
38. Yoon, T.J., Lee, W., Oh, Y.S., and Lee, J.K., *New J. Chem.* **2003**, 27, 227.
39. Liu, X.Q., Xing, J.M., Guan, Y.P., Shan, G.B., and Liu, H.Z., *Colloid Surf. A-Physicochem. Eng. Asp.* **2004**, 238, 127.
40. Lu, A.H., Schmidt, W., Matoussevitch, N., Bonnemann, H., Spliethoff, B., Tesche, B., Bill, E., Kiefer, W., and Schuth, F., *Angew. Chem. Int. Ed.* **2004**, 43, 4303.
41. Lu, A.H., Li, W.C., Kiefer, A., Schmidt, W., Bill, E., Fink, G., and Schuth, F., *J. Am. Chem. Soc.* **2004**, 126, 8616.
42. Hu, A.G., Yee, G.T., and Lin, W.B., *J. Am. Chem. Soc.* **2005**, 127, 12486.
43. Dijkstra, H.P., Van Klink, G.P.M., and Van Koten, G., *Accounts Chem. Res.* **2002**, 35, 798.
44. Bednarski, M.D., Chenault, H.K., Simon, E.S., and Whitesides, G.M., *J. Am. Chem. Soc.* **1987**, 109, 1283.
45. Woltinger, J., Bommarius, A.S., Drauz, K., and Wandrey, C., *Org. Process Res. Dev.* **2001**, 5, 241.
46. Wöltinger, J., Drauz, K., and Bommarius, A.S., *Appl. Catal. A: Gen.* **2001**, 221, 171.
47. Rondinone, A.J., Samia, A.C.S., and Zhang, Z.J., *J. Phys. Chem. B* **1999**, 103, 6876.
48. Shen, X.C., Fang, X.Z., Zhou, Y.H., and Liang, H., *Chem. Lett.* **2004**, 33, 1468.
49. Solinas, M., Jiang, J., Stelzer, O., and Leitner, W., *Angew. Chem.* **2005**, 117, 2331.
50. Solinas, M., Jiang, J.Y., Stelzer, O., and Leitner, W., *Angew. Chem. Int. Ed.* **2005**, 44, 2291.
51. Lakshmi, B.B. and Martin, C.R., *Nature* **1997**, 388, 758.
52. Hafez, A.M., Taggi, A.E., Dudding, T., and Lectka, T., *J. Am. Chem. Soc.* **2001**, 123, 10853.

CHAPTER 3

SULFONIC ACID FUNCTIONALIZED SILICA-COATED MAGNETIC NANOPARTICLE CATALYSTS †

3.1 Introduction

In Chapter 2, basic amine catalysts were immobilized on magnetic nanoparticles. This chapter presents the opposite case: sulfonic acid catalysts immobilized on MNP. Conflicting chemistries were encountered during this work, preventing the immobilization of sulfonic acid sites directly to the bare MNP. Instead, a protective silica shell was first applied to the MNP prior to surface functionalizations. Four MNP supported sulfonic acids were prepared and evaluated in acid catalyzed organic transformations.

The facile recovery and reuse of homogeneous catalysts via covalent tethering to a heterogeneous support while maintaining high catalytic activity has long been a goal in catalysis research [1]. These hybrid organic/inorganic catalysts have utilized a variety of support materials including porous inorganic oxides, such as zeolites, MCM, and SBA type silicas due to their high surface areas and well defined structures [2-5]. Additionally, organic polymers have also been extensively investigated as catalyst supports [6, 7]. However, these materials can suffer decreased catalytic activity resulting from diffusion limitations as chemicals diffuse through the porous silica networks or through swollen polymeric resins. Consequently recoverable soluble catalysts have received increasing

---

† Previously published work: C.S. Gill, C.W.Jones, *J. Catal.* **2007**, 251, 145-152.

attention in recent years. Several methods for the recovery of soluble catalysts include soluble polymer, multi-phase, membrane systems [8]. In the case of soluble polymer and multi-phasic systems, the addition of solvent to selectively precipitate polymer or extract homogeneous catalysts can prove costly.

Nanoparticles have received increasing attention as an alternative support for catalysis. As the diameter of the particle decreases to the nanometer scale, ample external surface area becomes available for surface modifications. Additionally, these particles can be dispersed into solvents, forming stable dispersions. However, these nanoparticles may be difficult to recover, as is the case with non-magnetic nanoparticle supported catalysts. Catalysts supported on magnetic nanoparticles (MNPs), usually iron oxides, can be quickly and easily recovered in the presence of external magnetic fields for reuse. Additionally, internal diffusion limitations can be avoided, since all the available surface area of the nonporous MNP is external. The surface of the MNPs can be functionalized to accommodate a wide variety of organic and organometallic catalysts. Several examples of transition metal catalyzed reactions grafted on MNPs have emerged recently: carbon-carbon cross-coupling reactions [9-14], hydroformylation [15, 16], hydrogenation [17-19], and polymerization [20] reactions. Other reports of MNP supported catalysts include enzymes for carboxylate resolution [21], amino acids for ester hydrolysis [22], and organic amine catalysts promoting Knoevenagel and related reactions [23, 24]. Despite the occurrence of these MNP supported base catalysts in the literature, no reports of acid functionalized MNP catalysts currently exist.

Acid catalysts are used in a variety of industrial organic transformations including aldol condensations, hydrolyses, acylations, nucleophilic additions, etc. [25]. However,

waste neutralization, difficult separations, reactor corrosion, and the inability for reuse hindered industrial reactions when using soluble, liquid acids [25]. Consequently, the need for solid acid catalysts arose. Proton exchanged aluminosilicate zeolites were well suited to the petrochemical industry due to their high selectivities and ability to be utilized in continuous processes [26]. However, the small pore diameter of these acidic aluminosilicate zeolites limited their utility in processes where larger molecules could not penetrate to the interior of the catalyst. Inorganic supports of larger pore diameters were developed to address such problems. However, acid sites in aluminosilicate derivatives of MCM-41 and SBA-15 materials were found to be only mildly acidic [27], and researchers began experimenting with covalently grafting sulfonic acids to these mesoporous supports to generate strong acid sites on these materials. These methods included oxidation of immobilized thiols to a sulfonic acids [28], hydrolysis of immobilized sulfonic acid chlorides [29], sulfonation of supported phenyl groups [30], ring opening of perfluorosulfonic acid sultones [31, 32], and via immobilization of perfluorosulfonic acid triethoxysilanes [33]. These methods and others were thoroughly discussed in two excellent reviews [25, 27].

This work builds upon prior work with magnetic nanoparticle base catalysts [23, 24] and illustrates for the first time the immobilization of sulfonic acid groups on magnetic nanoparticles for use as recyclable, solid acid catalysts (Figure 3.1). Various sulfonic acids were synthesized to compare the relative catalytic activity and stability of each. The magnetic nanoparticle supports were synthesized using known methods and silica-coated. This coating provided an inert barrier between the metal oxide core and surface functional groups. The hybrid organic/inorganic, magnetic, solid acid catalysts were characterized via nitrogen physisorption, FT-IR, titration, XRD, and TEM. The active

solid acid catalysts were easily recovered in the presence of an external magnetic field and exhibited good recyclability. Sulfonic acid catalysts grafted on mesoporous SBA-15 were observed to exhibit higher activities than those grafted on the silica coated magnetic nanoparticles.

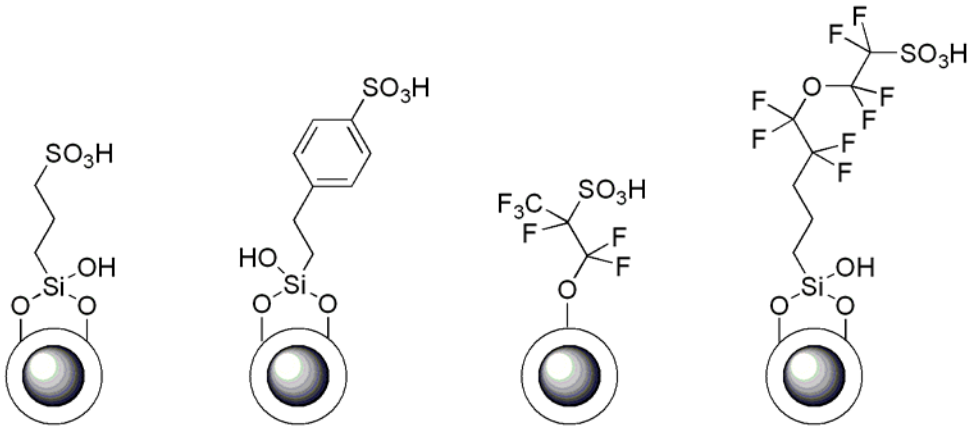

Figure 3.1 – Four new sulfonic acid catalysts supported on silica coated magnetic nanoparticles.

3.2 Experimental Procedures

3.2.1 Chemicals

Ammonium hydroxide (Fisher, 29%, v/v, aqueous solution), benzaldehydedimethylacetal (Acros, 99%), cobalt (II) chloride (Alfa Aesar, anhydrous, 99.5%), chloroform (Sigma-Aldrich, anhydrous, 99%), dichloromethane (DCM) (Sigma-Aldrich, 99.8%), diethylamine (Acros, 99%), dimethylsulfoxide (DMSO) (Alfa Aesar, anhydrous, 99.8%), dodecane (Acros, 99%), ethanol (J.T. Baker, anhydrous, 94.7%), hydrochloric acid (J.T. Baker, 37%), hydrogen peroxide (EMD, 30%, v/v, aqueous solution), iron (II) chloride (Alfa Aesar, anhydrous, 99.5%), methylamine (Alfa Aesar, 40%, w/w, aqueous solution), nitric acid (Sigma-Aldrich, 70%), Pluronic 123 (Aldrich),

sodium dodecylsulfate (SDS) (Acros, 85%), sulfuric acid (J.T. Baker, 96.4%), tetraethylorthosilicate (TEOS) (Acros, 98%), tetrahydrofuran (THF) (Sigma-Aldrich, 99%), *p*-toluenesulfonic acid monohydrate (Aldrich, 98.5%) and triethylamine (Alfa Aesar, 99%) were used as received. Toluene (J.T. Baker, anhydrous, 99.5%) was dried and deoxygenated with a solvent purification system [34] and stored in a nitrogen glove box. Silanes 3-mercaptopropyltrimethoxysilane (MPTMS) (Alfa Aesar, 97%) and chlorosulfonylphenyltrimethoxysilane (CSPTMS) (Gelest, 50% in dichloromethane) were stored in a nitrogen glove box. Hexafluoro(3-methyl-1,2-oxathietane)-2,2-dioxide (FSAS) (Synquest Labs, 95%) was stored at -35°C under dry nitrogen. Triethoxysilylperfluorosulfonyl fluoride $(EtO)_3Si(CH_2)_3(CF_2)_2O(CF_2)_2SO_2F$ (FSFTES) was obtained as a gift from DuPont and stored at 0°C.

3.2.2 Instrumentation

Standard schlenk techniques and an MBraun UniLab 2000 drybox were used as noted. A Sonics VCX 750 ultrasonic processor was used for sonication during the silica coating process. A Fischer Scientific FS60H sonication bath was used for all other sonication purposes. X-ray diffraction (XRD) spectra were obtained using a Scintag X1 powder diffractometer equipped with a Cu Kα source. Nitrogen physisorption experiements were conducted using a Micromeritics ASAP 2010 system. Samples were dried under vacuum at 150°C overnight prior to testing. Surface areas were calculated using the BET method. Microscopy studies were performed using a Hitachi HD-2000 field emission gun transmission electron microscope (TEM). Fourier transform infrared (FT-IR) experiments were conducted on a Bruker IFS 66v/s spectrometer. Samples were dispersed in potassium bromide pellets for analysis. Reaction conversions were

monitored based on gas chromatographic (GC) analyses in reference to a dodecane internal standard by a Shimadzu GC-2010 instrument furnished with a flame ionization detector (FID) and SHRX5 column (15 m length, 0.25 mm inner diameter, 0.25 μm film thickness). The oven profile heated from 50 - 140°C at 30°C/min, 140 - 300°C at 40°C/min, and held at 300°C for an additional two minutes.

3.2.3 Preparation of silica-coated magnetic nanoparticles

Cobalt spinel ferrite ($CoFe_2O_4$) magnetic nanoparticles (MNP) were synthesized according to literature methods [35]. The obtained MNP were washed three times with 100 mL ethanol. The MNP (about 1.7g) were recovered magnetically and finally dispersed in 100 mL ethanol. The MNP were then silica-coated using a slightly modified procedure [15]. A solution of 11.76 mL of the ethanol-MNP dispersion (200 mg MNP) in 522 mL isopropanol (IPA) and 40 mL water was sonicated with mechanical stirring for 30 min. To this solution was added 46.6 mL concentrated ammonium hydroxide followed by the dropwise addition of a solution of 1 mL tetraethylorthosilicate (TEOS) in 40 mL IPA. The solution was mechanically stirred and sonicated for an additional one hour. The silica-coated magnetic nanoparticles (SiMNP) were recovered by centrifugation and washed three times with water. The SiMNP were dried under vacuum at room temperature overnight.

3.2.4 Synthesis of SBA-15

SBA-15 [36] was synthesized following literature methods [37]. To a 1L Erlenmeyer flask was added EO-PO-EO triblock copolymer (18.0 g), DI water (561 g), and concentrated HCl (99.5 g). This mixture was stirred overnight at room temperature to dissolve the polymer template. TEOS (39.8 g) was added to the solution and stirred for 5

min followed by stirring at 35°C for 20 hours. A static treatment for 24 hours at 80°C was utilized to swell the pores. The mixture was decanted to remove the majority of the solution, and the white solid was filtered with 3L DI water, recovered, and dried at 60°C for 24 hours. The white powder was calcined to remove the polymer template using the following temperature profile: (1) heating to 200°C at 1.2°C/min, (2) holding at 200°C for one hour, (3) heating to 550°C at 1.2°C/min, (4) holding at 550°C for six hours, and (5) cooling to 200°C at 1.2°C/min.

3.2.5 Preparation of supported alkyl-sulfonic acid 1

Supported sulfonic acid **1** was prepared (Scheme 3.1) via the oxidation of surface thiol functionalities [28]. To a solution of 1 g MPTMS in 10 mL ethanol and 10 mL water was added 250 mg SiMNP. The mixture was sonicated for 15 minutes and refluxed overnight. The SiMNP supported thiols (SiMNP-SH) were recovered magnetically and washed three times with 20 mL water. The recovered SiMNP-SH was oxidized by reaction with 10 mL 30% hydrogen peroxide in 10 mL water and 10 mL methanol overnight at room temperature. The product was recovered magnetically, washed three times with 20 mL water, and reacidified with 10 mL of 1 M H_2SO_4. The obtained sulfonic acid modified SiMNP (SiMNP-SO_3H) were washed three times with water and dried under vacuum at room temperature overnight.

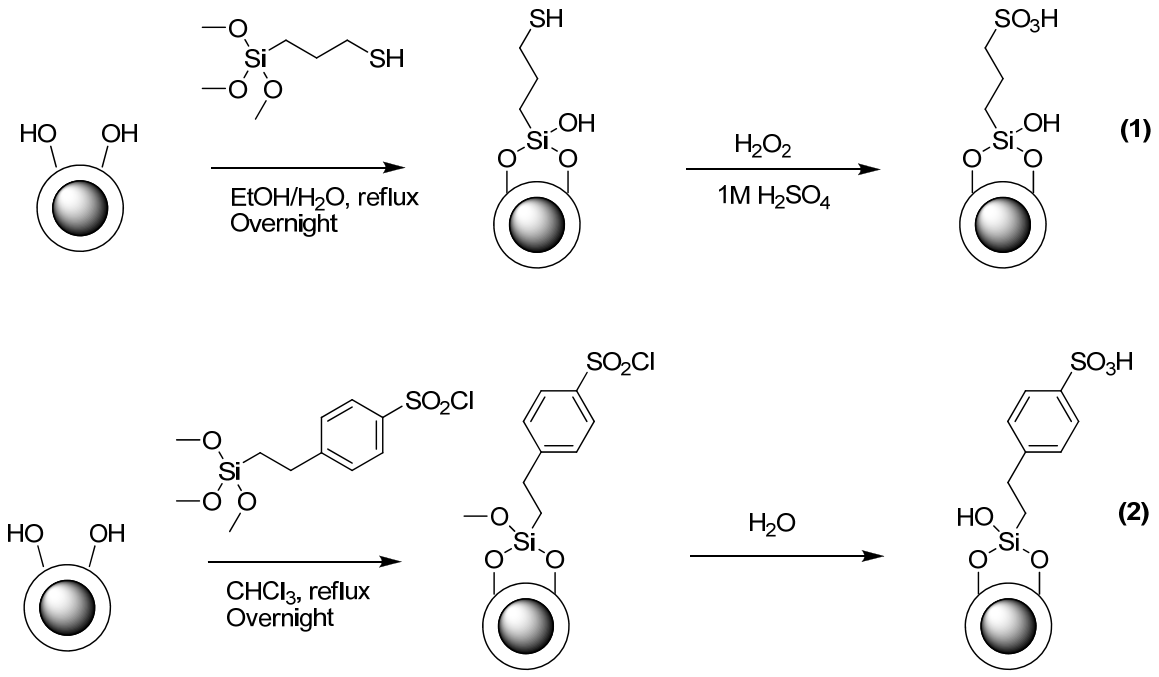

Scheme 3.1 – Synthesis of SiMNP supported alkyl (**1**) and phenyl (**2**) sulfonic acids.

3.2.6 Preparation of supported phenyl-sulfonic acid 2

Supported phenyl sulfonic acid **2** was prepared (Scheme 3.1) via the hydrolysis of supported phenyl-sulfonic acid chlorides [29]. Using schlenk techniques, 250 mg of SiMNP were dried under vacuum at 150°C overnight. In a nitrogen glove box, 1 g of CSPTMS 50% in DCM was diluted into 20 mL chloroform. This solution was added to the SiMNP and removed from the glove box. The mixture was sonicated for 15 minutes prior to refluxing overnight under an argon atmosphere. The phenyl-sulfonic acid chloride product (SiMNP-$PhSO_2Cl$) was exposed to the air, recovered magnetically, washed three times with 20 mL DCM, and dried under vacuum at room temperature overnight. The SiMNP-$PhSO_2Cl$ was hydrolyzed to the phenyl-sulfonic acid product (SiMNP-$PhSO_3H$) by stirring in water overnight. The SiMNP-$PhSO_3H$ was washed three times with water and dried overnight under vacuum at room temperature.

3.2.7 Preparation of supported perfluoroalkylsulfonic acid 3

Supported perfluoroalkylsulfonic acid **3** was prepared (Scheme 3.2) in a one-step reaction with 1,2,2-trifluoro-2-hydroxy-1-trifluoromethyl-ethane sulfonic acid beta-sultone (FSAS) [32]. Using schlenk techniques, 250 mg of SiMNP were dried under vacuum at 150°C overnight. In a nitrogen glove box, 1 g of FSAS was diluted into 20 mL anhydrous toluene. This solution was added to the SiMNP in a 125 mL screw-cap pressure reactor and removed from the glove box. The mixture was sonicated for 15 minutes prior to stirring at 100°C for four hours. The fluoro-sulfonic acid product (SiMNP-FSO_3H) was washed three times with 20 mL anhydrous toluene and dried under vacuum at room temperature overnight.

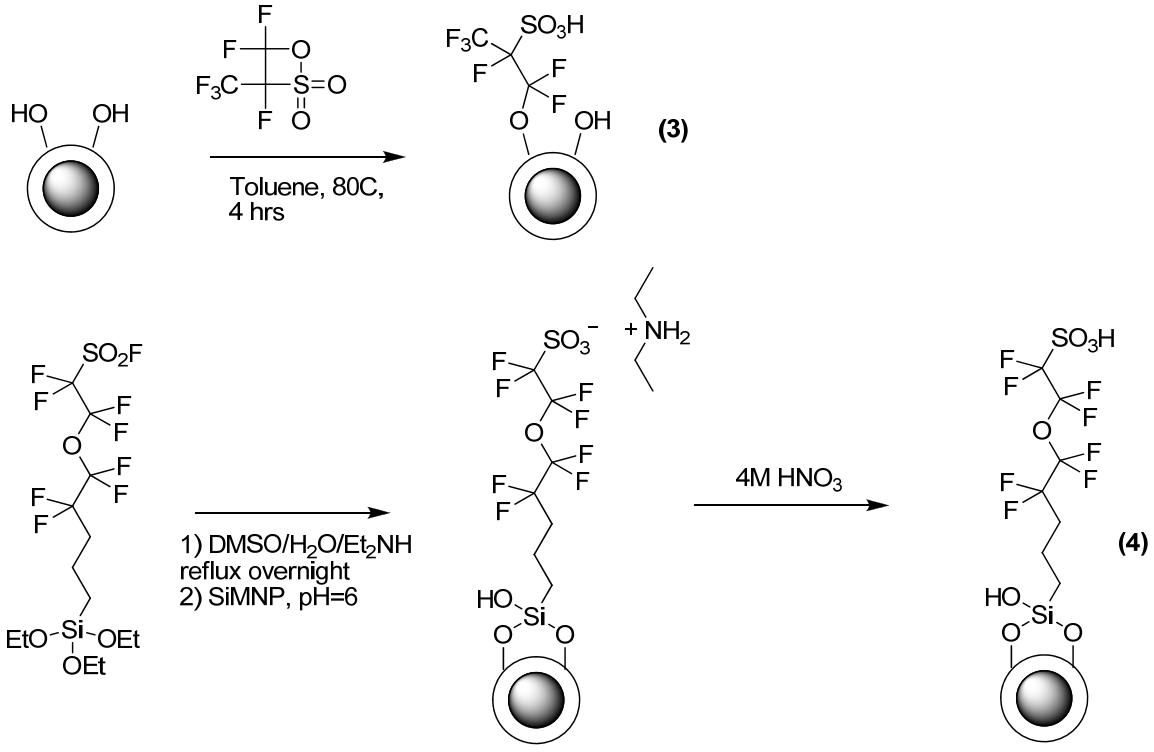

Scheme 3.2 - Synthesis of SiMNP supported perfluorinated sulfonic acids (**3**) and (**4**).

3.2.8 Preparation of supported perfluorosulfonic acid 4

Supported perfluorosulfonic acid **4** was prepared (Scheme 3.2) according to slightly modified procedures [33]. A mixture of 2.32 mL water, 1.2 mL DMSO, 0.48 mL diethylamine, and 250 mg triethoxysilylperfluorosulfonyl fluoride (FSFTES) was refluxed overnight. SiMNP (300 mg) were added to this solution and sonicated for 30 minutes. The solution was neutralized with the dropwise addition of 1M HCl until pH = 6. The dispersion was refluxed overnight. The recovered nanoparticles were washed three times with 20 mL water and acidified by stirring in 20 mL 4 M nitric acid overnight. The perfluorosulfonic acid functionalized SiMNP (SiMNP-$SiFSO_3H$) were washed three times with 20 mL water and dried overnight under vacuum at 80°C.

3.2.9 Solid acid titrations

Titrations were utilized to determine the acid loading of the catalysts. The surface bound acidic protons were ion exchanged with a brine solution by sonicating SiMNP catalyst (50 mg) in saturated aqueous NaCl solution (10 mL). The SiMNP catalyst was recovered magnetically and the brine solution was decanted and saved. This process was repeated two more times yielding 30 mL of proton exchanged brine solution. Two drops of phenol red indicator solution (2 mg in 10 ml water) were added to the brine solution. The solution was titrated to neutrality using 0.1 M NaOH solution to determine the loading of acid sites on the SiMNP catalysts.

3.2.10 Acid catalyzed reactions

The four solid acid catalysts were evaluated in the deprotection reaction of benzaldehyde dimethylacetal (Scheme 3). Into a 10 mL reactor was added 1 mol percent SiMNP catalyst (0.004 mmol H^+) and 2 mL tetrahydrofuran (THF). This mixture was

sonicated for 10 minutes to disperse the catalyst. The reaction was initiated by the addition of a solution of benzaldehyde dimethylacetal (BADMA) (60 μL, 0.4 mmol), THF (2 mL), dodecane (45.5 μL, 0.2 mmol), and water (7.2 μL, 0.4 mmol). Reaction conversion was monitored by GC in reference to the dodecane internal standard.[1] Catalysts **1 - 4** were compared against several homogeneous and heterogeneous sulfonic acid catalysts including methanesulfonic acid, *p*-toluenesulfonic acid, triflic acid, Amberlyst A-15 resin, and Nafion powder.[2] Catalysts **1** and **4** were also prepared on mesoporous SBA-15 (denoted **SBA1** and **SBA4**) to investigate the influence of the support on catalyst activity.[3]

Control reactions were performed to confirm sulfonic acid sites were the catalytically active species. Controls were performed on the bare supports: MNP, SiMNP, and SBA-15. Additional controls were performed on intermediates in the syntheses of the catalysts **SBA1** and **SBA4** (Schemes 1 and 2). A final control was carried out on SiMNP treated with 4M HNO_3 to determine if the washing steps in the synthesis of **4** were sufficient to remove all homogeneous acid from the support.

Recycle reactions were performed using the four SiMNP catalysts. Upon completion of the initial reaction, the catalyst was recovered magnetically, and the reaction solution was decanted. The catalyst was redispersed in THF (5 mL) by sonication for 10 minutes and recovered magnetically. This process was repeated two

---

[1] In cases requiring less than 5 mg SiMNP catalyst, a tenfold mass of catalyst was thoroughly dispersed into a THF solution and fractionated to yield the correct mass of catalyst. The volume of THF solvent added to the reaction was adjusted accordingly to total 4 mL.
[2] Loadings for Amberlyst A-15 and Nafion were obtained from manufacturers' literature.
[3] In cases requiring less than 5 mg of SBA catalyst, the reaction was scaled up to utilize >10 mg to minimize error when measuring catalyst masses.

additional times. After the third wash, the catalyst was dried under vacuum at room temperature. Recycle reactions were performed as described above.

Recovery tests were performed on the catalysts to evaluate if the catalysis was occurring via surface bound sulfonic acids. These reactions were prepared as specified above. However, the SiMNP were recovered magnetically after a given time period (either 10 or 20 minutes), and the solution was decanted into a clean 10 mL reactor. The reaction solution was stirred and sampled until 60 minutes to elucidate if conversion resulted from surface bound acid sites or homogeneous acid leached from the support.

3.3 Results

3.3.1 Catalyst synthesis and characterization

Cobalt spinel ferrite magnetic nanoparticles (MNP) were chosen as a catalyst support for their high magnetic susceptibility [38] and ability for surface functionalizations. These MNP were silica-coated to provide an inert barrier between the reaction solution and the metal oxide core while maintaining the capacity for surface modifications and thermal stability. The silica coating was found to be necessary after failed attempts of immobilizing sulfonic acids via the oxidation of surface thiol groups [28]. The bare MNP were found to be excellent catalysts for the rapid decomposition of hydrogen peroxide, preventing the thiols from being oxidized to the desired sulfonic acid. The incorporation of a silica shell was found to prevent peroxide decomposition and maintain the ability for surface functionalizations. The four immobilized sulfonic acids were chosen to illustrate a range in acidity from the less acidic alkyl-sulfonic acid to the perfluorinated superacids. The deprotection of benzaldehyde dimethylacetal was chosen as a simple benchmark reaction to evaluate the activity of the catalysts.

The solid acid catalysts were characterized using a variety of methods. X-ray diffraction (XRD) of the bare MNP displayed patterns consistent with the literature patterns of spinel ferrites (Figure 3.2) [35]. The same peaks were observed in the both the bare and silica-coated nanoparticle XRD patterns, indicating retention of the crystalline spinel ferrite core structure during the silica coating process. The broad peak from 2θ = 20° to 30° was consistent with an amorphous silica phase in the shell of the SiMNP [39].

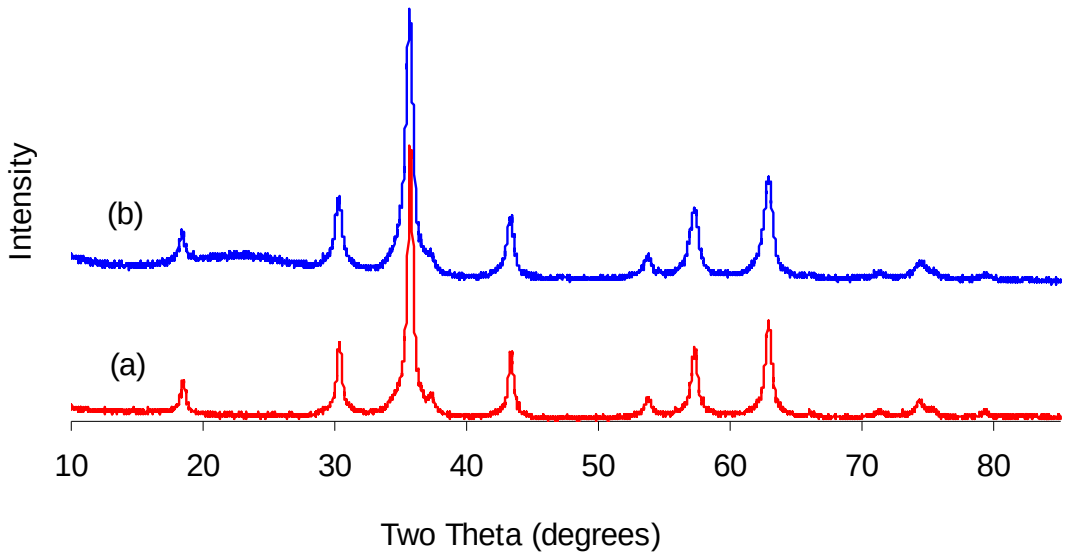

Figure 3.2 - XRD pattern of (a) bare MNP and (b) silica-coated MNP.

TEM images of the bare MNP displayed aggregated nanoclusters, roughly 50 nm in diameter (Figure 3.3). A close inspection of the images reveals the clusters are formed of primary particles with diameters in the range of 6-8 nm. Images of the silica-coated magnetic nanoparticles displayed dark MNP cores surrounded by a lighter amorphous silica shell about 5-10 nm thick (Figure 3.4). Instead of the desired core-shell architecture observed by others [15], the SiMNP appeared to have been aggregated prior to silica

coating.[4] Hence, they were coated as aggregates, leading to irregular shaped particles ranging in size from 50 nm up to 1 μm.

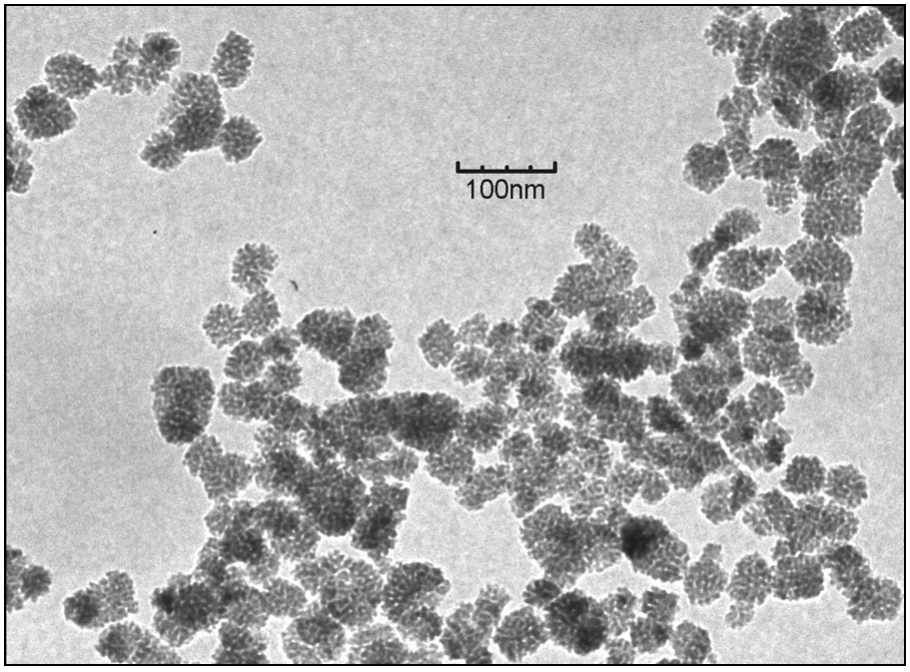

Figure 3.3 - TEM image of $CoFe_2O_4$ magnetic nanoparticles.

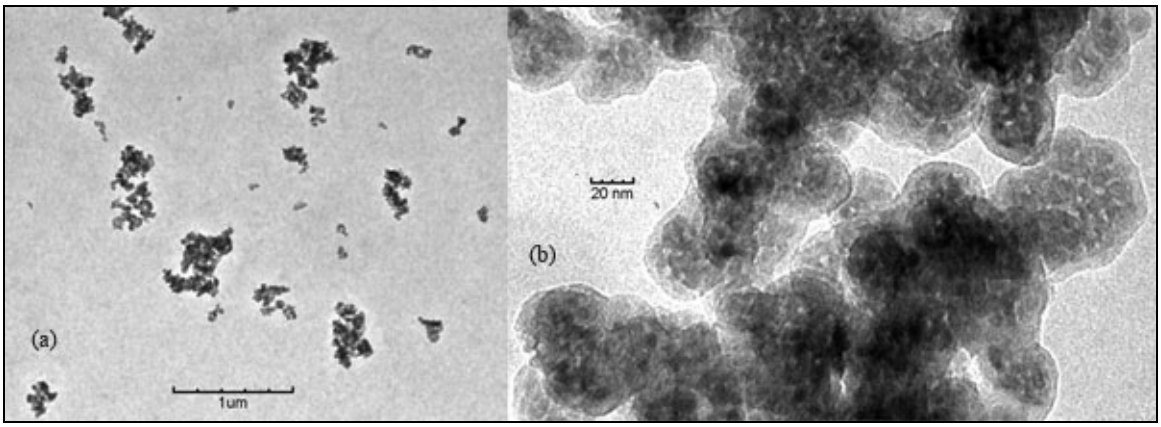

Figure 3.4 - TEM image of silica coated $CoFe_2O_4$ magnetic nanoparticle supports at (a) 10,000 and (b) 200,000 magnification.

[4] The desired core-shell architecture was observed on smaller scale experiments. However, these results were difficult to replicate on the larger scale required for the chemical syntheses in this paper.

Nitrogen physisorption experiments displayed a decrease in surface area upon silica coating the MNP. The bare MNP and SiMNP yielded BET surface areas of 126 m^2/g and 48 m^2/g, respectively. The decrease in surface area resulted from aggregation of the particles prior to silica coating. Despite the non-uniform particle size and lessened surface area, the SiMNP were suitable for surface funtionalization and use as catalyst supports. Nitrogen physisorption experiments revealed a BET surface area of 837 m^2/g and an average pore diameter of 64 angstroms for the synthesized SBA-15 mesoporous silica.

Due to the paramagnetic nature of the nanoparticle core, nuclear magnetic resonance (NMR) techniques could not be utilized to confirm surface modifications on the SiMNP. Instead titrations and FT-IR were utilized to characterize organic functionalities. Sulfonic acid loadings were calculated based on titrations of the proton exchanged brine solutions. These data are summarized in Table 3.1. FT-IR analysis of the SiMNP showed similar spectra as seen in literature [40]. The O-H stretch and vibration of surface hydroxyl groups or physisorbed water were present as broad peaks from 3000 – 3700 cm^{-1} and a sharper peak at 1640 cm^{-1}, respectively. An intense peak from 1000 – 1250 cm^{-1} corresponded to the Si-O stretch in the amorphous silica shell. Evidence of the surface functionalizations were difficult to observe due to the low loadings of catalysts **1 - 4**. The C-H stretch and C-H bend are visible in the spectra for catalysts **1, 2,** and **4** at 2800 – 3000 cm^{-1} and 1400 cm^{-1}, respectively (Figure 3.5). These peaks are absent from catalyst **3**, because no C-H bonds are present.

Table 3.1 - Sulfonic acid loadings of catalysts.

Catalyst	Titration Loading (mmol/g)
(**1**) SiMNP-SO_3H	0.47
(**2**) SiMNP-$PhSO_3H$	0.12
(**3**) SiMNP-FSO_3H	0.78[a]
(**4**) SiMNP-$SiFSO_3H$	0.055
(**SBA1**) SBA-SO_3H	0.32
(**SBA4**) SBA-$SiFSO_3H$	0.42

[a] Sulfonic acid loading for catalyst **3** calculated via thermogravimetric analysis due to leaching of the active acid.

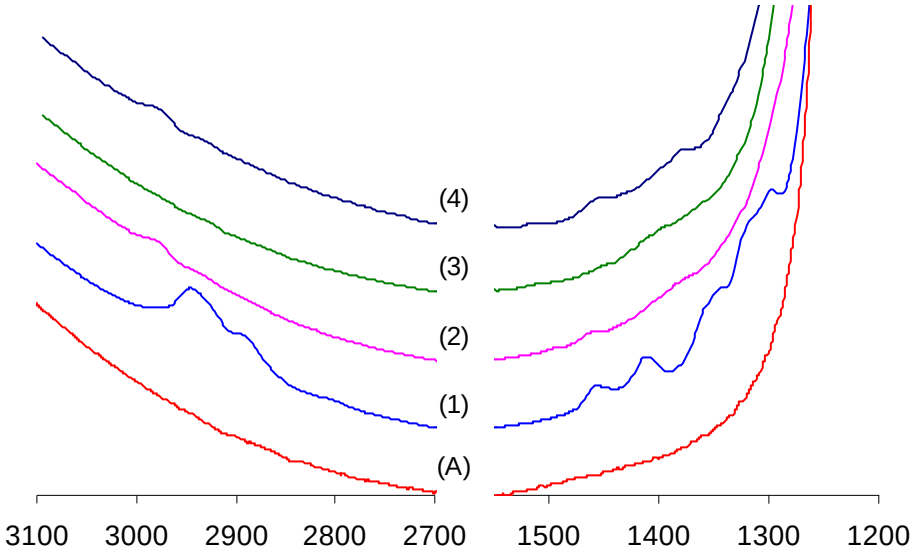

Figure 3.5 - FT-IR spectra of non-functionalized SiMNP (A), SiMNP-SO_3H (**1**), SiMNP-$PhSO_3H$ (**2**), SiMNP-FSO_3H (**3**), and SiMNP-$SiFSO_3H$ (**4**).

3.3.2 Catalytic studies

Kinetic profiles for the initial and recycle reactions of catalyst **1** closely overlapped each other within experimental error, reaching conversions of >75% in 60 minutes (Figure 3.6). The close overlap indicated the catalyst was recyclable. The initial kinetic profile for catalyst **2** (Figure 3.7) closely resembled that of catalyst **1**. However,

the recycle reaction displayed a notable decrease in activity. A third recycle of this catalyst displayed no activity at all. In recovery tests, catalysts **1** and **2** were recovered after 20 minutes, as indicated by the vertical line at 20 minutes in Figures 3.6 and 3.7. The cessation of conversion after this time indicated catalysis was occurring from surface bound sulfonic acid sites. Control reactions on bare MNP and bare SiMNP displayed no activity after 60 minutes, indicating neither the MNP core or silica-coated surface were responsible for the observed catalytic activity of catalysts **1 – 4**.

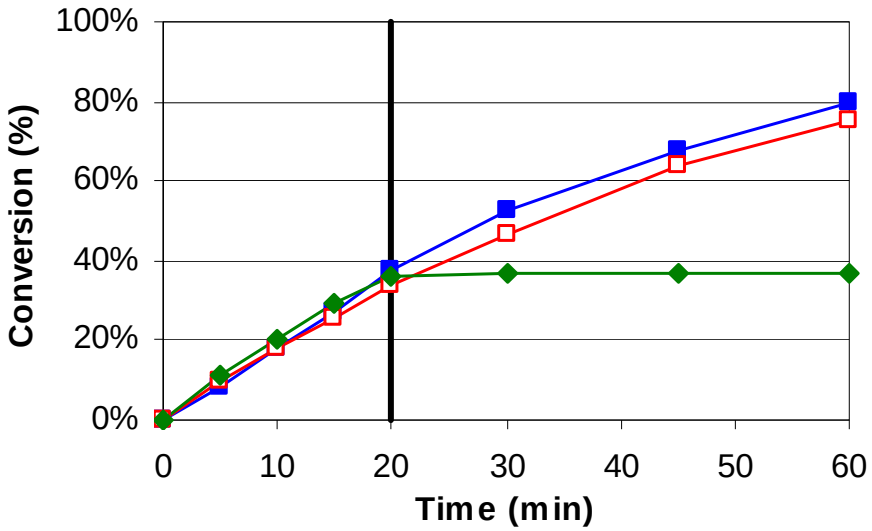

Figure 3.6 – Reaction conversion data for (**1**) SiMNP-SO_3H catalyst at 1 mol%: initial (■), recycle (□), and recovery test (◆).

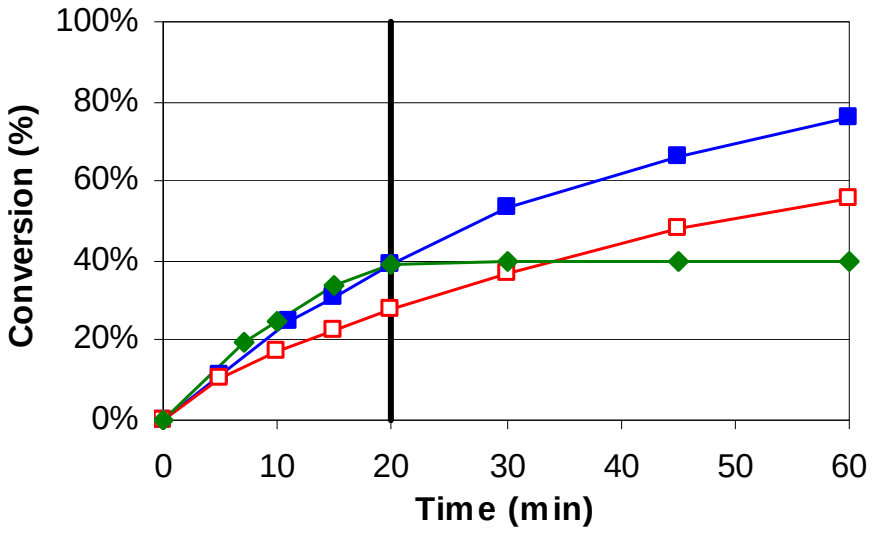

Figure 3.7 - Reaction conversion data for (**2**) SiMNP-$PhSO_3H$ catalyst at 1 mol%: initial (■), recycle (□), and recovery test (◆).

Initial kinetic profiles of catalysts **3** and **4** were markedly faster than **1** and **2** due to the strongly electronegative perfluoroalkyl linker adjacent to the sulfonic acid. Catalyst **3** reached 91% conversion in 20 minutes at 0.12 mol% catalyst (Figure 3.8). However, a recycle reaction displayed no activity at all, suggesting all active sulfonic acid species had been removed prior to running the recycle reaction. A recovery test for catalyst **3** at 0.12 mol% displayed no cessation of conversion upon removal of the SiMNP support after ten minutes. Additionally, the kinetic profiles for the initial test and leaching test closely overlapped one another, indicating catalyst **3** was not a heterogeneous catalyst but simply a source of leached catalytically active acid. The acid loss was presumed to occur via the reaction of water with the Si-O-C bond formed during the ring-opening reaction of the perfluorosulfonic acid sultone with surface silanol groups. The reaction was thought to hydrolize the Si-O-C bond, reforming surface silanol groups and a leached perfluorosulfonic acid species in accordance with literature reports [25]. Hence, when the

SiMNP support was removed after ten minutes, the leached active species continued catalyzing the reaction, leading to similar kinetics as observed in the initial reaction.

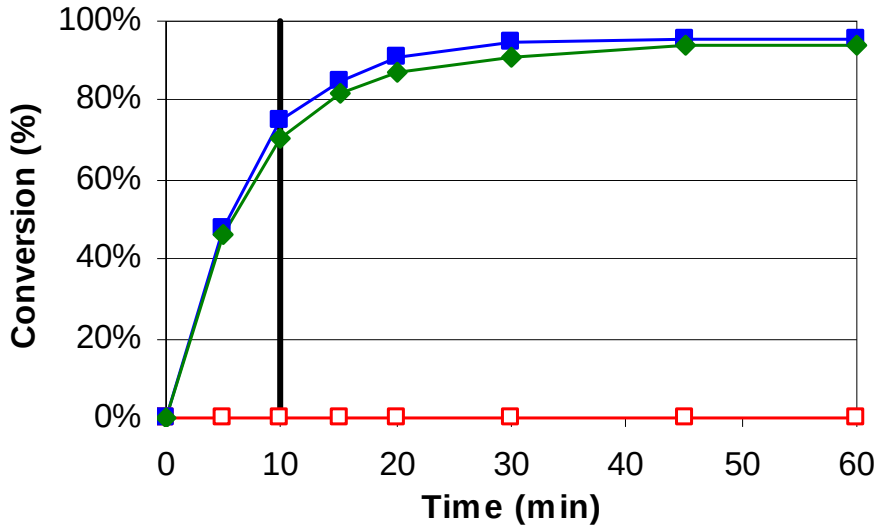

Figure 3.8 - Reaction conversion data for (**3**) SiMNP-FSO_3H catalyst: initial at 0.12 mol% (■), recycle (□), and recovery test (◆).

Conversion for **4** reached 96% in five minutes at 1 mol% and 72% in 20 minutes at 0.1 mol% catalyst. In contrast to **3**, the recovery test for catalyst **4**, showed a cessation of activity after 20 minutes, indicating a surface bound active catalyst (Figure 3.9). A recycle reaction of catalyst **4** showed similar activity as the initial reaction at 1 mol%, indicating the catalyst was recyclable. A control reaction was performed to determine if any physisorbed acid was responsible for the observed catalysis. Non-functionalized SiMNP were treated with nitric acid, washed, and dried according to the synthetic procedure for catalyst **4**. This control reaction showed zero conversion after 60 minutes. These controls and kinetic data indicate the catalytic activity resulted from surface bound acid sites.

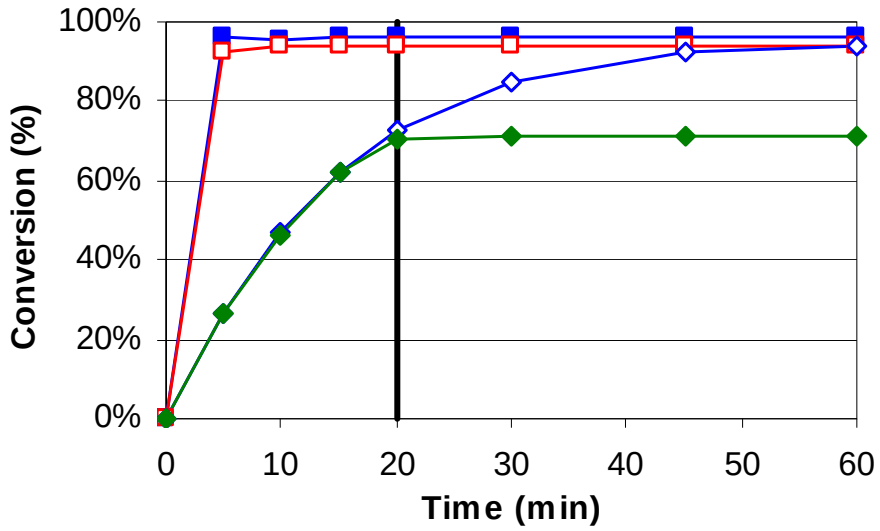

Figure 3.9 - Reaction conversion data for (4) SiMNP-$SiFSO_3H$ catalyst: initial at 1 mol% (■), recycle at 1 mol% (□), initial at 0.1 mol% (◇), and recovery test at 0.1 mol% (◆).

The alkylsulfonic acid and perfluoroalkylsulfonic acid catalysts **1** and **4** were prepared on mesoporous SBA-15 (**SBA1** and **SBA4**) to investigate any potential differences in catalytic activity arising from the different supports. Kinetics were compared for the two catalysts at 1 mol% for **1** and **SBA1** and at 0.1 mol% for **4** and **SBA4** (Figure 3.10). The concentration of perfluoroalkylsulfonic acid catalysts **4** and **SBA4** had to be compared at 0.1 mol%, since these catalysts reached 96% and 99% conversions in five minutes at 1 mol%, respectively. Conversions reached 96% for **SBA4** and 72% for **4** after 20 minutes at 0.1 mol%. A larger disparity in rates was observed for the alkylsulfonic acids **1** and **SBA1**. After 20 minutes, conversions reached 95% for **SBA1** but only 38% for **1** at 1 mol%. In both comparisons, the SBA grafted catalysts exhibited faster rates than the SiMNP catalysts. A possible explanation may result from enhanced physisorption of water in the SBA mesopores, resulting in higher local concentrations of water near the active sites. Diffusion limitations may slow kinetics for

mesoporous silicas of smaller pore diameters [24], however, the 65 anstrom SBA-15 pores appeared sufficiently large to mitigate any diffusion effects in this case, since the SBA catalysts displayed faster kinetics than the non-porous SiMNP catalysts. Control reactions were performed on the intermediates in the syntheses of **SBA1** and **SBA4** to determine if any unconverted, intermediary species were responsible for the activity in Figure 9. SBA-SH and SBA-$SiFSO_3^-NH_2Et_2^+$ (intermediates of **SBA1** and **SBA4**) and non-functionalized SBA all displayed negligible conversion after 60 minutes, indicating the sulfonic acid sites were responsible for the kinetic activity and not an intermediary species.

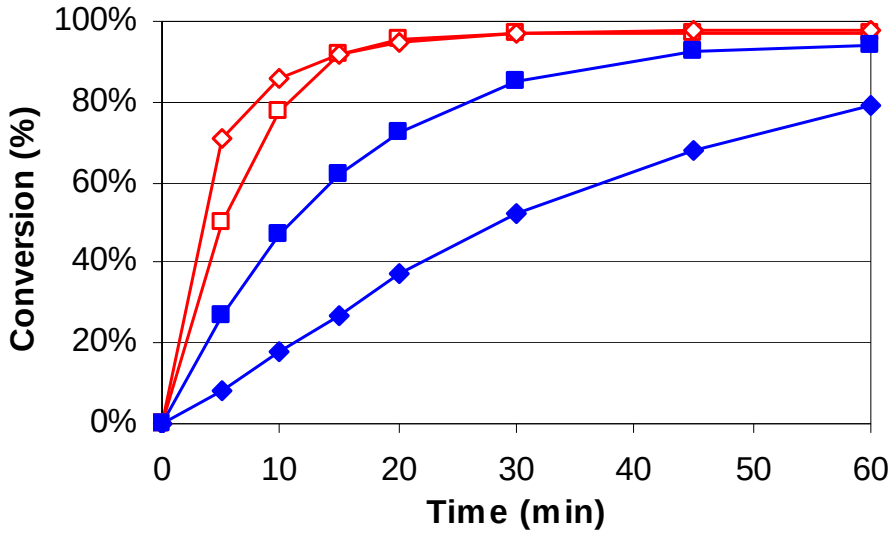

Figure 3.10 - Reaction conversion data for (**SBA4**) SBA-$SiFSO_3H$ at 0.1 mol% (□), (**SBA1**) SBA-SO_3H at 1 mol% (◇), (**4**) SiMNP-$SiFSO_3H$ at 0.1 mol% (■), and (**1**) SiMNP-SO_3H at 1 mol% (◆).

Several commercially available sulfonic acids of varying strengths were tested at 1 mol% to compare to the synthesized catalysts (Figure 3.11). The activity of the catalysts followed the order: methanesulfonic acid < *p*-toluenesulfonic acid (*p*-TSA) < Amberlyst A-15 < Nafion powder < triflic acid at 0.1 mol%. The trend followed the order

of increasing electron withdrawing capability of the functional groups adjacent to the sulfonic acid: alkylsulfonic acid < phenylsulfonic acid < perfluorosulfonic acid. The *p*-TSA and Amberlyst A-15 exhibited comparable kinetics for the first 15 minutes. After this time, the Amberlyst kinetics appeared marginally faster than for *p*-TSA. This was presumed to occur due to reactant absorption into the polystyrene beads of the Amberlyst, resulting in slightly faster kinetics. The macroreticular polymer resin appeared to swell sufficiently in the THF solvent to mitigate any diffusion limitations resulting in slowed kinetics. In contrast, the activity of Nafion powder was much lower than for its homogeneous comparison, triflic acid. This discrepancy in rates was attributed to diffusion limitations of reactant into the polytetrafluoroethylene (PTFE) support due to poor polymer swelling and inaccessibility of reactant to some internal, catalytically active sites [41]. Differences in polymer swelling properties may explain the similar activities observed for *p*-TSA and Amberlyst but distinctly different rates seen for triflic acid and Nafion.

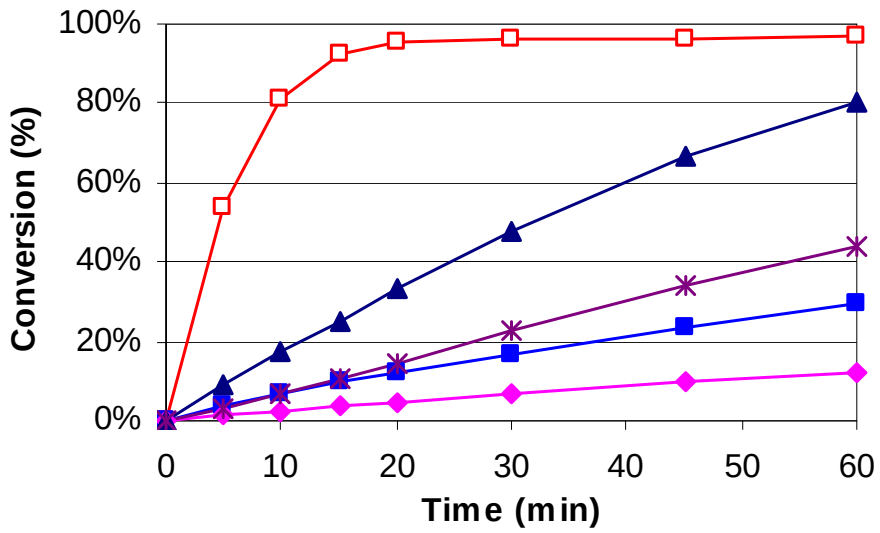

Figure 3.11 - Reaction conversion data for sulfonic acid catalysts at 1 mol%: methanesulfonic acid (◆), *p*-toluenesulfonic acid (■), Amberlyst A-15 (✳), Nafion powder (▲), and triflic acid at 0.1 mol% (□).

The maximum initial turn over frequencies (TOF) for all catalysts in this study were summarized in Table 3.2. Curiously, the TOFs for catalysts **1** and **2** were higher than for their homogeneous comparisons: methanesulfonic acid and *p*-toluenesulfonic acid, respectively. Surface adsorption of reactants giving high local concentrations of reactant near the active sites could explain these enhanced rates. The opposite case was observed for the TOFs of catalyst **4**, which was roughly half that of triflic acid. Catalyst **3** showed deceivingly high rates, although it must be regarded as a solid source of homogeneous catalyst, rather than a heterogeneous catalyst under the conditions investigated.

Table 3.2 - Sulfonic acid catalyst inititial turn over frequencies (TOF).

Catalyst	Homogeneous (min^{-1})	Heterogeneous (min^{-1})
Methanesulfonic acid	0.3	
Amberlyst A-15		0.8[a]
p-toluenesulfonic acid	0.8	
(**1**) SiMNP-SO_3H		1.9
Nafion		1.9[a]
(**2**) SiMNP-$PhSO_3H$		2.2
(**SBA1**) SBA-SO_3H		14
(**3**) SiMNP-FSO_3H		52[b]
(**4**) SiMNP-$SiFSO_3H$		54
(**SBA4**) SBA-$SiFSO_3H$		101
Triflic acid	108	

[a] TOFs for Amberlyst A-15 and Nafion were artificially low due to poor polymer swelling and inaccessibility of reactant to internal active sites.

[b] Catalyst **3** acted as a solid source of leached homogeneous acid.

3.4. Conclusions

Hybrid organic/inorganic sulfonic acid/magnetic nanoparticle catalysts offer an alternative support to silica based materials. Supporting these acid catalysts on silica-coated magnetic nanoparticles offers a simple and non-energy intensive method for recovery and reuse of these catalysts. The silica coating provides an inert barrier to adverse interactions between surface functionalizations and the metal oxide core. The magnetic, solid acid catalysts exhibited comparable or better activities to other commercially available sulfonic acid catalysts: Amberlyst A-15 and Nafion. SiMNP catalysts **1**, **2**, and **4** were found to be easily recoverable, recyclable, and surface bound, solid acid catalysts. Catalyst **3** was observed to act as a source of homogeneous acid under these conditions, and may only act as a recyclable, heterogeneous catalyst under specific, anhydrous conditions. Catalyst **4** generated the highest TOFs of the magnetic, solid acid catalysts, with an activity one half that of triflic acid. Catalysts **SBA1** and **SBA4** displayed enhanced activities when immobilized on 65 angstrom, mesoporous SBA-15 versus the nonporous SiMNP. Further experimentation is necessary for optimization of the silica coating procedure on large scales to maximize surface area available for surface chemistry.

3.5 Acknowledgements

The authors acknowledge financial support for this research from the US Department of Energy, and Air Products for undergraduate research funding. The authors additionally thank Mark Harmer and DuPont for the gift of the perfluorinated silane. CWJ thanks the School of Chemical & Biomolecular Engineering at Georgia Tech for the J. Carl and Sheila Pirkle faculty fellowship.

3.6 References

1. Gladysz, J.A., *Chem. Rev.* **2002**, 102, 3215.
2. De Vos, D.E., Dams, M., Sels, B.F., and Jacobs, P.A., *Chem. Rev.* **2002**, 102, 3615.
3. Wight, A.P. and Davis, M.E., *Chem. Rev.* **2002**, 102, 3589.
4. Anwander, R., *Chem. Mater.* **2001**, 13, 4419.
5. Jones, C.W., Tsuji, K., and Davis, M.E., *Nature* **1998**, 393, 52.
6. Leadbeater, N.E. and Marco, M., *Chem. Rev.* **2002**, 102, 3217.
7. Dioos, B.M.L., Vankelecom, I.F.J., and Jacobs, P.A., *Adv. Synth. Catal.* **2006**, 348, 1413.
8. Cole-Hamilton, D.J., *Science* **2003**, 299, 1702.
9. Zheng, Y., Stevens, P.D., and Gao, Y., *J. Org. Chem.* **2006**, 71, 537.
10. Stevens, P.D., Li, G.F., Fan, J.D., Yen, M., and Gao, Y., *Chem. Commun.* **2005**, 4435.
11. Stevens, P.D., Fan, J.D., Gardimalla, H.M.R., Yen, M., and Gao, Y., *Org. Lett.* **2005**, 7, 2085.
12. Duanmu, C., Saha, I., Zheng, Y., Goodson, B.M., and Gao, Y., *Chem. Mater.* **2006**, 18, 5973.
13. Wang, Z.F., Xiao, P.F., Shen, B., and He, N.Y., *Colloids Surf., A* **2006**, 276, 116.
14. Wang, Z.F., Shen, B., Zou, A.H., and He, N.Y., *Chem. Eng. J.* **2005**, 113, 27.
15. Abu-Reziq, R., Alper, H., Wang, D.S., and Post, M.L., *J. Am. Chem. Soc.* **2006**, 128, 5279.
16. Yoon, T.J., Lee, W., Oh, Y.S., and Lee, J.K., *New J. Chem.* **2003**, 27, 227.
17. Hu, A.G., Yee, G.T., and Lin, W.B., *J. Am. Chem. Soc.* **2005**, 127, 12486.
18. Yi, D.K., Lee, S.S., and Ying, J.Y., *Chem. Mater.* **2006**, 18, 2459.
19. Guin, D., Baruwati, B., and Manorama, S.V., *Org. Lett.* **2007**,
20. Ding, S.J., Xing, Y.C., Radosz, M., and Shen, Y.Q., *Macromolecules* **2006**, 39, 6399.
21. Gardimalla, H.M.R., Mandal, D., Stevens, P.D., Yen, M., and Gao, Y., *Chem. Commun.* **2005**, 4432.
22. Zheng, Y., Duanmu, C., and Gao, Y., *Org. Lett.* **2006**, 8, 3215.
23. Phan, N.T.S., Gill, C.S., Nguyen, J.V., Zhang, Z.J., and Jones, C.W., *Angew. Chem., Int. Ed.* **2006**, 45, 2209.
24. Phan, N.T.S. and Jones, C.W., *J. Mol. Catal. A: Chem.* **2006**, 253, 123.
25. Corma, A. and Garcia, H., *Adv. Synth. Catal.* **2006**, 348, 1391.
26. Corma, A., *J. Catal.* **2003**, 216, 298.
27. Melero, J.A., van Grieken, R., and Morales, G., *Chem. Rev.* **2006**, 106, 3790.
28. Van Rhijn, W.M., De Vos, D.E., Sels, B.F., Bossaert, W.D., and Jacobs, P.A., *Chem. Commun.* **1998**, 317.
29. Melero, J.A., Stucky, G.D., van Grieken, R., and Morales, G., *J. Mater. Chem.* **2002**, 12, 1664.
30. Jones, C.W., Tsuji, K., and Davis, M.E., *Microporous Mesoporous Mater.* **1999**, 33, 223.
31. Alvaro, M., Corma, A., Das, D., Fornes, V., and Garcia, H., *Chem. Commun.* **2004**, 956.

32. Alvaro, M., Corma, A., Das, D., Fornes, V., and Garcia, H., *J. Catal.* **2005**, 231, 48.
33. Harmer, M.A., Sun, Q., Michalczyk, M.J., and Yang, Z.Y., *Chem. Commun.* **1997**, 1803.
34. Pangborn, A.B., Giardello, M.A., Grubbs, R.H., Rosen, R.K., and Timmers, F.J., *Organometallics* **1996**, 15, 1518.
35. Rondinone, A.J., Samia, A.C.S., and Zhang, Z.J., *J. Phys. Chem. B* **1999**, 103, 6876.
36. Zhao, D.Y., Huo, Q.S., Feng, J.L., Chmelka, B.F., and Stucky, G.D., *J. Am. Chem. Soc.* **1998**, 120, 6024.
37. Hicks, J.C. and Jones, C.W., *Langmuir* **2006**, 22, 2676.
38. Song, Q. and Zhang, Z.J., *J. Phys. Chem. B* **2006**, 110, 11205.
39. Haddad, P.S., Duarte, E.L., Baptista, M.S., Goya, G.F., Leite, C.A.P., and Itri, R., *Progress in Colloid and Polymer Science: Surface and Colloid Science* **2004**, 128, 232.
40. Du, G.H., Liu, Z.L., Xia, X., Chu, Q., and Zhang, S.M., *J. Sol-Gel Sci. Technol.* **2006**, 39, 285.
41. Harmer, M.A., Farneth, W.E., and Sun, Q., *J. Am. Chem. Soc.* **1996**, 118, 7708.

CHAPTER 4

ENHANCED COOPERATIVITY VIA DESIGN: PENDANT COBALT(III)-SALEN POLYMER BRUSH CATALYSTS FOR THE HYDROLYTIC KINETIC RESOLUTION OF EPICHLOROHYDRIN[†]

4.1 Introduction

While Chapters 2 and 3 discussed relative simple organic acid and base catalysts, this chapter presents more complicated supported Co-salen catalysts for the hydrolytic kinetic resolution of epoxides. The main focus of this chapter is designing a new type of supported catalyst, called polymer brushes, to promote site-site interactions as required in the bimetallic mechanism. Investigations into catalytic deactivation are also discussed.

The Co^{III}-salen catalyzed hydrolytic kinetic resolution (HKR) of racemic epoxides has emerged as a highly attractive and efficient method of synthesizing chiral C_3 building blocks for intermediates in larger, more complex molecules, especially useful in the pharmaceutical industry.[1, 2] The HKR reaction has been shown to involve a bimetallic mechanism as evident from a second order dependency of activity upon the concentration of Co^{III} sites (Figure 4.1). This second order dependency arose from a proposed dual activation pathway of the reaction.[3] The two cobalt centers are proposed to bind hydroxide and epoxide individually. The cobalt-activated hydroxide is suggested to perform a nucleophilic attack on the α-carbon of the epoxide. Hydrolysis of the intermediate species then purportedly regenerates the two active sites as the catalytic

---

[†] Previously published work: C.S. Gill, K. Venkatasubbaiah, N.T.S. Phan, C.W. Jones, *Chem. Eur. J.* **2008**, 14, 7306-7313.

cycle repeats. Accordingly, activities of the original homogeneous Co^{III}-salen catalyst suffered due to unfavorable statistical interactions between the catalytic active sites in solution, resulting in very slow rates at low catalyst concentrations. Researchers have noted significant increases in activity when utilizing multiple Co-salen oligomeric,[4-6] dendritic,[7] and polymeric catalysts.[8-14] These multi-sited, soluble catalysts gave significant increases in activity versus the homogeneous Co-salen but remained difficult to recycle via distillation, dialysis membranes, or polymer precipitation. To this end, many researchers studied heterogenization of the expensive Co^{III}-salen catalysts to aid in their recovery and reuse.[15-17] A variety of methods have been introduced including ship-in-a-bottle synthesis,[18, 19] grafting to silicas,[20, 21] membrane reactors,[22] ionic liquids,[23] and fluorous systems.[24, 25] Despite the ability to recover and recycle the catalysts, retention of the high activities remained difficult.

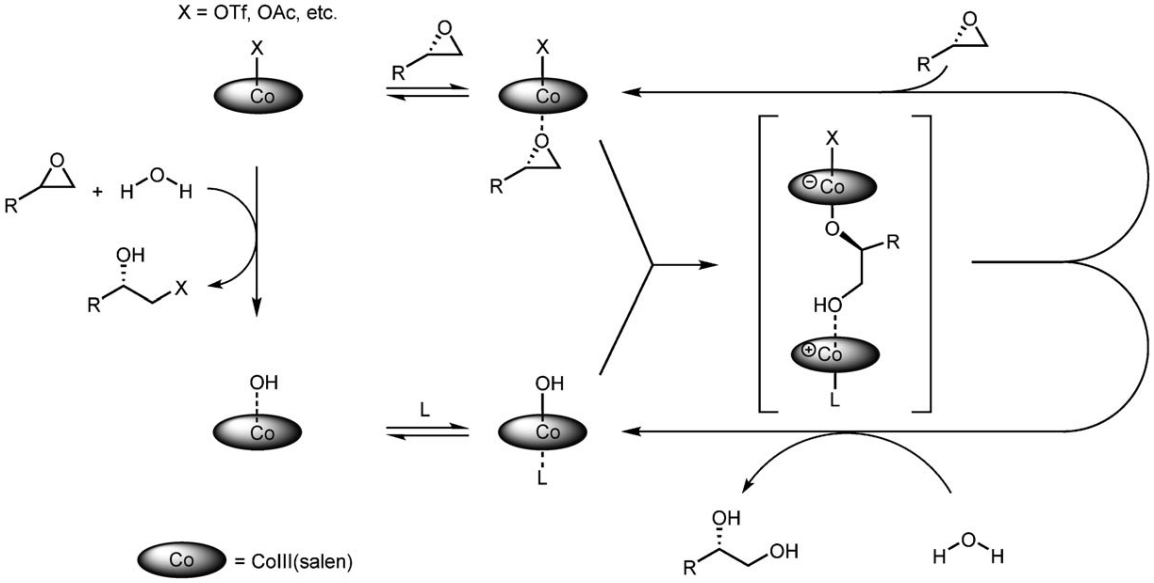

Figure 4.1 - Proposed mechanism for the Co-salen catalyzed HKR of epoxides. Image taken from published literature by Jacobsen.[26]

Grafting polymer brushes to solid surfaces has received increasing attention in recent years in several areas including microelectronics and biotechnology.[27] However, the use of grafted polymer brushes as heterogeneous catalyst supports has remained limited to isolated examples. These include palladium complexes for carbon-carbon coupling reactions [28, 29] and spherical polyelectrolyte brush supported nanoparticle catalysts, [30-35] where it appears that only site accessibility was the strategic aim.

Here, we demonstrate how high activities via site-site cooperativity can be achieved with a new catalyst design using an easily recoverable hybrid organic/inorganic catalyst.[36] The polymer brush architecture was employed to specifically promote the site-site interactions required by the increasing array of catalytic reactions with quasi-planar coordination complexes.[37-42] This site-site cooperativity is achieved via strategic design of the pendant Co^{III}-salen active sites supported on polymer brushes to promote the cooperative bimetallic interactions required for the HKR reaction (Scheme 4.1). Specifically, the polymer brush architecture addresses issues of increased mobility, enhanced proximity of the catalytic sites, and facile recovery. By grafting polymer chains with pendant Co-salen sites to silica supports, the flexibility and proximity of the catalyst centers can be enhanced leading to increased activities in the HKR of epichlorohydrin,[43] while allowing for simple recovery and reuse via the insoluble support. In addition to demonstration of the use of polymer brushes as catalyst supports, this work highlights catalyst recyclability and investigates causes of catalyst deactivation.

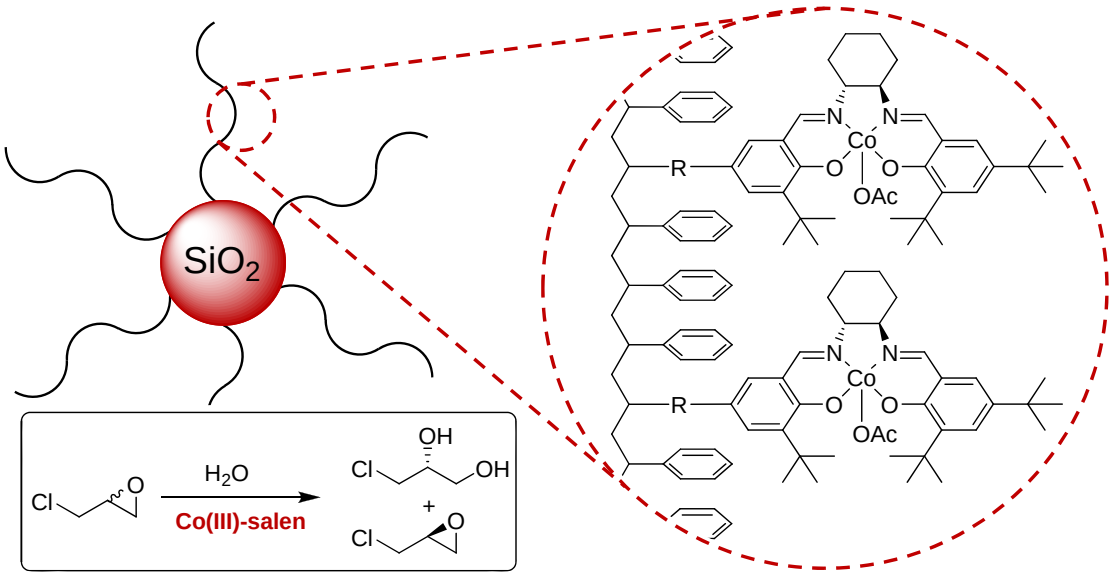

Scheme 4.1 – HKR of epichlorohydrin by polymer brush supported Co-salen catalysts.

4.2 Experimental procedures

4.2.1 Chemicals

Reagents were used as received unless otherwise noted. Dichloromethane (DCM) was dried by passing through columns of activated alumina. Toluene and tetrahydrofuran (THF) were dried by passing through columns of activated copper oxide and alumina successively.[44] Styrene was dried over activated 3 Å molecular sieves, purified by distillation, degassed, and stored in a nitrogen glove box at -20°C. Non-porous CAB-O-SIL M5 fumed silica (BET surface areas 200 m^2/g) was purchased from Cabot Corporation (Tuscola, IL, USA), dried under vacuum (200°C, 3 hours), and stored in a nitrogen glove box prior to use.

4.2.2 Instrumentation

^{1}H and ^{13}C NMR spectra were acquired with a Varian Mercury 400 MHz spectrometer, and chemical shifts were reported in ppm with reference to the corresponding residual nuclei of the deuterated solvents. Cross-polarization magic angle spinning (CP-MAS) solid-state NMR spectra were collected on a Bruker DSX 300-MHz instrument. Samples were packed in 7-mm zirconia rotors and spun at 6.6 kHz. Typical ^{13}C CP-MAS parameters were 3000 scans, a 90° pulse length of 4 μs, and recycle times of 4 s. Typical ^{29}Si CP-MAS parameters were 5000 scans, a 90° pulse length of 5 μs, and recycle times of 5 s. Mass spectra were analyzed using a VG 7070 EQ-HF hybrid tandem mass spectrometer. Transmission electron microscopy experiments (TEM) was performed using a Hitachi HD-2000 field emission gun microscope. Gel-permeation chromatography (GPC) analyses were performed with American Polymer Standards columns equipped with a Waters 510 pump and UV detector, using poly(styrene)s as standards for calibration and THF at a flow rate of 1.0 mL/min as the mobile phase. Enantiomeric excesses were determined by capillary gas-phase chromatography (GC) analysis on a Shimadzu GC 14A instrument equipped with a FID detector and a Chiraldex γ-TA column (40 m × 25 mm × 0.25 μm). A Netzsch Thermoanalyzer STA 409 was used for thermogravimetric analysis (TGA) and differential scanning calorimetry (DSC) with a heating rate of 10°C/min in air. Fourier transform infrared (FT-IR) spectra were recorded on a Bruker IFS 66 V/S or Bruker Equinox 55 spectrometers by dispersing samples in potassium bromide pellets. A Fischer Scientific FS60H, was used for ultrasonication purposes to disperse samples in solution. Elemental analyses were performed by Desert Analytics Lab (Tucson, AZ, USA).

4.2.3 Polymer brush precatalyst synthesis

4.2.3.1 Overview of polymer brush precatalyst synthesis

Co^{II}-salen polymer brush precatalysts were synthesized via atom transfer radical polymerization (ATRP)[45] of styrene and styryl-modified salen ligands from a CAB-O-SIL supported ATRP initiator (**2**) [46] (Scheme 4.2). Two different styryl-modified salen monomers (**1a**, **1b**) [9, 47] were selected to investigate their effect upon catalytic activities resulting from contrasting hydrophilicities and flexibilities of the salen-styrene linker. Post-polymerization, the polymer brushes were metallated with cobalt (II) acetate, forming the Co^{II}-salen polymer brush precatalysts. The precatalysts were activated prior to testing in the HKR of epichlorohydrin.

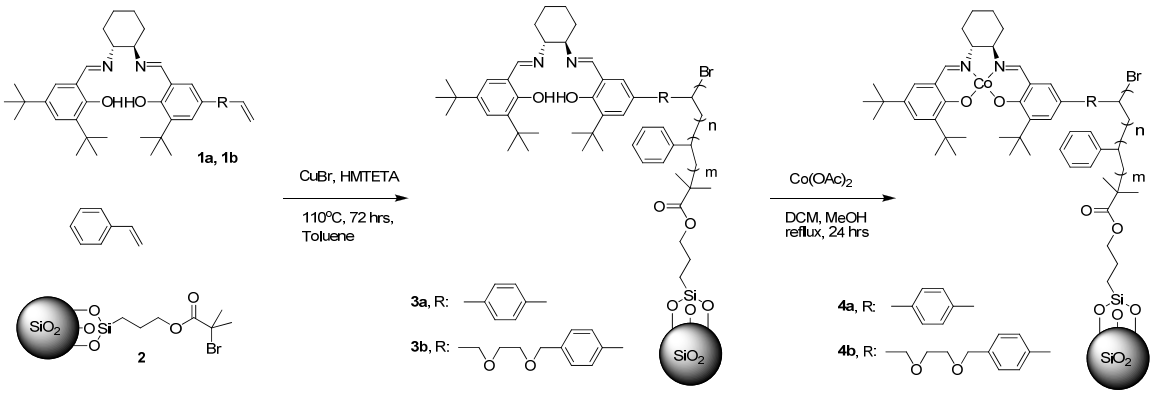

Scheme 4.2 – Polymer brush catalyst synthesis.

4.2.3.2 Synthesis of grafted ATRP initiator **2**

The initiator 3-(trimethoxysilyl)propyl 2-bromo-2-methylpropanoate was synthesized as previously reported.[46] The product was purified by distillation and stored in a nitrogen glove box. Non-porous CAB-O-SIL M-5 fumed silica (1.00 g), which was previously dried under vacuum (200°C, 3 hr) prior to use, was suspended in dry toluene

(30 mL) in a nitrogen glove box. 3-(Trimethoxysilyl)propyl 2-bromo-2-methylpropanoate (1.00 g) was added. The mixture was sonicated (15 min) to disperse the silica and refluxed under an argon atmosphere (48 hr). The solid was filtered and washed with copious amounts of toluene, hexanes, methanol, and diethyl ether. The immobilized bromoisobutyrate initiator (**2**) was dried under vacuum (150°C, 3 hr) and stored in a nitrogen glove box. TGA of the solid revealed that approximately 0.24 mmol/g of the bromoisobutyrate initiator was grafted on the silica surface. IR (KBr): ν_{max} = 3430, 2953, 2852, 1727 (C=O), 1630, 1100, 815 cm^{-1}.

4.2.3.3 Synthesis of polymer brushes (**3a**, **3b**)

A pressure reactor (50 mL) was charged with styryl-modified salen ligand (**1a** or **1b**, 0.5 mmol), [9, 47] toluene (5 mL), immobilized bromoisobutyrate initiator (**2**, 0.30 g), styrene (0.21g, 2 mmol), and 2.5 mL of a copper (I) bromide/ 1,1,4,7,10,10-hexamethyltriethylenetetramine (HMTETA) mixture (2 mmol HMTETA, 1 mmol CuBr, and 30 mL toluene) in a nitrogen glove box. The mixture was sonicated (15 min) to disperse the silica and stirred (110°C, 72 hr) under argon to initiate ATRP.[45] The reaction mixture was cooled to room temperature, opened to air, sonicated (30 min), and the solid was isolated by centrifugation. The particles were re-dispersed in dry toluene (40 mL), sonicated (30 min), and allowed to stand overnight. The green precipitate was removed, and the polymer brushes were then recovered by centrifugation. The particles were re-dispersed in dry toluene (40 mL), sonicated until no particles were visually observed (30 minutes), and the washing procedure was repeated 6 times. Thermal induced polymerization of styrene likely generated polymer chains not attached to the silica surface. The extensive washing steps were undertaken to minimize free polymer chains

from the solid material. The polymer brushes were dried under vacuum at room temperature overnight. TGA of **3a** indicated an organic loading of 50%. ^{13}C CP-MAS NMR (300 MHz, 25°C): δ= 25 - 50 (aliphatic), 73 (CH-N), 120 - 145 (aromatic), 158 (C-O), 165 ppm (C=N). ^{29}Si CP-MAS NMR (300 MHz, 25°C): δ= -110, -105, -90; and -65, -60, -50 ppm. IR (KBr): ν_{max} = 3430, 3086, 3063, 3031, 2957, 2934, 2865, 1727 (C=O), 1630 (C=N st), 1456, 1102, 815, 703. TGA of **3b** indicated an organic loading of 48%. ^{13}C CP-MAS NMR (300 MHz, 25°C): δ= 25 - 80 (aliphatic, cyclohexyl, CH_2-O), 120 - 145 (aromatic), 159 (C-O), 166 ppm (C=N) (Figure 4.2). ^{29}Si CP-MAS NMR (300 MHz, 25°C): δ= -110, -102, -90; and -66, -57, -50 ppm (Figure 4.3). IR (KBr): ν_{max} = 3416, 3084, 3061, 3028, 2951, 2930, 2863, 1724 (C=O), 1632 (C=N), 1456, 1104, 803, 700.

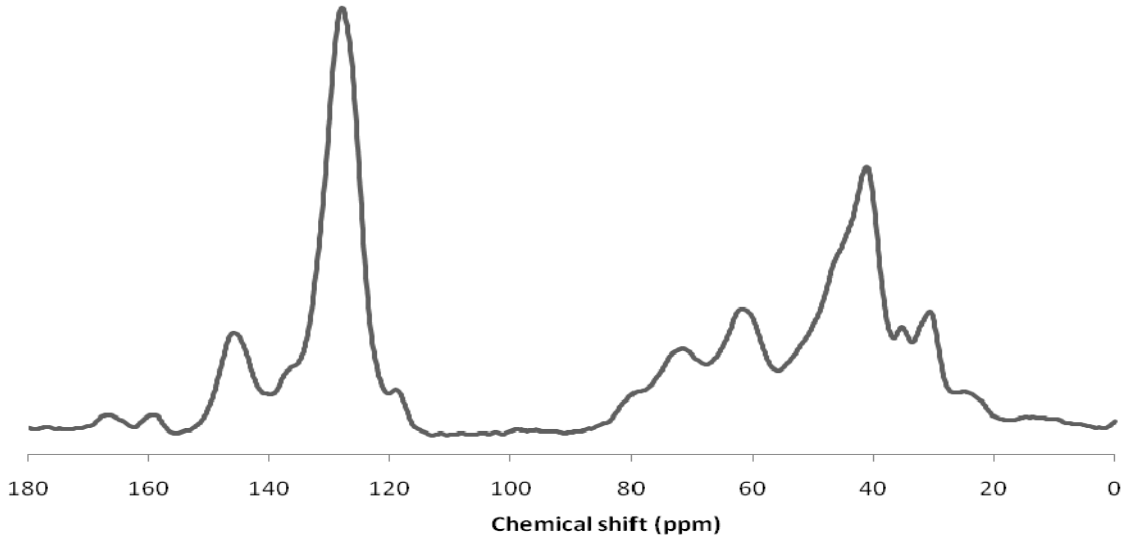

Figure 4.2 - ^{13}C CP MAS NMR for polymer brush **3b**.

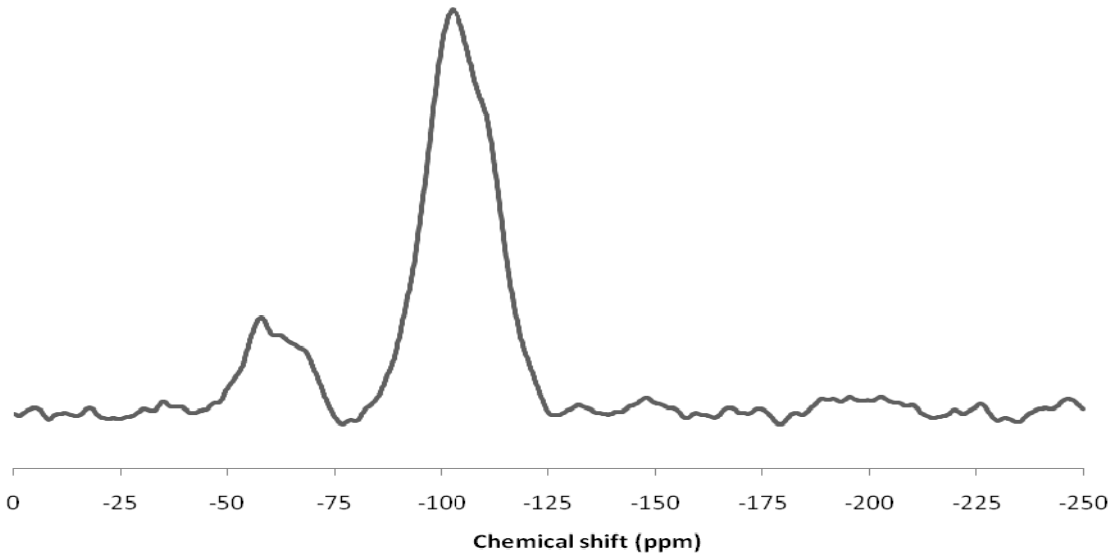

Figure 4.3 - ^{29}Si CP MAS NMR for polymer brush **3b**.

4.2.3.4 Cleavage of grafted polymer from silica

The polymer brushes (30 mg, **3a** or **3b**) were dispersed in DCM (20 mL) in a 50 mL polypropylene bottle, and the mixture was sonicated for 30 minutes. Using proper safety precautions, aqueous hydrofluoric acid solution (2M, 20 mL) was carefully added, and the mixture was shaken vigorously for 10 minutes. The bottle was then allowed to stand for 15 minutes. The DCM phase was then recovered, washed with water (20 mL) four times, and dried over anhydrous magnesium sulfate. The solvent was roughly removed by a rotovap, and the yellow residue was dried under vacuum at room temperature overnight. The polymer was characterized by ^{1}H NMR and GPC. Cleaved polymer from **3a**: ^{1}H NMR (400 MHz, $CDCl_3$, 25°C): 0.82 - 2.0 (m), 1.26 (s), 1.33 (s), 1.43 (s), 3.35 (br, 2NC*H*CH_2), 6.30 - 7.45 (aromatic), 8.35 ppm (br, C*H*=N). Traces of C*H*=O and Ar-O*H* groups were observed at 9.87 and 11.64 ppm, respectively. Integration of C*H*=N and C*H*=O indicated that approximately 5.1% of the salen ligand was

hydrolyzed by hydrofluoric acid. Integration of the imine, aldehyde, and aromatic protons indicated a styrene:salen ratio of 4.1, closely matching the desired ratio of 4.0. GPC indicated a multimodal distribution of polymeric molecular weights and M_n = 28,700 Da. It was calculated that only 15% of the available surface initiator sites were converted into polymer chains using equation 4.1.

$$I_{eff} = Org_{TGA} / (M_n * I_{loading}) \quad (4.1)$$

where I_{eff} = initiator efficiency, Org_{TGA} = TGA organic loss (g organic/g material), M_n = number average molecular weight of the cleaved polymer, and $I_{loading}$ = initiator loading (mmol/g). Cleaved polymer from **3b**: ^{1}H NMR (400 MHz, $CDCl_3$, 25°C): 0.8 - 2.0 (m), 3.31 (br, 2NC*H*CH_2), 3.56 (br, OCH_2CH_2O), 4.41 (br, Ar-CH_2-O), 6.30 - 7.45 (aromatic), 8.35 (br, C*H*=N), 9.87 (C*H*=O), 11.64 ppm (Ar-O*H*). Integration of C*H*=N and C*H*=O indicated that approximately 7.5% of the salen ligand was hydrolyzed by hydrofluoric acid. Integration of the imine, aldehyde, and aromatic protons confirmed a styrene:salen ratio of 4.3, closely matching the desired value of 4.0. GPC indicated a multimodal distribution of polymeric molecular weights and M_n = 21,500 Da. Using equation 4.1, it was calculated that only 19% of the available surface initiator sites were converted into polymer chains.

4.2.3.5 Synthesis of Co^{II}-salen polymer brush precatalysts (**4a**, **4b**)

A flask (100 mL) was charged with the polymer brushes (**3a** or **3b**, 400 mg) and anhydrous DCM (10 mL) in a nitrogen glove box. A solution of anhydrous cobalt (II) acetate (80 mg) in anhydrous methanol (10 mL) was then added. A brick-red powder was observed immediately in the reaction mixture. The brick-red suspension was sonicated (30 min) to disperse the particles in the solution. The reaction mixture was refluxed (40

hr) under an argon atmosphere. The suspension was then cooled to room temperature and transferred to a centrifuge tube in a nitrogen glove box. The solid was recovered by centrifugation. Anhydrous methanol (40 mL) was added, the suspension was sonicated (30 min), and the solid was recovered by centrifugation. The washing procedure was repeated 6 times. The brick-red Co^{II}-salen precatalyst was dried under vacuum at room temperature overnight. Elemental analysis (ICP-MS) of the pre-catalyst indicated a cobalt loading of 0.30 mmol/g. for **4a** and 0.28 mmol/g for **4b**. The cobalt loading on the polymer chains were calculated from equation 4.2.

$$Co_{exp} = Co_{EA} / Org_{TGA} \quad (4.2)$$

where, Co_{exp} = experimental polymeric cobalt loading (mmol Co / g polymer) and Co_{EA} = cobalt loading of the solid catalyst as determined via elemental analysis (mmol Co / g solid). The theoretical maximum cobalt loading was calculated from equation 4.3.

$$Co_{th} = 1 / (MW_{styrene} * R + MW_{salen}) \quad (4.3)$$

where, Co_{th} = theoretical polymeric cobalt loading assuming complete metallation of the salen monomers (mmol Co / g polymer), $MW_{styrene}$ = styrene molecular weight (g/mol), R = styrene:salen ratio as determined via ^1H NMR, and MW_{salen} = styryl-salen molecular weight (g/mol). The effectiveness of the cobalt metallation step was calculated via equation 4.4.

$$M_{eff} = Co_{exp} / Co_{th} \quad (4.4)$$

where, M_{eff} = percent efficiency of the metallation procedure. From these calculations, it was determined only 62% and 68% of the salen ligands were metallated with cobalt for species **4a** and **4b**, respectively.

4.2.4 SBA-15 supported Co^{II}-salen precatalyst synthesis (7)

4.2.4.1 Overview of SBA-15 supported Co^{II}-salen precatalyst synthesis

For comparison of the catalyst architectures, an analogous Co^{II}-salen precatalyst was grafted (Scheme 4.3) on mesoporous SBA-15 silica (**7**) similar to previous reports of silica supported salen catalysts.[48, 49] Compound **1a** was reacted with 3-mercaptopropyltrimethoxysilane (MPTMS), forming salen-modified silane **5** via a thiol coupling. Compound **5** was metallated with cobalt(II) acetate, forming Co^{II}-salen-modified silane **6**. Compound **6** was reacted with mesoporous SBA-15, generating the silica supported Co^{II}-salen precatalyst **7**.

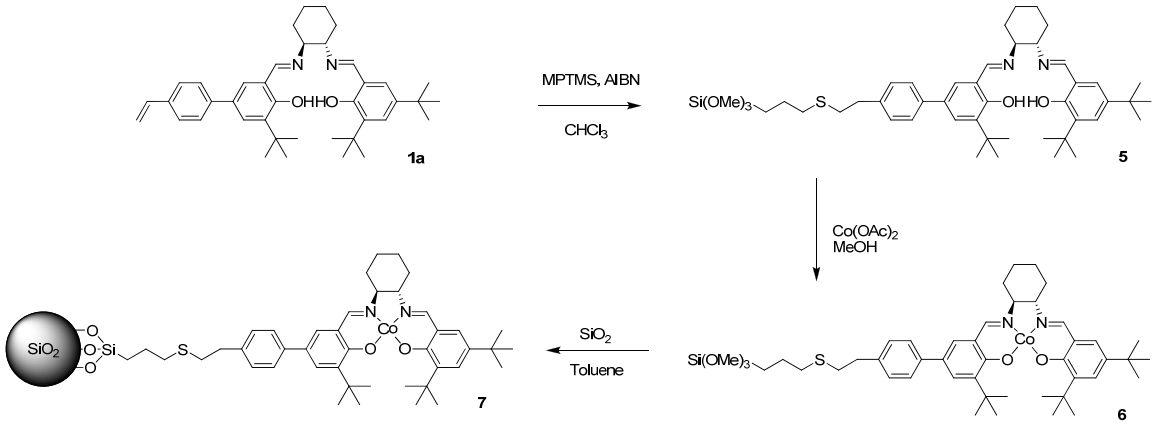

Scheme 4.3 - Synthesis of SBA-15 grafted Co^{II}-salen precatalyst.

4.2.4.2 Methoxysilane modified salen ligand synthesis

Salen ligand was grafted onto an SBA-15 support using modified methods from literature.[48] A solution of styryl-modified salen ligand (1.80 g, 3.0 mmol, **1a**) in dry chloroform was added to a solution of 3-mercaptopropyltrimethoxysilane (MPTMS, 0.72 g, 3.6 mmol) and AIBN (0.24 g, 1.5 mmol) in dry chloroform. The solution was heated at

80°C for 24 hours and then cooled to room temperature. The solvent was removed under vacuum. Flash chromatography of the crude product with ethyl actetate/hexanes afforded the compound (*R*,*R*)-*N*-(3,5-Di-*tert*-butylsalicylidene)-*N'*-(3-(4'-(2-(3-trimethoxysilyl-propylsulfanyl)-ethyl)benzene)-5-*tert*-butylsalicylidene)-1,2-cyclohexanediamine (**5**) as yellow oil. ^{1}H NMR (400 MHz, $CDCl_3$, 25 °C) δ= 14.15 (brs, 1H, -OH), 13.60 (brs, 1H, -OH), 8.41 (s, 1H, N=CH), 8.18 (s, 1H, N=CH), 7.48 (d, *J* = 2.4 Hz, 1H, ArH), 7.40 (s, 1H, ArH), 7.38 (s, 1H, ArH), 7.32 (d, *J* = 2.4 Hz, 1H, ArH), 7.24 (s, 1H, ArH), 7.23 (s, 1H, ArH), 7.20 (d, *J* = 2.4 Hz, 1H, ArH), 6.99 (d, *J* = 2.4 Hz, 1H, ArH), 3.59 (s, 9H, OMe), 3.36-3.23 (m, 2H, CH_2), 2.93-2.89 (m, 2H, CH_2), 2.82-2.78 (m, 2H, CH_2), 2.62-2.58 (m, 2H, CH_2), 2.04-1.97 (m, 2H, CH_2), 1.90-1.88 (m, 2H, CH_2), 1.77-1.73 (m, 4H, CH_2), 1.47 (s, 9H, CMe_3), 1.48-1.46(m, 2H, CH_2), 1.43 (s, 9H, CMe_3), 1.23 (s, 9H, CMe_3), 0.81-0.78 ppm (m, 2H, CH_2) (Figure 4.4). ^{13}C NMR (100.6 MHz, $CDCl_3$, 25 °C) δ= 165.72, 165.31, 159.56, 157.66, 139.68, 138.97, 138.65, 137.18, 136.09, 130.37, 128.56, 128.02 127.85, 126.62, 126.52, 125.80, 118.52, 117.60, 72.33, 72.28, 50.56, 36.01, 35.19, 34.95, 34.05, 33.49, 33.20, 31.44, 29.44, 27.62, 24.39 23.05, 8.69, 8.32 ppm (Figure 4.5). MS-ESI (m/z): 789 [M^+].

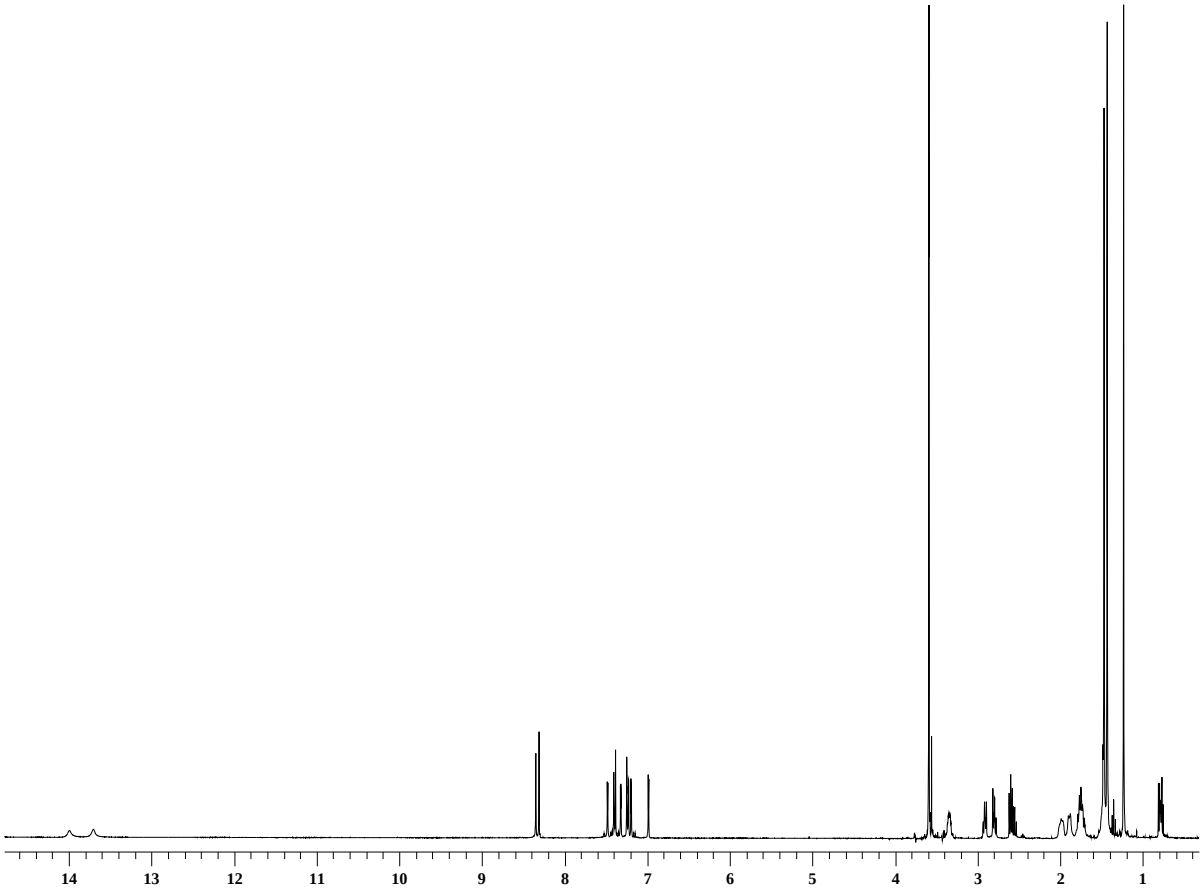

Figure 4.4 - Solution ^{1}H NMR for trimethoxysilane-modified salen **5**.

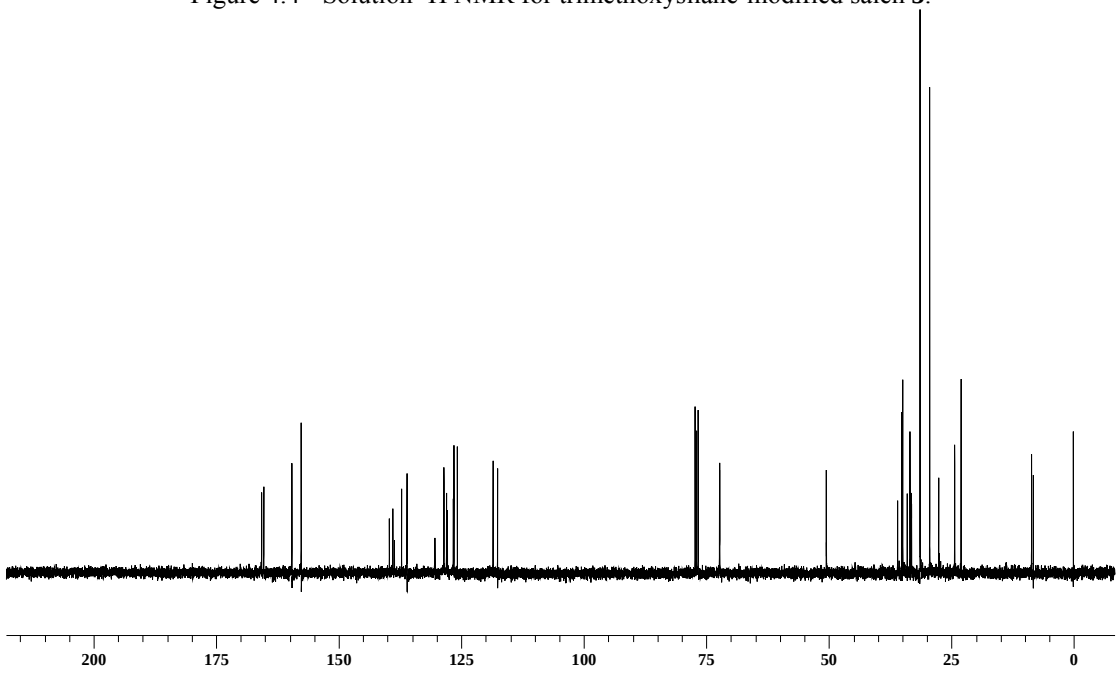

Figure 4.5 - Solution ^{13}C NMR for trimethoxysilane-modified salen **5**.

4.2.4.3 Methoxysilane modified Co^{II}-salen

A solution of the salen-modified silane (2.06 g, 2.6 mmol, **5**) in dry chloroform was added to a solution of cobalt(II) acetate (0.46 g, 2.6 mmol) in dry methanol. The solution was stirred at room temperature for 4 hours and then filtered to afford 6 as a red colored solid. MS-ESI (m/z): 846 [M^+]. elemental analysis calcd (%) for $C_{46}H_{66}N_2SSiO_5Co$: C 65.30, H 7.86, N 3.31, Co 6.97; found: C 65.74, H 7.63, N 3.56, Co 6.22.

4.2.4.4 SBA-15 modified Co^{II}-salen precatalyst

SBA-15 was synthesized by a slightly modified method[50] based on published procedures.[51] A solution of (2.0 g) of compound **6** in dry toluene was added to a mixture of SBA-15 (2.0 g) in dry toluene in a nitrogen dry box. The reaction was stirred under reflux conditions for 24 h, filtered and washed with toluene and hexanes. The red solid obtained was soxhlet extracted with dichloromethane for 12 hours, and the resulting solid was dried under vacuum at 50 °C, overnight. Elemental analysis of precatalyst **7** indicated a cobalt loading of 0.35 mmol/g. IR (KBr): ν_{max} = 2952, 2863, 1610, 1521, 1434, 1388 cm^{-1}. UV/Vis: λ_{max} (ε) = 375, 420 nm.

4.2.5 Procedure for the hydrolytic kinetic resolution of epichlorohydrin

In order to test the catalyst at 0.5 mol%, a 5 mL pear shaped flask was charged with the Co^{II}-salen polymer brush precatalyst (0.015 mmol using a cobalt basis, **4a**, **4b**, or **7**), DCM (1 mL), glacial acetic acid (0.1 mL), and a triangular stir bar. The flask was sonicated (5 min) to disperse the particles and stirred under air (30 min). The solvent and acetic acid were removed via rotovap and dried under high vacuum (30 min) leaving the

solid, brown activated Co^{III}-salen polymer brush catalyst. The catalyst was dispersed into racemic epichlorohydrin (234.6 μL, 3 mmol) and chlorobenzene (27.3 μL, internal standard) and immersed into a water bath at room temperature. Deionized water (0.6 equiv, 32.4 μL, 1.8 mmol) was added to initiate the reaction. Samples (2 μL) were periodically removed from the reaction mixture via micropipette, diluted with anhydrous diethyl ether (2 mL), and passed through a plug of silica gel in a Pasteur pipette to remove the catalyst and water. Conversions and enantiomeric excesses of epichlorohydrin were measured by GC with a Chiraldex γ-TA column with reference to the chlorobenzene internal standard.

4.2.6 Procedure for recycle experiments

Recycle experiments of the polymer brush catalyst were started similarly to the intitial experiments. The mass of the dry flask and stir bar was recorded. Catalyst (0.025 mmol using a cobalt basis) was added (scaling other parameters appropriately) and the reaction was performed as described above. The reaction was terminated by addition of excess THF (3 mL). The solid catalyst was recovered via centrifuge (2500 rpm, 30 min) and the solution was decanted. Fresh THF (3 mL) was added, and the solid was dispersed via sonication. The washing procedure was repeated four times to remove water, chlorobenzene, 3-chloro-1,2-propanediol, and epichlorohydrin. The solid was dried under high vacuum, and the mass of the flask, stir bar, and recovered catalyst was recorded. Recycle experiments were scaled according to the mass of recovered catalyst, as the centrifuge proved insufficient to completely remove the solid particles. Reactivation of the catalyst with acetic acid was performed before each cycle, because it has been shown important for retention of high activities.[52]

4.3 Results and Discussion

4.3.1 Catalyst characterization

CAB-O-SIL silica displayed a fractal-like structure with particle thicknesses of roughly 20 nm via TEM (Figure 4.6), in agreement with company literature. Thermogravimetric analysis (TGA) of the ATRP initiator modified CAB-O-SIL silica **2** indicated a loading of 0.24 mmol/g of the initiator on the silica surface. Post-ATRP polymerization, calculations using equation 4.1 indicated roughly 17% of the surface initiator sites resulted in polymer chains, a result consistent with prior reports of low initiator efficiencies for polymer brush systems.[53] TGA confirmed a surface initiated polymerization by indicating organic contents of 50% and 48% for polymer brushes **3a** and **3b**, respectively. TEM images also supported surface-bound polymer initiation by displaying similar fractal-like structures for **3a** and **3b** as with the bare silica, but the particle thicknesses increased to roughly 40 nm (Figure 4.6)

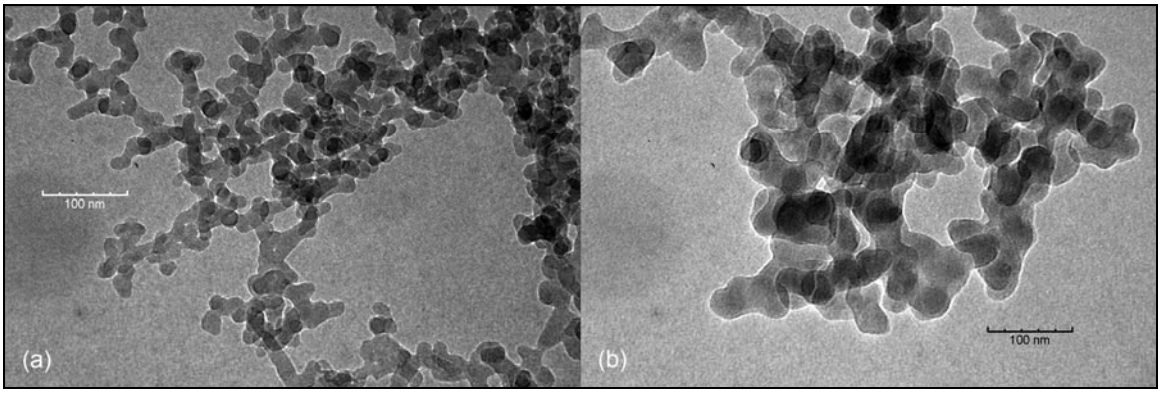

Figure 4.6 - TEM images at 100,000X of (a) CAB-O-SIL silica and (b) polymer brush **3b**.

FT-IR bolstered the postulated structure of the organic species present in the solid catalyst (Figure 4.7). Aromatic C-H stretches were observed in each of the polymer brushes (**3a**, **3b**) not present in the immobilized ATRP initiator (**2**) at 3086, 3063, and

3031 cm^{-1}. A significant growth in the aliphatic C-H stretches at 2957, 2934, and 2865 and the imine (C=N) stretch at 1630 was also observed. The growths of the aromatic and aliphatic C-H stretches from the poly(styrene) backbone and the imine stretch from the salen ligand in the FT-IR spectra indicated the organic loadings observed by TGA were indeed the desired styrene/styryl-salen copolymer.

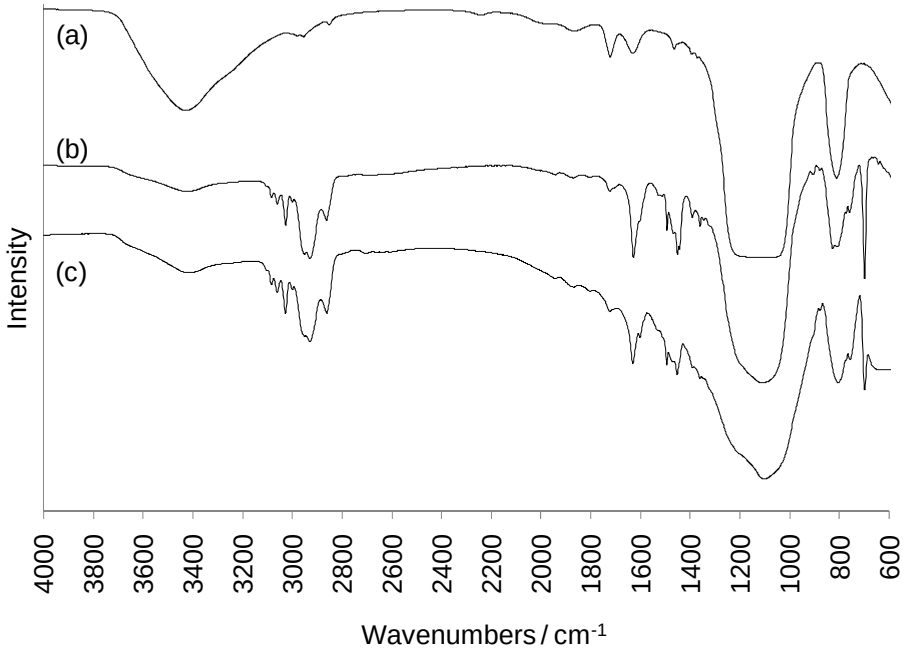

Figure 4.7 - FT-IR spectra of (a) ATRP initiator functionalized silica **2**, (b) polymer brush **3a**, and (c) polymer brush **3b**.

This formation was confirmed with CP MAS ^{13}C NMR, which displayed peaks in the regions 25-80 (*C*Me_3, *C*H_2, O-*C*H_2, cyclohexyl-*C*H_2, cyclohexyl *C*H), 120-145 (aromatic *C*), 160 ppm (*C*=N) (Figure 4.2). CP MAS ^{29}Si NMR also indicated the presence of Q^2, Q^3, and Q^4 silicon resonances ($^-$90 to $^-$110 ppm) and resonances corresponding to reaction of 1, 2, and 3 methoxy groups of the polymer initiator to the silica surface ($^-$51 to $^-$67 ppm) in the material, confirming a covalent linkage between the silica support and surface organic functionalities. Cleavage of the polymer from the silica

surface by treatment with aqueous HF allowed for analysis of the polymer by GPC and solution ^{1}H NMR. GPC indicated multi-modal distributions of polymer molecular weights with number average molecular weights of 28,700 Da and 21,500 Da relative to poly(styrene) standards for **3a** and **3b**, respectively. Integration of the imine, aldehyde, and aromatic protons in ^{1}H NMR yielded styrene:styryl-salen ratios of 4.1 and 4.3 for **3a** and **3b**, respectively, closely matching the targeted ratio of 4.0. The polymer brushes were metallated with cobalt(II) acetate, forming the Co^{II}-salen polymer brush precatalysts (**4a**, **4b**). Elemental analysis indicated loadings of 0.30 and 0.28 mmol/g on the basis of cobalt for **4a** and **4b**, respectively. Calculations estimated roughly 65% of the salen ligands chelated cobalt. Since this work utilizes heterogeneous systems, polymer initiation and ligand metallation suffer from steric hinderance from the silica support and polymer chains. In additional studies using solely polymeric Co-salen systems, elemental analysis indicates slightly higher metallation to the Co-salen complex (70%) indicating complete formation of the complex may only be possible using small molecules rather than the polymeric or polymer brush systems.

SBA-15 supported CoII-salen precatalyst **7** was characterized via nitrogen physisorption and elemental analysis. Using nitrogen physisorption experiments, decreasing BET surface areas (888 m^2/g to 537 m^2/g) and average pore diameters (80 angstroms to 65 angstroms) were observed after grafting **5** to the silica surface, indicating the organic species were being immobilizing within the mesopores after modifying bare SBA-15 to form precatalyst **7**. Elemental analysis confirmed a cobalt loading of 0.35 mmol/g on the silica support.

4.3.2 Catalyst performance

The polymer brush catalysts were activated with acetic acid in air and evaluated in the hydrolytic kinetic resolution (HKR) of epichlorohydrin. A dramatic difference in activity was observed between **4b** and the homogeneous Co-salen catalyst at 0.01 mol% loading (Figure 4.8). After 20 hours, the enantiomeric excesses of the polymer brush catalyst approached 85% versus 10% by the benchmark homogeneous Co-salen catalyst. Enantiomeric excesses surpassed 94% at longer times (72 hrs, 48% conversion). This difference in activity was attributed to enhanced cooperativity of the active sites via the polymer brush architecture. In contrast, the bimetallic interactions of the homogeneous catalyst were governed by statistical interactions of the active site in solution. These interactions became increasingly unfavorable, especially at the low 0.01 mol% catalyst concentration, leading to the low activity of the catalyst. Unlike the homogeneous catalyst, lowering catalyst concentration of the polymer brush catalysts only decreased the total mass of catalyst present, without affecting the local concentrations of active sites on the poly(styrene) brush.

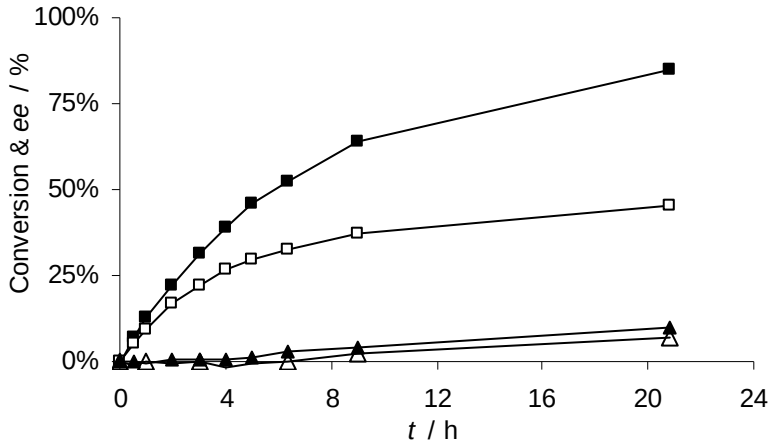

Figure 4.8 - Kinetic data for the HKR of epichlorohydrin at 0.01 mol%: 4b ee (■), 4b conversion (□), homogeneous Co^{III}-salen ee (▲), and homogeneous Co^{III}-salen conversion (△).

At 0.5 mol%, activity of the homogeneous catalyst improved due to the increased probability of interactions of active sites in solution (Figure 4.9). However, **4b** still retained higher activities compared to the homogeneous Co^{III}-salen catalyst. Additionally, **4b** exhibited increased activities over **4a**, a result attributed to two improvements in design: increased flexibility and hydrophilicity of the salen-poly(styrene) linker. The flexibility of the six atom linker between the salen and poly(styrene) backbone permitted three dimensional translational and rotational freedoms, potentially leading to enhanced site-site interactions.[47] The rigid phenylene linker was hypothesized to permit rotational freedom but restrict translational freedom of the pendant catalyst in **4a**, lessening these interactions. In addition, the hydrophilicity of the ethylene glycol linker of **4b** was envisioned to further aid activities in this multi-phase system due to its affinity for water near the Co^{III}-salen active sites. Additionally, the longer linker in **4b** would result in less steric hinderance from the poly(styrene) backbone than **4a**. Both catalysts displayed high enantioselectivities during the HKR reaction. Catalyst **4a** displayed 95% *ee* for epichlorohydrin and >99% *ee* for the 3-chloro-1,2-propanediol product after 120 minutes. Catalyst **4b** displayed >99% *ee* for both epichlorohydrin and the diol product after 60 minutes.

Precatalyst **7** showed greatly reduced *ee*'s of 31% at 22% conversion after 30 minutes. The low activity and selectivity of **7** versus **4a** or **4b** was attributed to poor site-site interactions and hindered Co-salen cooperativity, resulting from the inability to graft high local densities of the salen ligand on the silica surface. This is consistent with related work on epoxide ring-opening with Cr-salen catalysts.[49] Despite possessing lower

cobalt loadings, polymer brushes **4a** and **4b** were thought to contain higher local concentrations of the cobalt(III)-salen active site, leading to the greatly enhanced activities versus the silica grafted material **7**.

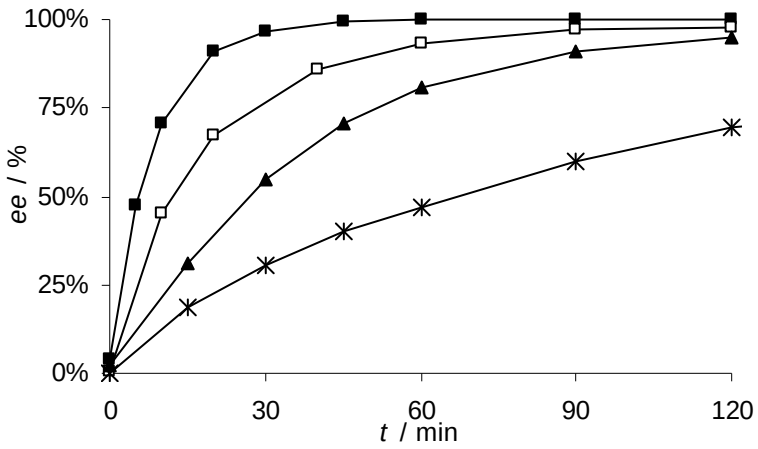

Figure 4.9 - Enantiomeric excesses for the HKR of epichlorohydrin at 0.5 mol%: 4b (■), homogeneous Co^{III}-salen (□), 4a (▲), and 5 (∗).

In recycle studies on the most active catalyst **4b**, high enantioselectivities of the remaining epoxide (≥ 99%) were retained after each of five runs, however the reaction rates were observed to decrease after each subsequent run (Table 4.1). The time required to achieve ≥ 99% *ee*'s increased by roughly a factor of ten (45 to 420 min) and maximum initial turnover frequencies (TOFs) dropped from 30.2 to 4.1 min^{-1} after five cycles. These results echo observations by other researchers of retained high selectivities with decreasing activities (or lengthened reaction times) upon recycle of Co-salen catalysts.[9, 18, 19, 52] However, the deactivation mechanism has yet to be thoroughly investigated.

Table 4.1 - Recycle data for catalyst **4b** at 0.5 mol% catalyst.

Cycle	Time [min]	Conv. [%]	*ee*[a] [%]	Max Initial TOF [min^{-1}]
1	45	55%	> 99%	30.2
2	60	55%	> 99%	25.5
3	120	55%	> 99%	9.4
4	210	55%	99%	4.8
5	420	52%	99%	4.1

[a] *ee* corresponds to the enantiomeric excess of the unreacted epichlorohydrin.

4.3.3 Catalyst deactivation

Several possibilities existed to explain the catalyst deactivation: cobalt leaching, ligand decomposition, polymer loss (non-surface-bound or cleavage of surface-bound polymer), and/or counter-ion exchange.[3, 52] Elemental analysis (EA) and FT-IR of fresh and spent catalysts were compared to elucidate possible deactivation mechanisms. EA indicated significant losses of cobalt and nitrogen in the fresh versus spent catalysts (Figure 4.10). EA also indicated a 10% carbon loss, 6% hydrogen loss and similar silicon content after five cycles. These data indicated ligand decomposition as the underlying cause of catalyst deactivation. If cobalt leached and the salen ligand remained intact, one would not expect to observe 60% N or 10% C losses. If polymer cleavage or removal of non-surface-bound polymer were the suspected cause, one might expect to observe a linear relationship between Co, and C, H, N losses. Instead the data indicate slight C and H losses and significant Co and N losses, an observation much more consistent with decomposition of the salen ligand.

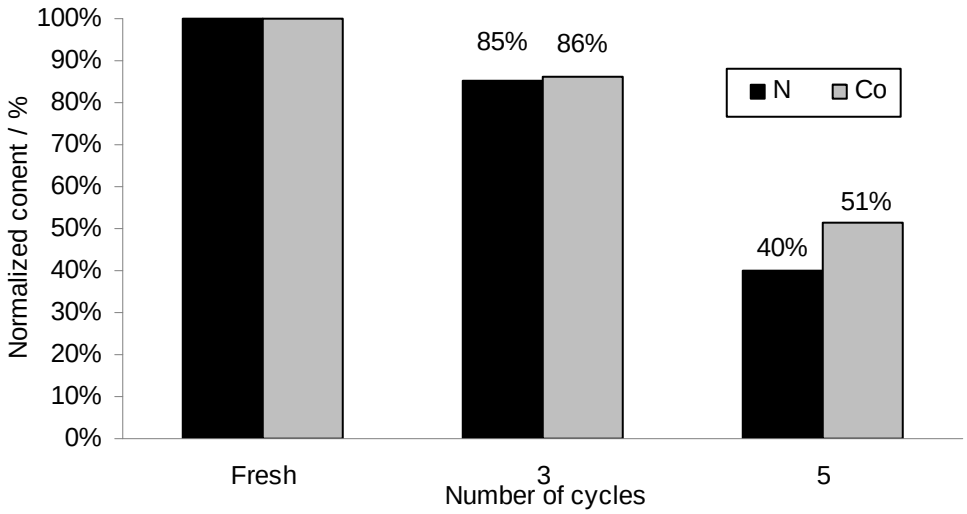

Figure 4.10 - Retention of nitrogen and cobalt in catalyst **4b** upon recycle.

The hypothesized mechanism for this decomposition is presumed to involve cleavage of the imine bonds in the salen ligand. Imines are known to cleave in the presence of water with an acid catalyst. Any acetic acid remaining from the activation step of the Co^{II}-salen to the Co^{III}-salen could catalyze the decomposition of the Schiff base in the presence of water during the HKR reaction. Alternately, unremoved water from the HKR reaction or water vapor absorbed from the air could produce the same result during the activation step with acetic acid (although extensive washing steps with dry THF between cycles was undertaken to minimize residual water). The resulting amine and cobalt species would be removed during the THF washing steps, leading to catalyst loss and possibly explaining the EA results and observed deactivation. It may also be possible that counter-ion exchange was occurring at long reaction times, compounding the problem of salen decomposition. Jain *et. al.* recently suggested counter-ion exchange of Co-OAc to Co-OH could lead to catalyst deactivation.[52] This is consistent with the previous report that the fastest HKR rates were observed when a

roughly equal ratio of Co-X (X=SbF_6^-) to Co-OH was used, with the Co-OH performing the nucleophilic attack on the epoxide.[3] It has thus suggested that a balance of Co-OH and Co-X is required for good activity, although it should be mentioned that no report of the experimental observation or verification of Co-OH species has appeared. In the present work, decomposition of the salen ligand was the presumed cause of deactivation of catalyst **4b**, resulting in reduced rates after two cycles. As the reaction time lengthened, counter-ion exchange to high fractions of Co-OH could be compounding problems, leading to further deactivation of the catalyst. This possibility could not be discounted.

To further investigate catalyst deactivation, FT-IR was utilized to compare the fresh and spent catalysts (Figure 4.11). The imine bands were the main peaks of interest. Non-metallated salen ligand displayed a large imine stretch at 1631 cm^{-1} which shifted to 1596 cm^{-1} upon incorporation of cobalt into the ligand. Unmetallated and metallated polymer brushes **3b** and **4b** displayed similar shifts from 1629 cm^{-1} to 1601 cm^{-1}, respectively. After 1 and 5 cycles of catalyst **4b**, the imine stretch at 1603 cm^{-1} displayed a substantial decrease in intensity. Additionally, evidence of an unmetallated imine stretch in the 1630 cm^{-1} region began to reappear as a shoulder, although not nearly as intense as the unmetallated polymer brush **3b**. These results indicate a significant reduction in the Co-salen structure upon reuse of the catalyst. The FT-IR results support the hypothesis of cleavage of the C=N bond, accompanied by loss of cobalt from the fragmenting ligand. Since a strong imine stretch at 1630 cm^{-1} did not reappear in the FT-IR spectra of the spent catalysts, it may be reasoned that just leaching of the cobalt from the intact ligand was not the underlying cause of deactivation.

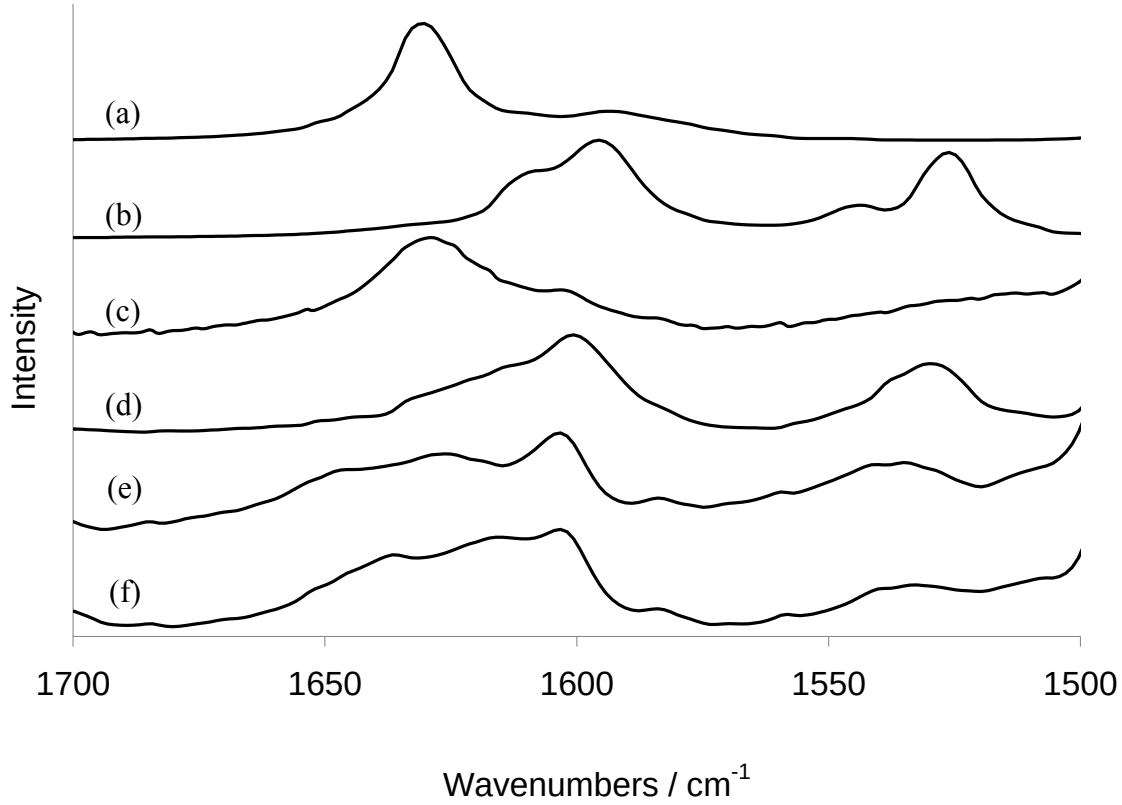

Figure 4.11 - FT-IR spectra of (a) non-metallated homogeneous salen ligand, (b) homogeneous Co-salen complex, (c) non-metallated polymer brush **3b**, (d) Co-salen polymer brush **4b**, (e) polymer brush catalyst **4b** after 1 cycle, and (f) polymer brush catalyst **4b** after 5 cycles.

4.4 Conclusion

Presented here is the first example of utilizing pendant polymer brush catalysts for enhancing cooperative catalysis. It is also one of very few examples of polymer brush catalysts in general.[28-35] Additionally, catalyst **4b** appears to be among the most active, solid, insoluble Co-salen HKR catalysts. Results indicate this novel catalyst promotes bimetallic interactions of the Co-salen catalyst, leading to high activities. This type of catalyst could be especially useful for a variety of reactions that are proposed to require cooperative catalysis.[37-42] This architecture could also be beneficial to obtain higher loadings and/or higher local concentrations of catalyst on insoluble supports versus

traditional grafting approaches. The silica support provided for facile recovery of the catalyst in contrast to highly active, but more difficult to recover examples of oligomeric, polymeric, and dendritic materials. In addition to catalyst architecture, a flexible/hydrophilic linker was hypothesized to further aid activity. The polymer brush catalyst was observed to retain high enantioselectivities up to five cycles in the HKR of epichlorohydrin, despite a drop in activity. Cleavage of the salen ligand was the suggested cause of the catalyst deactivation as indicated by FT-IR and elemental analysis investigations of the spent catalyst.

4.5 Acknowledgements

The US DOE Office of Basic Energy Science is acknowledged for financial support through Catalysis Contract No. DEFG02-03ER15459. The authors acknowledge collaborators Dr. Xiaolai Zheng of GT and Dr. Robert J. Davis of UVA. CWJ acknowledges ChBE at GT for the J. Carl & Shiela Pirkle Faculty Fellowship.

4.6 References

1. Schaus, S.E., Brandes, B.D., Larrow, J.F., Tokunaga, M., Hansen, K.B., Gould, A.E., Furrow, M.E., and Jacobsen, E.N., *J. Am. Chem. Soc.* **2002**, 124, 1307.
2. Kumar, P., Naidu, V., and Gupta, P., *Tetrahedron* **2007**, 63, 2745.
3. Nielsen, L.P.C., Stevenson, C.P., Blackmond, D.G., and Jacobsen, E.N., *J. Am. Chem. Soc.* **2004**, 126, 1360.
4. Ready, J.M. and Jacobsen, E.N., *J. Am. Chem. Soc.* **2001**, 123, 2687.
5. Ready, J.M. and Jacobsen, E.N., *Angew. Chem. Int. Ed.* **2002**, 41, 1374.
6. Kureshy, R.I., Singh, S., Khan, N.U.H., Abdi, S.H.R., Ahmad, I., Bhatt, A., and Jasra, R.V., *Chirality* **2005**, 17, 590.
7. Breinbauer, R. and Jacobsen, E.N., *Angew. Chem. Int. Ed.* **2000**, 39, 3604.
8. Annis, D.A. and Jacobsen, E.N., *J. Am. Chem. Soc.* **1999**, 121, 4147.
9. Zheng, X.L., Jones, C.W., and Weck, M., *Chem. Eur. J.* **2006**, 12, 576.
10. Holbach, M. and Weck, M., *J. Org. Chem.* **2006**, 71, 1825.
11. Rossbach, B.M., Leopold, K., and Weberskirch, R., *Angew. Chem. Int. Ed.* **2006**, 45, 1309.
12. Kwon, M.A. and Kim, G.J., *Catal. Today* **2003**, 87, 145.

13. Song, Y.M., Chen, H.L., Hu, X.Q., Bai, C.M., and Zheng, Z., *Tetrahedron Lett.* **2003**, 44, 7081.
14. Song, Y.M., Yao, X.Q., Chen, H.L., Bai, C.M., Hu, X.Q., and Zheng, Z., *Tetrahedron Lett.* **2002**, 43, 6625.
15. Li, C., *Catal. Rev. - Sci. Eng.* **2004**, 46, 419.
16. Baleizao, C. and Garcia, H., *Chem. Rev.* **2006**, 106, 3987.
17. Heitbaum, M., Glorius, F., and Escher, I., *Angew. Chem. Int. Ed.* **2006**, 45, 4732.
18. Yang, H.Q., Zhang, L., Zhong, L., Yang, Q.H., and Li, C., *Angew. Chem. Int. Ed.* **2007**, 46, 6861.
19. Yang, H.Q., Zhang, L., Su, W.G., Yang, Q.H., and Li, C., *J. Catal.* **2007**, 248, 204.
20. Kim, G.J. and Park, D.W., *Catal. Today* **2000**, 63, 537.
21. Thakur, S.S., Chen, S.W., Li, W.J., Shin, C.K., Kim, S.J., Koo, Y.M., and Kim, G.J., *J. Organomet. Chem.* **2006**, 691, 1862.
22. Choi, S.D. and Kim, G.J., *Catal. Lett.* **2004**, 92, 35.
23. Oh, C.R., Choo, D.J., Shim, W.H., Lee, D.H., Roh, E.J., Lee, S., and Song, C.E., *Chem. Commun.* **2003**, 1100.
24. Shepperson, I., Cavazzini, M., Pozzi, G., and Quici, S., *J. Fluorine Chem.* **2004**, 125, 175.
25. Cavazzini, M., Quici, S., and Pozzi, G., *Tetrahedron* **2002**, 58, 3943.
26. Belser, T. and Jacobsen, E.N., *Adv. Synth. Catal.* **2008**, 350, 967.
27. Mori, H., Boker, A., Krausch, G., and Muller, A.H.E., *Macromolecules* **2001**, 34, 6871.
28. Mayr, M., Mayr, B., and Buchmeiser, M.R., *Angew. Chem. Int. Ed.* **2001**, 40, 3839.
29. Buchmeiser, M.R., Lubbad, S., Mayr, M., and Wurst, K., *Inorg. Chim. Acta* **2003**, 345, 145.
30. Sharma, G. and Ballauff, M., *Macromol. Rapid Commun* **2004**, 25, 547.
31. Mei, Y., Sharma, G., Lu, Y., Ballauff, M., Drechsler, M., Irrgang, T., and Kempe, R., *Langmuir* **2005**, 21, 12229.
32. Sharma, G., Mei, Y., Lu, Y., Ballauff, M., Irrgang, T., Proch, S., and Kempe, R., *J. Catal.* **2007**, 246, 10.
33. Mei, Y., Lu, Y., Polzer, F., Ballauff, M., and Drechsler, M., *Chem. Mater.* **2007**, 19, 1062.
34. Schrinner, M., Polzer, F., Mei, Y., Lu, Y., Haupt, B., Ballauff, M., Goldel, A., Drechsler, M., Preussner, J., and Glatzel, U., *Macromol. Chem. Phys.* **2007**, 208, 1542.
35. Proch, S., Mei, Y., Villanueva, J.M.R., Lu, Y., Karpov, A., Ballauff, M., and Kempe, R., *Adv. Synth. Catal.* **2008**, 350, 493.
36. Zheng, X., Gill, C.S., Phan, N.T.S., Weck, M., and Jones, C.W., *Design of Highly Active and Enantioselective Recyclable Oligomeric/Polymeric Co-Salen Catalysts for the Hydrolytic Kinetic Resolution of Epoxides*, in *20th North American Catalysis Society National Meeting*. 2007: Houston, TX USA.
37. Sammis, G.M. and Jacobsen, E.N., *J. Am. Chem. Soc.* **2003**, 125, 4442.
38. Sammis, G.M., Danjo, H., and Jacobsen, E.N., *J. Am. Chem. Soc.* **2004**, 126, 9928.

39. Noh, E.K., Na, S.J., Sujith, S., Kim, S.W., and Lee, B.Y., *J. Am. Chem. Soc.* **2007**, 129, 8082.
40. Lu, X.B., Shi, L., Wang, Y.M., Zhang, R., Zhang, Y.J., Peng, X.J., Zhang, Z.C., and Li, B., *J. Am. Chem. Soc.* **2006**, 128, 1664.
41. Chen, F.X., Qin, B., Feng, X.M., Zhang, G.L., and Jiang, Y.Z., *Tetrahedron* **2004**, 60, 10449.
42. Kim, S.S. and Kwak, J.M., *Tetrahedron* **2006**, 62, 49.
43. Zheng, X.L., Jones, C.W., and Weck, M., *J. Am. Chem. Soc.* **2007**, 129, 1105.
44. Pangborn, A.B., Giardello, M.A., Grubbs, R.H., Rosen, R.K., and Timmers, F.J., *Organometallics* **1996**, 15, 1518.
45. Xia, J.H. and Matyjaszewski, K., *Macromolecules* **1997**, 30, 7692.
46. Marsh, A., Khan, A., Garcia, M., and Haddleton, D.M., *Chem. Commun.* **2000**, 2083.
47. Zheng, X.L., Jones, C.W., and Weck, M., *Adv. Synth. Catal.* **2008**, 350, 255.
48. Baleizao, C., Gigante, B., Garcia, H., and Corma, A., *J. Catal.* **2003**, 215, 199.
49. Baleizao, C., Gigante, B., Sabater, M.J., Garcia, H., and Corma, A., *Appl. Catal., A* **2002**, 228, 279.
50. Hicks, J.C. and Jones, C.W., *Langmuir* **2006**, 22, 2676.
51. Zhao, D.Y., Huo, Q.S., Feng, J.L., Chmelka, B.F., and Stucky, G.D., *J. Am. Chem. Soc.* **1998**, 120, 6024.
52. Jain, S., Zheng, X.L., Jones, C.W., Weck, M., and Davis, R.J., *Inorg. Chem.* **2007**, 46, 8887.
53. Sun, Y.B., Ding, X.B., Zheng, Z.H., Cheng, X., Hu, X.H., and Peng, Y.X., *Eur. Polym. J.* **2007**, 43, 762.

CHAPTER 5

MAGNETIC NANOPARTICLE POLYMER BRUSH CATALYSTS: ALTERNATIVE HYBRID ORGANIC/INORGANIC STRUCTURES TO OBTAIN HIGH, LOCAL CATALYST LOADINGS FOR USE IN ORGANIC TRANSFORMATIONS

5.1 Introduction

Chapters 2 and 3 discussed use of magnetic nanoparticle supports for acid and base catalysis, and Chapter 4 discussed use of silica supported Co-salen polymer brush catalysts. This chapter demonstrates how these two grafting techniques were combined to form magnetic polymer brush catalysts. These materials allow for high, local catalyst concentrations with magnetic recovery. Co-salen and basic piperazine modified magnetic polymer brush catalysts were synthesized to highlight the utility of this new type of hybrid organic/inorganic catalyst in enantiomeric resolutions and organic transformations.

A long standing goal in catalysis has been the simple recovery and reuse of highly active, single-sited, homogeneous catalysts via surface grafting to heterogeneous supports.[1] A large variety of hybrid organic/inorganic materials have been developed in response to this challenge. Numerous porous and nonporous heterogeneous supports have been utilized to this end: silicas, polymers, zeolites, etc.[2-4] Unfortunately, recovery and reuse of these materials has been relegated to energy intensive techniques such as filtration or centrifugation for batch processes or via packed bed or slurry reactors for continuous processes. A relatively new type of hybrid organic/inorganic material utilizes magnetic nanoparticles (MNPs) for the catalyst support[5] and offers a simple and non-energy-intensive method for recovery and reuse. Examples include MNP supported

organic acids[6] and bases[7-10] as well as organometallic complexes[11-20] for various small molecule reactions. Furthermore, these particles can be easily modified in terms of hydrophilicity/hydrophobicity to tune their dispersion stability in organic or aqueous media. Unfortunately, magnetic nanoparticles often have lower surface areas compared to other, more traditional, microporous/mesoporous materials used as catalyst supports, limiting the total amount of active sites that can be grafted to the surface.

This work aims to illustrate the versatility of magnetic nanoparticle polymer brush (MPB) materials for catalyst supports as well as demonstrating how increased catalyst loadings at high local concentrations can be achieved using this novel architecture. This goal is achieved by grafting functionalized polymer chains from surface bound polymer initiators via ATRP polymerization of styrene-modified catalyst (or precatalyst) monomers. The resulting polymer brushes mimic soluble polymer catalysts, but offer facile recovery and reuse via the covalent attachment to the magnetic nanoparticle support.

This method has been applied to two different catalyst systems to illustrate the utility of this versatile catalyst architecture (Figure 5.1). The first utilizes pendant, organometallic, Co(III)-salen catalysts for the hydrolytic kinetic resolution (HKR) of epichlorohydrin. In this case, the high, local concentration of active sites becomes extremely important, since the transition state of the HKR mechanism has been theorized to follow a bimetallic pathway.[21] The second example illustrates a versatile organic, piperazine base catalyst for the Knoevenagel reaction of benzaldehyde with malononitrile. Using this type of catalyst architecture, a large variety of magnetic, organometallic and organic catalysts may be developed with high catalyst loading at high local concentrations.

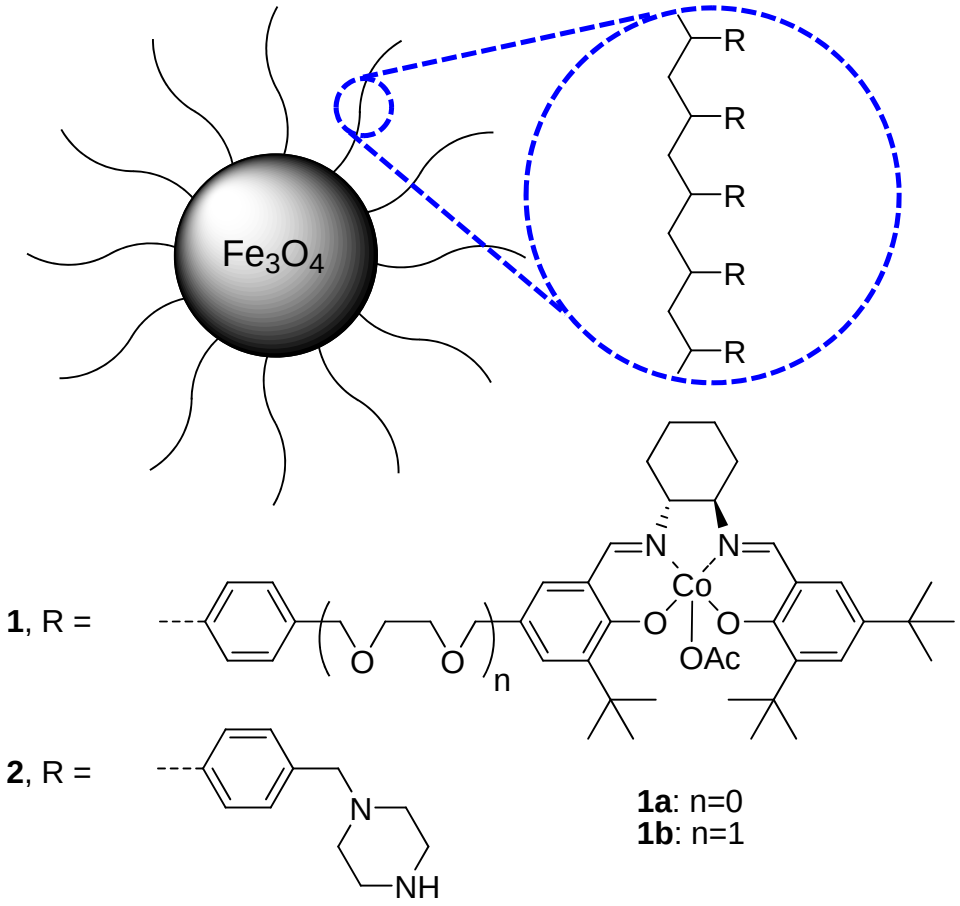

Figure 5.1 - Magnetic polymer brush catalysts used in this work: (**1a**, **1b**) Co(III)-salen MPB and (**2**) piperazine MPB.

5.2 Experimental procedures

5.2.1 General remarks

All chemicals were used as received unless specified otherwise. Air and water sensitive reactions were performed in a nitrogen glove box unless described otherwise. Dichloromethane (DCM, <50 ppm water) was further dried over columns packed with activated alumina. Anhydrous tetrahydrofuran (THF), hexane, and toluene (all <50 ppm water) were further dried over columns of activated copper oxide and alumina.[22] Styrene was washed with 5% NaOH to remove inhibitors, dried over magnesium sulfate, distilled over calcium hydride, and stored at -23°C in a nitrogen glove box prior to use.

5.2.2 Instrumentation

Enantiomeric excesses (*ee*'s) of epichlorohydrin were measured by capillary gas-phase chromatography analysis on a Shimadzu GC 14A instrument equipped with a FID detector and a Chiraldex γ-TA column (40 m × 0.25 mm × 0.12 μm). A Netzsch Thermoanalyzer STA 409 was used for thermogravimetric analysis (TGA) and differential scanning calorimetry (DSC) with a heating rate of 10°C/min in air. Elemental analyses were performed by Columbia Analytics Lab (Tucson, AZ, USA) or Galbraith (Knoxville, TN, USA). FT-IR spectra were obtained on a Perkin Elmer Spectrum 1000 spectrometer using KBr pellets.

5.2.3 Synthesis of ATRP initiator functionalized Fe_3O_4 nanoparticles

Oleic acid stabilized Fe_3O_4 nanoparticles[23] and an ATRP initiator silane[24] were synthesized following published procedures. A dispersion of oleic acid stabilized Fe_3O_4 nanoparticles in toluene (215 mL, 0.014 mg/mL, 3.01 g Fe_3O_4-OA) was combined with additional toluene (35 mL), ATRP initiator silane (3.01 g), and triethylamine (8.5 g).[23] The mixture was stirred for three days under nitrogen atmosphere at room temperature. The resulting ATRP initiator functionalized magnetic nanoparticles (MNPs) were recovered by magnetic separation from slow addition of the toluene dispersion into petroleum ether (100 mL). The MNPs were isolated and redispersed into toluene (20 mL). The MNPs washed five additional times by repeating this procedure. Finally, the MNPs were dried under high vacuum at room temperature overnight and stored in a nitrogen glovebox.

5.2.4 Synthesis of Co-salen MPB catalysts 1a, 1b

Styryl-modified salen monomers[25-28] were synthesized according to reported procedures. In a nitrogen glovebox, copper (I) bromide (34 mg, 0.23 mmol) was dissolved in hexamethyltriethylenetetramine (HMTETA, 59 mg, 0.26 mmol) and DMF

(100 mg) in a 15 mL pressure tube reactor. Styryl-modified salen (1.63 mmol, 1 eq.) dissolved in toluene (8.2 g), ATRP initiator modified Fe_3O_4 nanoparticles (680 mg) and styrene (680 mg, 6.5 mmol, 4 eq.) were added to the pressure tube, sequentially. The reactor was sealed, removed from the glovebox, stirred, and heated (110°C, 60 hours) to form the magnetic polymer brush material. The MPB was precipitated into anhydrous DMF (80 mL) by dropwise addition of the reaction mixture and recovered magnetically. The recovered particles were decanted and dispersed in toluene (20 mL) via ultrasonication (10 min). The dropwise precipitation and magnetic recovery in DMF was repeated three times to remove the copper bromide catalyst. The recovered particles were decanted and redispersed in toluene (50 mL), followed by dropwise addition and precipitation into hexane (100 mL). This process was repeated two more times to remove DMF. Finally, the recovered particles were decanted and dried under high vacuum (24 hrs, room temperature). The dry particles (560 mg) were metallated with anhydrous cobalt acetate (127 mg) in 50/50 methanol/DCM (16 mL total) by refluxing under argon (48 hrs). In a glovebox, the particles were recovered magnetically and subsequently washed three times with a 50/50 methanol/DCM solution (20 mL total) to remove excess cobalt acetate. The particles were dried under high vacuum (24 hrs) and stored in a glovebox.

5.2.5 Synthesis of MPB catalyst 2

Magnetic polymer brush catalyst **2** was synthesized similar to **1a** and **1b**. In a nitrogen glovebox, copper (I) bromide (24 mg, 0.17 mmol) was dissolved in HMTETA (43 mg, 0.19 mmol) and DMF (121 mg) in a 15 mL pressure tube reactor. N-(4-vinylbenzyl)piperazine[29] (1.21 g, 6 mmol) dissolved in toluene (6.0 g) and ATRP initiator modified Fe_3O_4 nanoparticles (500 mg) were added to the pressure tube. The reactor was sealed, removed from the glovebox, stirred, and heated (110°C, 60 hrs) to form catalyst **2**. The catalyst was washed and dried similar to catalysts **1a** and **1b**.

5.2.6 General procedure for HKR reactions

Precatalyst **1a** and **1b** were tested in the hydrolytic kinetic resolution of epichlorohydrin. Precatalyst **1** (0.5 mol% Co(III)-salen sites, 34 mg for **1a**, 38 mg for **1b**) was activated with DCM (1 mL) and glacial acetic acid (100 uL) in a 5 mL pear shaped flask. The catalyst particles were dispersed via ultrasonication (5 min) and stirred open to air (30 min, 23°C). The solution was removed by rotovap followed by drying under high vacuum (30 min). Epichlorohydrin (234.6 uL, 3 mmol, 1 eq.) and chlorobenzene (27.3 uL, internal standard) were added to the flask. The reaction was initiated by addition of water (32.4 uL, 1.8 mmol, 0.6 eq.) and stirred at room temperature. Samples (2 uL) were removed, diluted with acetone (1 mL), decanted from the magnetically separated catalyst, and analyzed via chiral GC. Upon reaching 99% *ee* of the remaining epichlorohydrin, the reaction was quenched with excess anhydrous THF (3 mL). The catalyst was recovered magnetically and decanted. Fresh anhydrous THF (3 mL) was added and the catalyst was dispersed via ultrasonication (5 min). This procedure was repeated four times to remove water, epichlorohydrin, and the diol product. The remaining catalyst was dried under high vacuum (12 hours). Recycle experiments were performed by scaling the amounts of epichlorohydrin, water, and chlorobenzene to the mass of recovered catalyst. The catalyst was reactivated with acetic acid prior to each cycle.

5.2.7 General procedure for Knoevenagel reactions

Catalyst **2** was tested in the Knoevenagel reaction of benzaldehyde with malononitrile. A solution of benzaldehyde (203.8 uL, 2 mmol), dodecane (454.2 uL, 2 mmol, internal standard), and THF (1.0 mL) was added to catalyst **2** (39 mg, 10 mol% piperazine) in a pear shaped flask (10 mL). The reaction was initiated by quick addition of a solution of malononitrile (264 mg, 4 mmol) in THF (1.0 mL). Samples (10 uL) were removed periodically, diluted with acetone (1 mL), decanted from the magnetically separated catalyst, and analyzed via GC. Upon completion, the reaction was diluted with

excess anhydrous THF (5 mL). The catalyst was recovered magnetically, and the solution was decanted. Fresh anhydrous THF (5 mL) was added and the catalyst was dispersed via ultrasonication (5 min). This procedure was repeated four times to thoroughly wash the catalyst. The remaining catalyst was dried under high vacuum (12 hours). Recycle experiments were performed by scaling the reaction to the mass of recovered catalyst.

5.3 Results and discussion

The magnetic polymer brush catalysts were synthesized based on modified published procedures. Oleic acid stabilized, superparamagnetic iron oxide nanoparticles (Fe_3O_4) were synthesized via an aqueous method followed by extraction into an organic phase.[23] Silane modified ATRP initiators were then synthesized and grafted to the nanoparticles.[24] Salen[27, 28, 30] and piperazine[29] modified styrene monomers were synthesized, and polymerized via ATRP[23, 30] to form the magnetic polymer brush (MPB) catalysts (Figure 5.1). The salen-modified polymer brushes were subsequently metallated with cobalt acetate and activated with acetic acid to form the Co(III)-salen catalysts **1a** and **1b** while the piperazine modified polymer brush catalyst **2** required no subsequent modification.

5.3.1 TEM, EA, and TGA characterization of magnetic polymer brush catalysts

The oleic acid stabilized and ATRP functionalized magnetic nanoparticles both displayed very monodisperse, non-aggregated nanoparticles roughly 10 to 14 nm in diameter (Figures 5.2 and 5.3). Upon ATRP polymerization, the organic content of MPB catalysts **1a** and **2** were observed to be 65 and 58%, respectively, via thermogravimetric analysis. This organic polymer was visible via TEM as a roughly 5 nm thick coating encasing the Fe_3O_4 nanoparticles (Figures 5.4 and 5.5). These particles exhibited some aggregation, and as such, care was taken to wash the particles thoroughly and disperse them in solution prior to catalytic reactions via sonication. Elemental analysis indicated

cobalt loadings of 0.45 and 0.39, respectively, for **1a** and **1b** and a nitrogen content of 7.2% (2.6 mmol piperazine/g) for **2**.

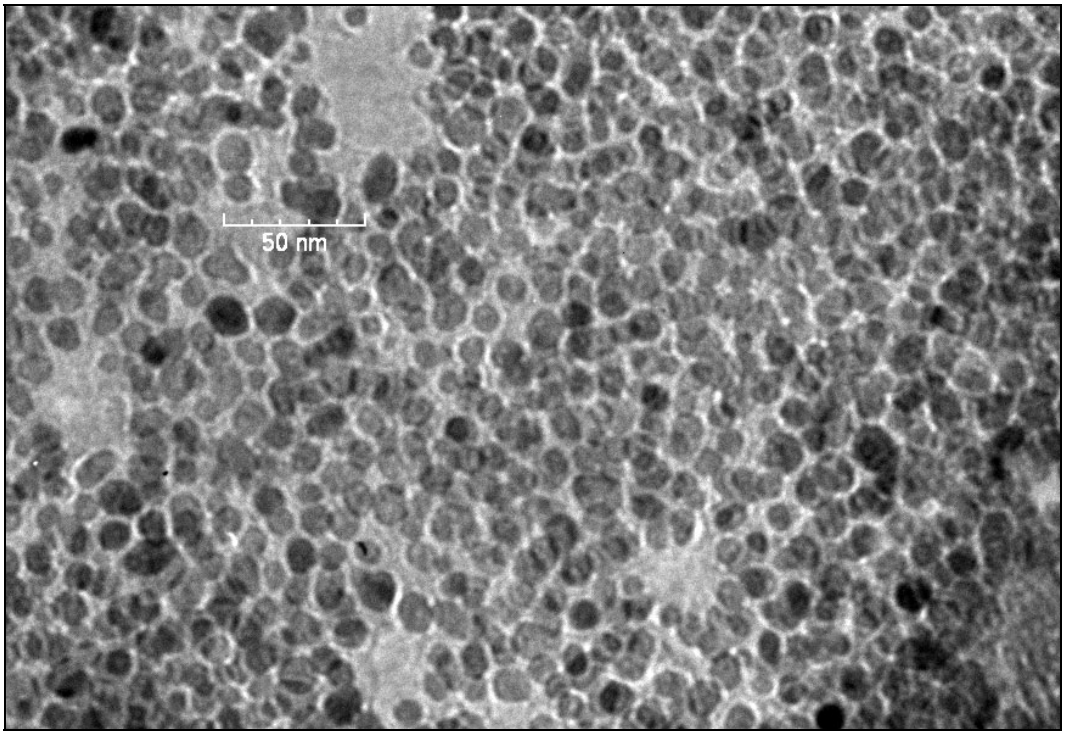

Figure 5.2 - TEM image of oleic acid stabilized Fe_3O_4 magnetic nanoparticles. Scale bar denotes 50 nm.

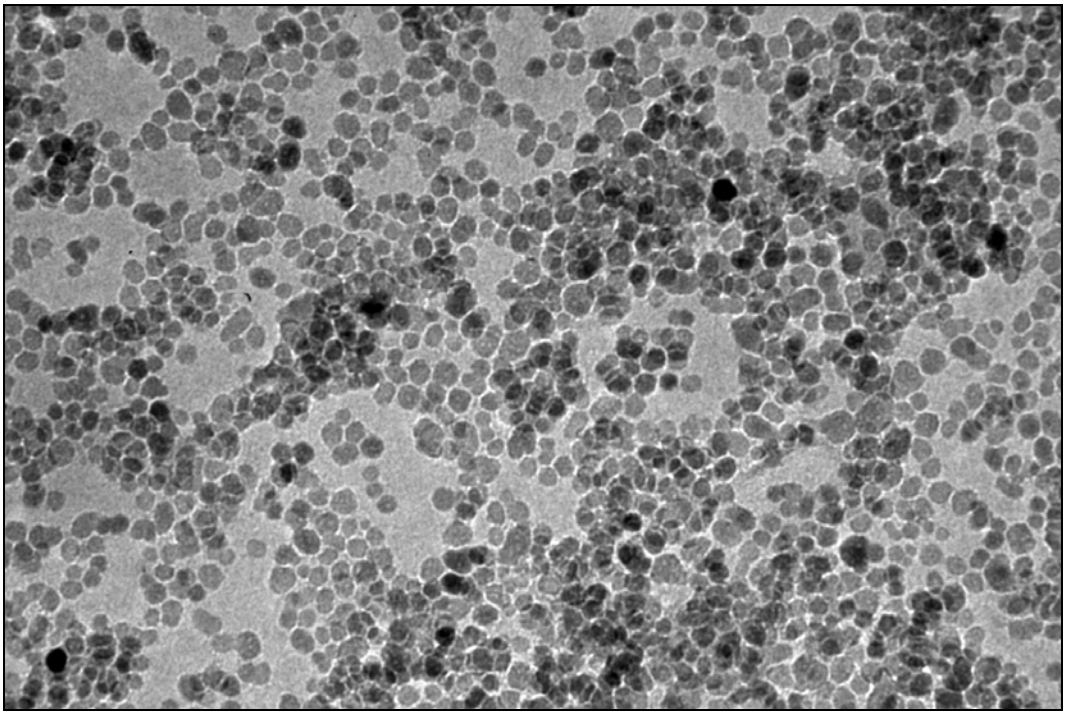

Figure 5.3 - TEM image of ATRP initiator functionalized Fe_3O_4 magnetic nanoparticles.

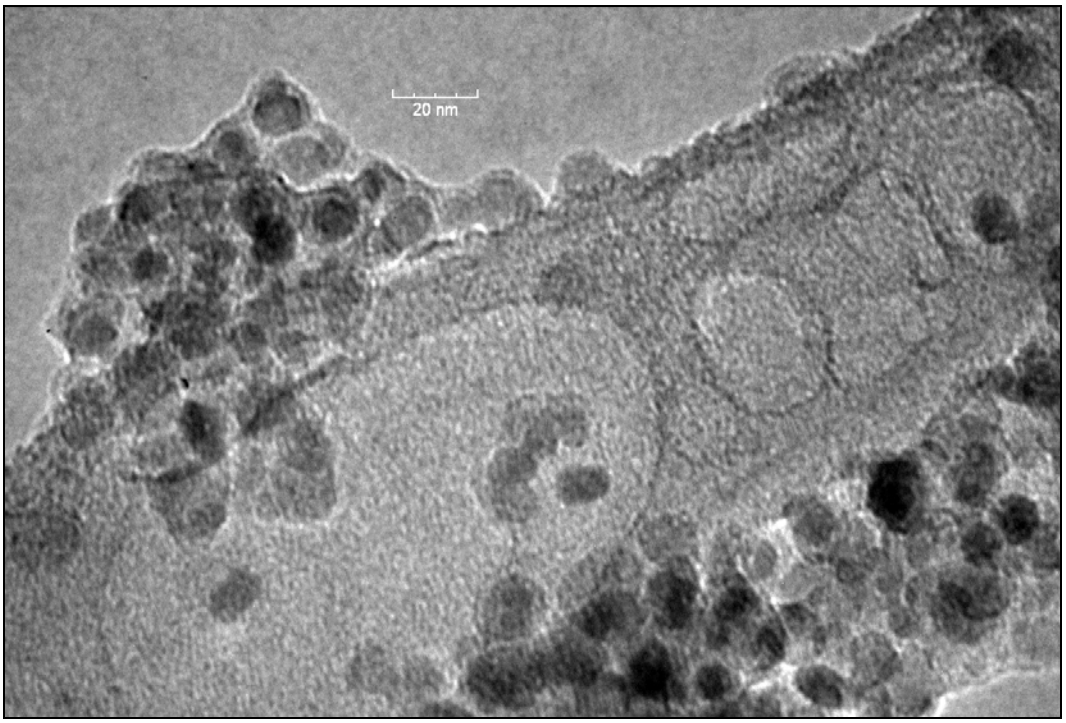

Figure 5.4 - TEM image of magnetic polymer brush catalyst **1a** on lacey grids. Scale bar denotes 20 nm.

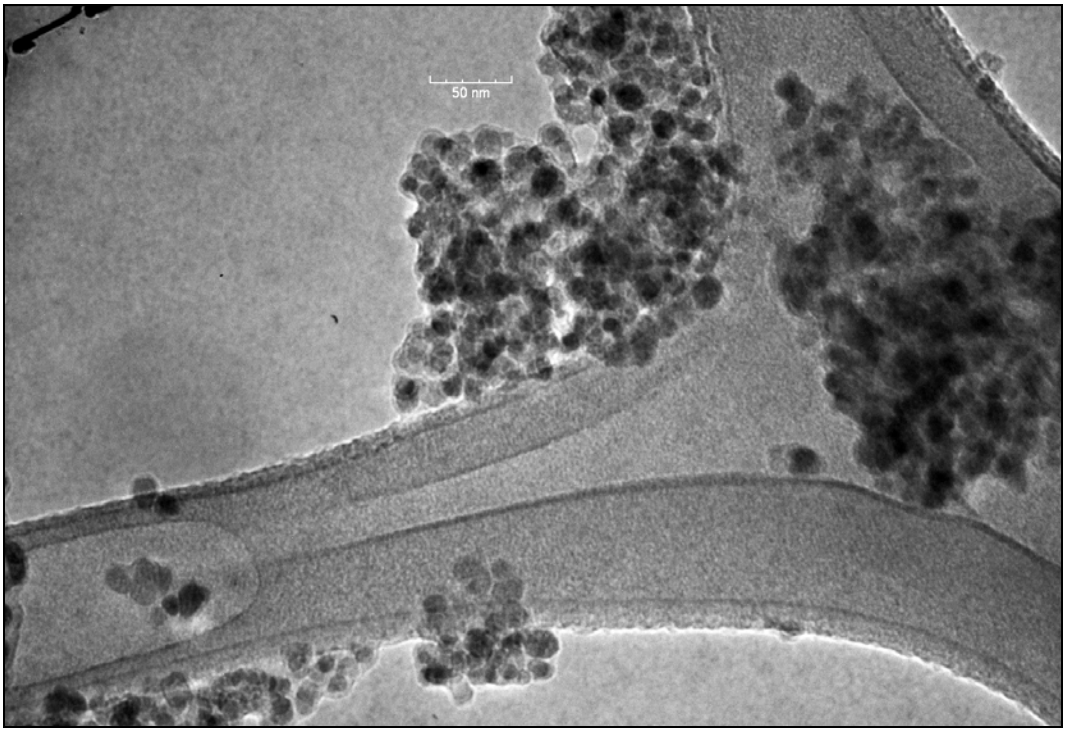

Figure 5.5 - TEM image of Co-salen functionalized polymer brush catalyst **1a** on lacey grids. Scale bar denotes 50 nm.

5.3.2 FT-IR characterization of magnetic polymer brushes

The expected peaks were observed in the FT-IR spectra for the oleic acid stabilized Fe_3O_4 nanoparticles (Figure 5.6). The main peaks were the 1560 and 1540 cm^{-1} peaks associated with the COO^- stretch, aliphatic C-H stretches at 2920 and 2850 cm^{-1}, and the Fe-O stretching vibration at 594 and 630 cm^{-1}. Upon grafting of the ATRP surface initiator, the 1560 cm^{-1} COO^- stretch was replaced with the 1735 cm^{-1} carbonyl stretch in the ester group of the initiator. An additional Si-O vibration appeared at 1036 cm^{-1}.

Catalyst **2** displayed weak aromatic C-H stretches at 3030 cm^{-1}, strong aliphatic C-H stretches, and strong, broad N-H stretch around 3400 cm^{-1}, supporting formation of the piperazine modified polymer brush. Catalysts **1a** and **1b** displayed aromatic and aliphatic C-H stretches, indicating presence of polymer. A sharp imine stretch appeared at 1626 cm^{-1} for the non-metallated H_2salen MPB, which shifted to 1602 cm^{-1} upon metallation to form Co(II)-salen MPB catalysts **1a** and **1b**.

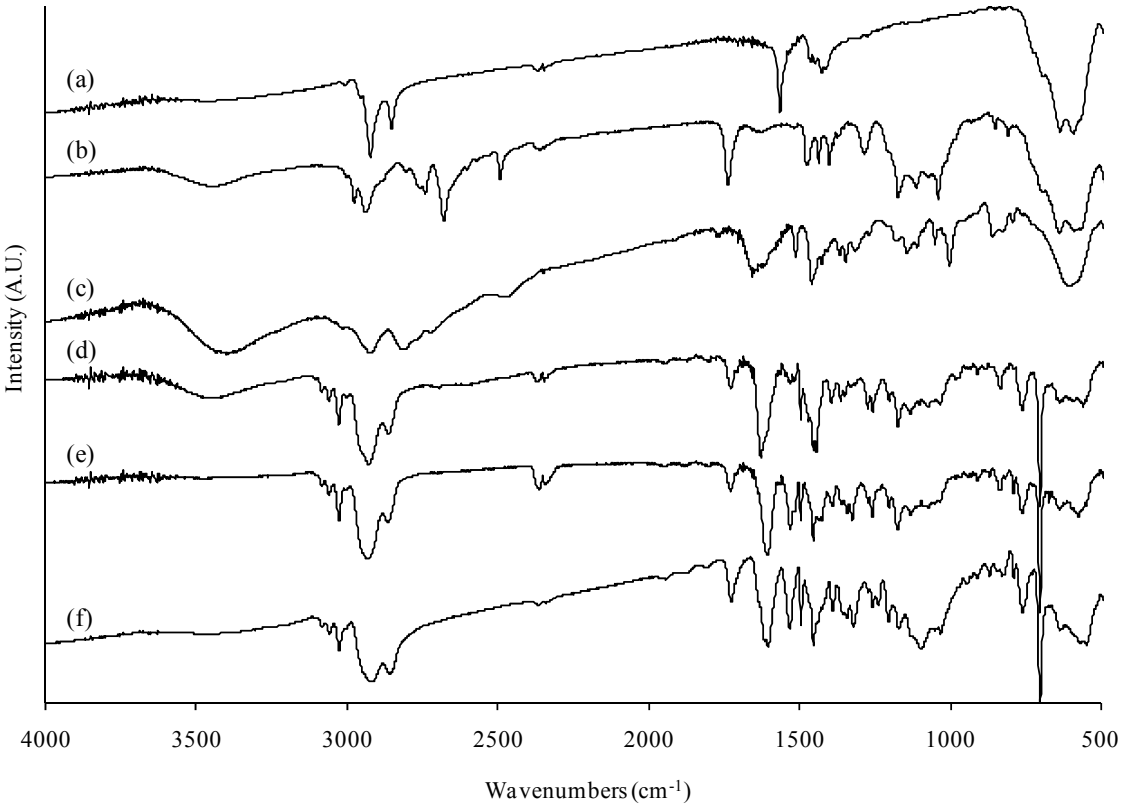

Figure 5.6 - FT-IR spectra of (a) oleic acid stabilized Fe_3O_4 nanoparticles, (b) ATRP initiator functionalied Fe_3O_4 nanoparticles, (c) piperazine functionalized magnetic polymer brush **2**, (d) non-metallated H_2salen polymer brush (precursor to **1a**), (e) metallated Co-salen polymer brush catalyst **1a**, and (f) metallated Co-salen polymer brush catalyst **1b**.

5.3.3 Catalytic studies

Two different catalysts were selected to illustrate the versatility of the magnetic polymer brush materials to accommodate a variety of functional groups: organometallic Co-salen and organic piperazine catalysts. Catalysts **1a** and **1b** were tested and recycled in the HKR of epichlorohydrin. Catalyst **1a** reached 98% ee at 54% conversion after 120 min using 0.5 mol% loading. Catalyst **1b** was observed to be more active than **1a**, in agreement with previous reports due to enhanced cooperativity allowed by the flexible linker.[28, 30] It achieved >99% ee after 60 minutes and generated high enantioselectivities (≥99 to 98%) of the remaining epoxide after each of three cycles (Table 5.1). The polymer brush architecture was exploited in this reaction, as kinetic studies of the HKR

reaction have indicated a second order rate dependence on the concentration of catalyst, presumably resulting from a bimetallic reaction mechanism.[21] Since the MPB architecture promotes high local catalyst concentrations, these bimetallic interactions are enhanced, resulting in surprisingly high activities for the hybrid catalyst. In comparison, the homogeneous Co(III)-salen only generated 93% *ee* at 48% conversion after 60 minutes at 0.5 mol%. At lower catalyst concentrations of 0.01 mol%, polymer brush Co-salen catalysts have been shown to be 18 times more active than the homogeneous catalysts due to the inherent cooperativity built into the polymer brush materials.[30] Although selectivities for catalyst **1b** remained high after three cycles, initial rates and activities decreased marginally, as was observed with previous supported Co-salen catalysts (Figure 5.7).[30] The likely deactivation pathway likely proceeded via decomposition of the salen ligand by cleavage of the imine as outlined in Chapter 4.

Table 5.1 - Recycle data for the HKR by catalyst **1b** at 0.5 mol%.

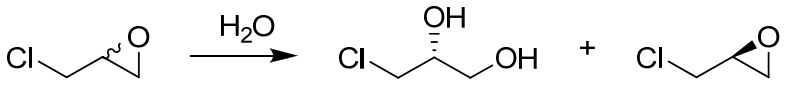

Cycle #	Time (min)	Conversion (%)	*ee* (%)[a]
1	60	54	>99
2	90	56	>99
3	120	51	98

[a] *ee* of the remaining epichlorohydrin determined by chiral GC.

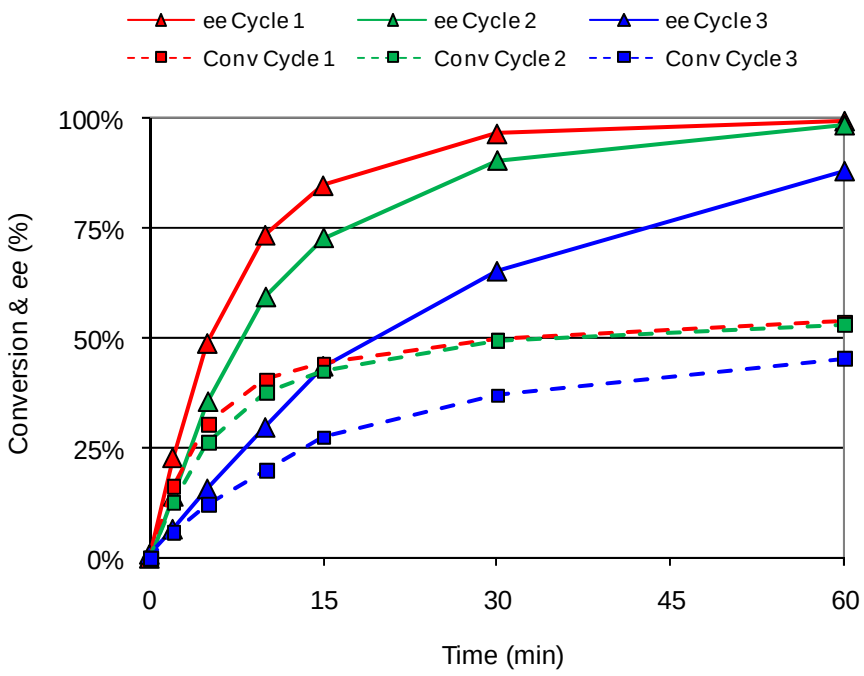

Figure 5.7 - Recyclability of Co-salen functionalized MPB catalyst **1b**.

Catalyst **2** displayed ≥99% conversion in the Knoevenagel reaction after 3 cycles at 18 hrs, showing the catalyst is recyclable (Table 5.2). While piperazine is generally not a commonly used Knoevenagel catalyst, this base was chosen to illustrate how a MPB can be synthesized that gives quantitative conversion due to high catalyst loadings. Conversely, only moderate to high yields could be obtained using other supported piperazine catalysts under using microreactor[31] or microwave conditions.[32] Catalyst **2** was run at 10 mol% but only 15% w/w (catalyst to benzaldehyde limiting reactant), demonstrating how high loadings can be achieved with low mass fractions of catalyst. Additionally, unlike soluble polymeric catalysts, the MPB catalysts are easily recovered using readily available NdFeB rare earth magnets.

Even though the catalyst is recyclable, decreasing activities were observed from kinetic data (Figure 5.8). Unlike the Co-salen MPB, the likely deactivation pathway using this catalyst involved loss of active sites on the MNP support by hydrolysis of the ester

group in the linker. In the presence of the piperazine base catalyst and water, a byproduct in the reaction, the ester group can cleave and the resulting polymer would be removed during the washing cycles prior to reuse of the catalyst. Although the ester containing ATRP initiator silane was sufficient for proof of concept of MPB catalysts, a more stable linker is necessary for future studies. Syntheses for four novel non-hydrolyzable ATRP initiator silanes are outlined in the future work section of Chapter 7.

Table 5.2 - Recycle data for the Knoevenagel reaction by catalyst **2** at 10 mol%.

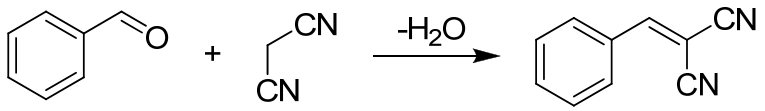

Cycle #	Time (hr)	Conv. (%)[a]
1	18	100
2	18	100
3	18	99

[a] Conversion of benzaldehyde.

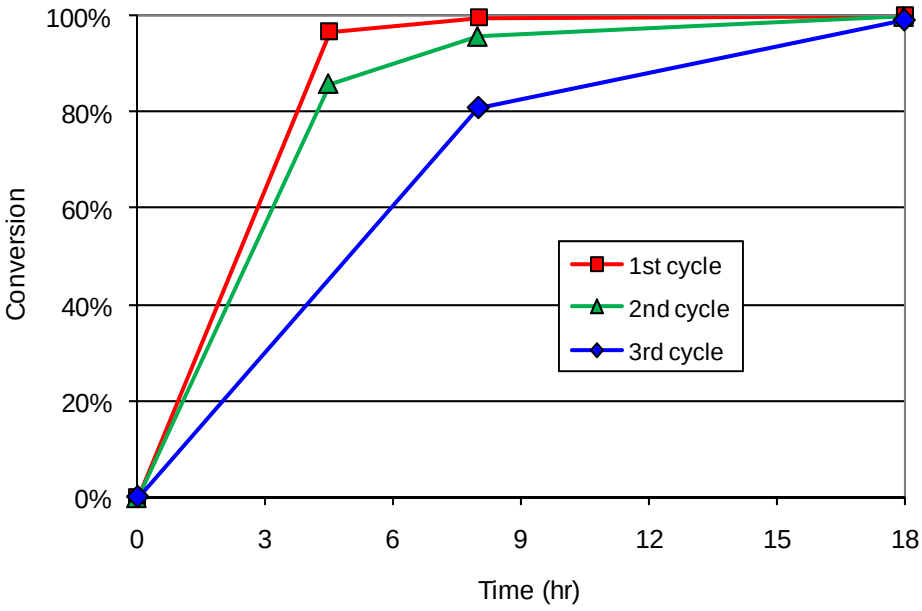

Figure 5.8 - Recyclability of piperazine modified MPB **2**.

5.4 Summary

In conclusion, magnetic nanoparticle polymer brush materials can offer a versatile new support for hybrid organic/inorganic catalysis. The ability to polymerize modified styrene monomers from surface bound initiators allows for a wide variety of functionalized polymers. These type materials could have a wide variety of applications ranging from catalyst supports to metal scavengers to targeted drug delivery vehicles, simply by synthetically modifying the organic or organometallic functionalities on the polymer chain either pre- or post- ATRP polymerization from the supported initiators. Future work will be devoted to detailed rate studies and characterization of the MPB catalysts as well as investigating effects of varying ATRP initiators upon catalyst stability.

5.5 Acknowledgements

The authors would like to thank DOE-BES through Catalysis Science contract DE-FG02-03ER15459 for financial support.

5.6 References

1. Gladysz, J.A., *Chem. Rev.* **2002**, 102, 3215.
2. Benaglia, M., Puglisi, A., and Cozzi, F., *Chem. Rev.* **2003**, 103, 3401.
3. Hoffmann, F., Cornelius, M., Morell, J., and Froba, M., *Angew. Chem. Int. Ed.* **2006**, 45, 3216.
4. Wight, A.P. and Davis, M.E., *Chem. Rev.* **2002**, 102, 3589.
5. Fan, J. and Gao, Y., *J. Exp. Nanosci.* **2006**, 1, 457.
6. Gill, C.S., Price, B.A., and Jones, C.W., *J. Catal.* **2007**, 251, 145.
7. Phan, N.T.S., Gill, C.S., Nguyen, J.V., Zhang, Z.J., and Jones, C.W., *Angew. Chem. Int. Ed.* **2006**, 45, 2209.
8. Phan, N.T.S. and Jones, C.W., *J. Mol. Catal. A: Chem.* **2006**, 253, 123.
9. Luo, S.Z., Zheng, X.X., Xu, H., Mi, X.L., Zhang, L., and Cheng, J.P., *Adv. Synth. Catal.* **2007**, 349, 2431.
10. O' Dalaigh, C., Corr, S.A., Gun'ko, Y., and Connon, S.J., *Angew. Chem. Int. Ed.* **2007**, 46, 4329.
11. Yoon, T.J., Lee, W., Oh, Y.S., and Lee, J.K., *New J. Chem.* **2003**, 27, 227.
12. Stevens, P.D., Li, G.F., Fan, J.D., Yen, M., and Gao, Y., *Chem. Commun.* **2005**, 4435.

13. Stevens, P.D., Fan, J.D., Gardimalla, H.M.R., Yen, M., and Gao, Y., *Org. Lett.* **2005**, 7, 2085.
14. Hu, A.G., Yee, G.T., and Lin, W.B., *J. Am. Chem. Soc.* **2005**, 127, 12486.
15. Zheng, Y., Stevens, P.D., and Gao, Y., *J. Org. Chem.* **2006**, 71, 537.
16. Duanmu, C., Saha, I., Zheng, Y., Goodson, B.M., and Gao, Y., *Chem. Mat.* **2006**, 18, 5973.
17. Abu-Reziq, R., Alper, H., Wang, D.S., and Post, M.L., *J. Am. Chem. Soc.* **2006**, 128, 5279.
18. Ding, S.J., Xing, Y.C., Radosz, M., and Shen, Y.Q., *Macromolecules* **2006**, 39, 6399.
19. Lv, G.H., Mai, W.P., Jin, R., and Gao, L.X., *Synlett* **2008**, 1418.
20. Arai, T., Sato, T., Kanoh, H., Kaneko, K., Oguma, K., and Yanagisawa, A., *Chem. Eur. J.* **2008**, 14, 882.
21. Nielsen, L.P.C., Stevenson, C.P., Blackmond, D.G., and Jacobsen, E.N., *J. Am. Chem. Soc.* **2004**, 126, 1360.
22. Pangborn, A.B., Giardello, M.A., Grubbs, R.H., Rosen, R.K., and Timmers, F.J., *Organomet.* **1996**, 15, 1518.
23. Sun, Y.B., Ding, X.B., Zheng, Z.H., Cheng, X., Hu, X.H., and Peng, Y.X., *Eur. Polym. J.* **2007**, 43, 762.
24. Marsh, A., Khan, A., Garcia, M., and Haddleton, D.M., *Chem. Commun.* **2000**, 2083.
25. Holbach, M. and Weck, M., *J. Org. Chem.* **2006**, 71, 1825.
26. Holbach, M., Zheng, X.L., Burd, C., Jones, C.W., and Weck, M., *J. Org. Chem.* **2006**, 71, 2903.
27. Zheng, X.L., Jones, C.W., and Weck, M., *Chem. Eur. J.* **2006**, 12, 576.
28. Zheng, X.L., Jones, C.W., and Weck, M., *Adv. Synth. Catal.* **2008**, 350, 255.
29. Gross, A., Maier, G., and Nuyken, O., *Molec. Chem. Phys.* **1996**, 197, 2811.
30. Gill, C.S., Venkatasubbaiah, K., Phan, N.T.S., Weck, M., and Jones, C.W., *Chem. Eur. J.* **2008**, 14, 7306.
31. Nikbin, N. and Watts, P., *Org. Process Res. Dev.* **2004**, 8, 942.
32. Yang, G., Chen, Z., Xu, G., and Nie, X., *Catal. Commun.* **2004**, 5, 75.

CHAPTER 6

RECYCLABLE POLYMER AND SILICA SUPPORTED RUTHENIUM(II)-SALEN BIS-PYRIDINE CATALYSTS FOR THE ASYMMETRIC CYCLOPROPANATION OF OLEFINS

6.1 Introduction

Like the supported Co-salen catalysts discussed in Chapters 4 and 5, Ru-salen catalysts also promote enantioselective, or asymmetric, reactions. Although reports of supported Co-salen catalysts are common in the open literature, very few reports of supported Ru-salen catalysts appear. Furthermore, no examples of supported Ru-salen catalysts for the asymmetric cyclopropanation of olefins could be found. For this reason, developing techniques for supporting these catalysts on insoluble supports was difficult but warranted. This chapter discusses immobilization of Ru-salen catalysts on silica and polymer supports and compares them to other leading supported asymmetric cyclopropanation catalysts.

Asymmetric synthesis of chiral cyclopropyl chemicals is of particular importance in the pharmaceutical and agro-chemical industries as an alternative method of procuring these important chiral building blocks used in the preparation of drugs and pesticides.[1-3] Researchers have developed numerous homogeneous catalysts to facilitate synthesis of these chiral cyclopropyl products.[4-10] Optimizing catalysts to produce desired products in high atom economy has been of particular importance. Consequently, all asymmetric cyclopropanation catalysts are judged based on their activity, diasteroselectivity to *cis* or *trans* cyclopropyl products, and enatioselectivities (*ee*) of the resulting *cis* and *trans*

products. Recently, ruthenium-salen catalysts have been shown to demonstrate high activities and selectivities for the cyclopropanation of olefins (Scheme 6.1), while maintaining functional group tolerance for a range of electronically diverse olefins.[11-13]

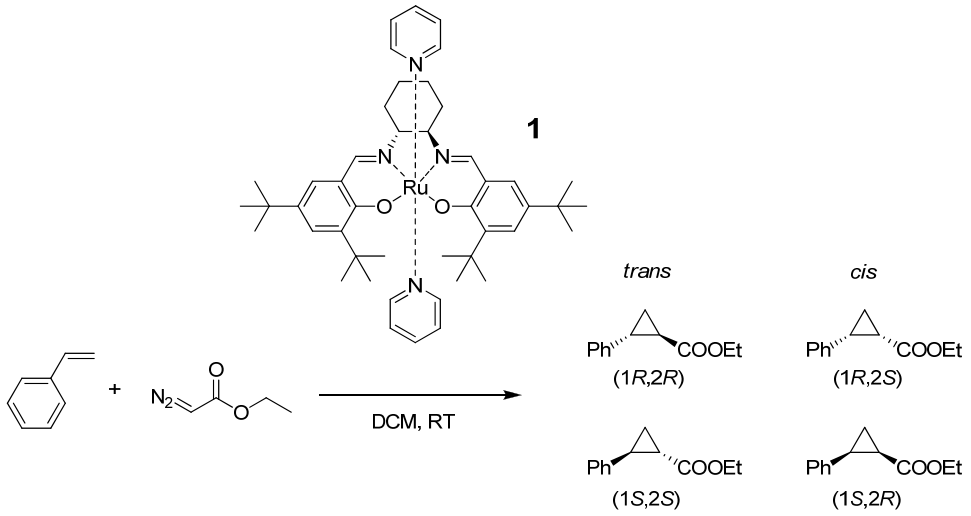

Scheme 6.1 - Ru(II)-salen bis-pyridine catalyzed asymmetric cyclopropanation of styrene with ethyldiazoacetate.

In addition to ruthenium, a number of other salen complexes with cobalt and iridium have shown activity in the cyclopropanation of olefins.[9, 10, 14, 15] It is commonly accepted this mechanism proceeds via the addition of carbene intermediates across the C=C double bond of the olefin to form the cyclopropyl products. A recent density functional theory (DFT) simulation predicted a ruthenium-2,6-bis(oxazolin-2-yl)pyridine (pybox) catalyst follows a concerted pathway for the cyclopropanation of olefins, meaning that all bond breaking and creation occurs in a single step.[16] The ruthenium-salen and ruthenium-pybox cyclopropanation reactions likely follow similar mechanisms due to the similarity of the ligands (Figure 6.1). Previous work using cobalt-Schiff base catalysts for cyclopropanation reactions predicted the mechanism followed a concerted pathway only when the Schiff bases are bridged by an ethylene unit, otherwise called

salen ligands.[17] When the Schiff bases were not connected, the complex was able to contort, creating two vacant coordination sites and resulting in metallacyclobutane intermediates. Thus, both researchers proposed metallacycle intermediates were only probable in ligands allowing for adjacent vacant coordination sites, as is the case with ruthenium based olefin metathesis chemistry. Since the pybox and salen ligands do not permit adjacent coordination sites, the metallacycle pathway for formation of cyclopropanes is not predicted, and a concerted pathway is favored. This also explains why olefin metathesis products are not observed during Ru-salen or Ru-pybox cyclopropanation reactions.

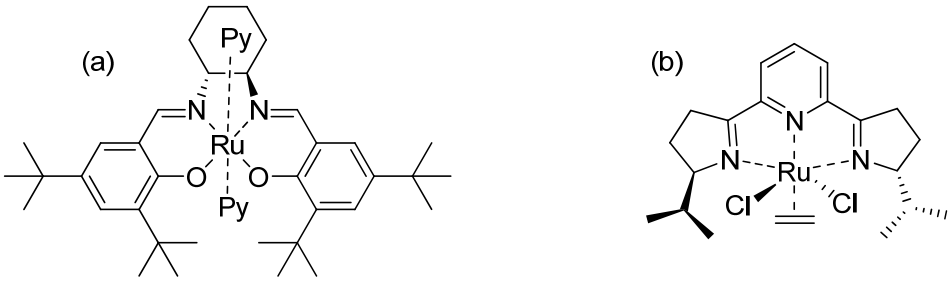

Figure 6.1 – (a) Ru-salen and (b) Ru-pybox asymmetric cyclopropanation catalysts.

The Ru-salen catalyzed cyclopropanation mechanism is redrawn based on the DFT predicted Ru-pybox mechanism (Figure 6.2).[16] The Ru-salen-bis(pyridine) precatalyst dissociates one pyridine ligand, creating a vacant coordination site to enter the catalytic cycle. Ethyldiazoacetate then coordinates to ruthenium at the vacant site. A ruthenium carbene intermediate is formed by simultaneous nitrogen extrusion. Olefin association and carbene addition across the C=C double bond then occur in a concerted reaction. A new intermediate is formed with the carbonyl of the ester group coordinated to the ruthenium center. The product dissociates, closing the catalytic cycle.

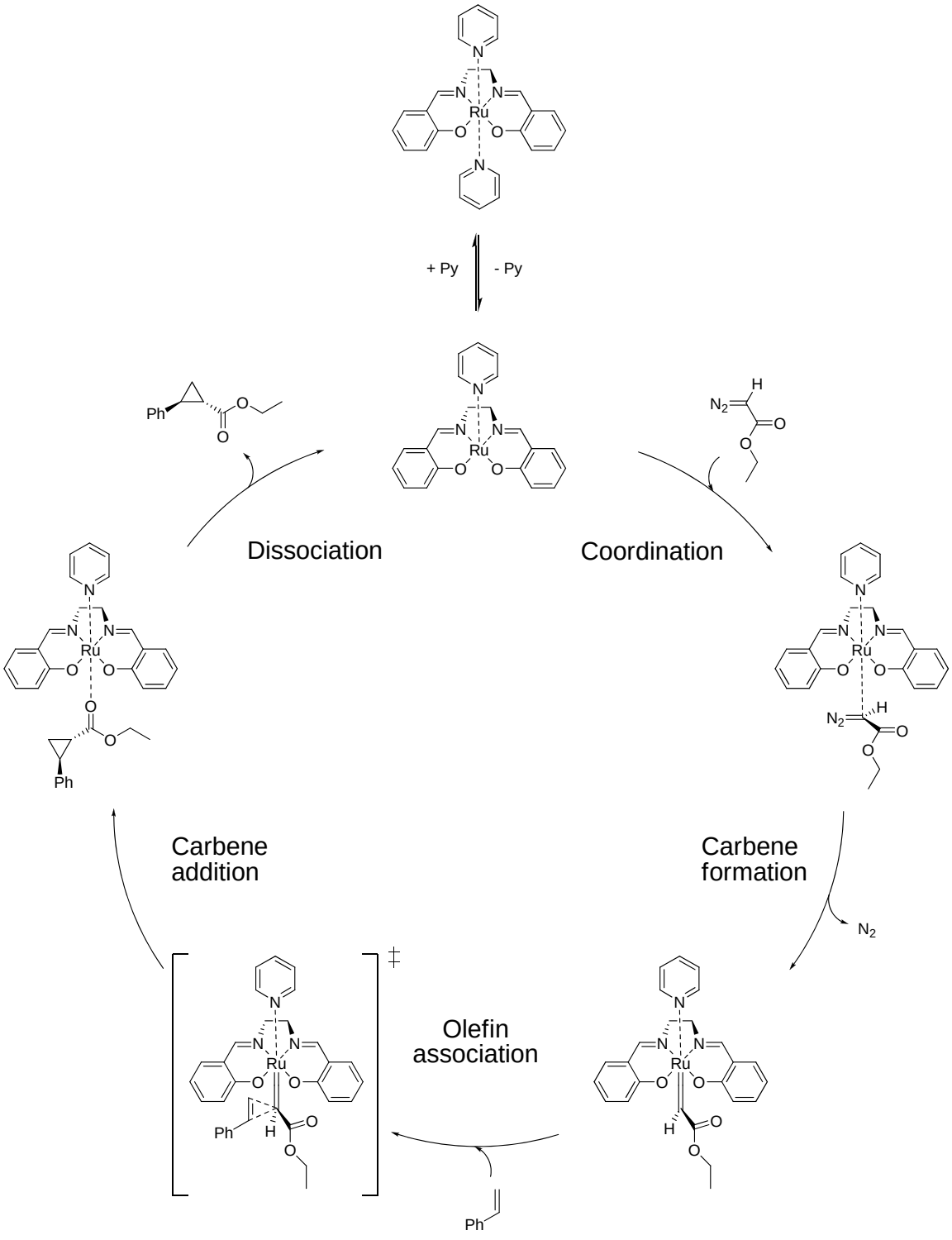

Figure 6.2 – Probable mechanism for the cyclopropanation of styrene by Ru-salen catalyzed decomposition of ethyldiazoacetate. Cyclohexyl and *t*-butyl groups in salen ligand omitted for clarity.

The Ru-pybox DFT study proposed the enantioselectivity and diastereoselectivity of the reaction resulted from steric interactions between the incoming olefin and one of the bulky isopropyl groups on the pybox ligand. The bulky t-butyl groups in the salen ligand likely affect the approach of the olefin in a similar manner, resulting in the high diastereoselectivities and enantioselectities observed.

With advancements in homogeneous asymmetric cyclopropanation catalysis, several researchers have been working on development of supported, single-sited heterogeneous catalysts in parallel. Immobilization of these catalysts on solid phase supports allows for the facile recovery and reuse of the asymmetric catalyst, which can be important for a variety of economic, environmental, and quality control reasons. Research in this area has mainly focused on supported copper, rhodium, and ruthenium complexes.[18-20] While much research has focused on supported copper bis(oxazoline) (Box) and related complexes,[20] increasing reports of supported ruthenium catalysts have appeared due to their high activity, selectivity, and advantages of ruthenium over the copper based systems: superior diastereoselectivities, functional group tolerance, and ease of use. These reports include ruthenium pyridine-bis(oxazoline) (PyBox) complexes grafted to polymers,[21, 22] encapsulated within polymers,[23] and grafted to silica.[24] Additional examples of polymer[25] and silica[26] supported ruthenium porphyrins exist. Despite the promising results of homogeneous Ru-salen cyclopropanation catalysts, no reports of Ru-salen catalysts covalently grafted to solid supports exists at present. Only a single report of Ru-salen catalysts coordinated to poly(4-vinylpyridine) for aldehyde olefination appears, but this catalyst was hampered by poor recyclability due to leaching

of the active Ru-salen catalyst by dissociation of the Ru-N coordination to the polymer support,[27] thus highlighting the need for covalent immobilization to solid supports.

Building on past work in our research group focused on development of supported Co-salen catalysts,[28-32] alternative techniques are developed here to produce the first report of heterogenized Ru-salen complexes covalently grafted to solid supports. The goal of this work was to develop a solid catalyst, stable over multiple cycles which retained the high activity, diastereoselectivity, and enantioselectivities exhibited by the homogeneous analogue in the asymmetric cyclopropanation of olefins with ethyldiazoacetate (EDA). This was accomplished via the immobilization of monofunctionalized, unsymmetrical, chiral salen ligands on polymer and silica supports to eventually produce covalently bound, surface-grafted Ru(II)-salen bis-pyridine catalysts. These catalysts were characterized via solid state CP MAS ^{13}C and ^{19}Si NMR, FT-IR, elemental analysis, and thermogravimetric analysis. This report highlights the synthesis and characterization of these immobilized catalysts, as well as investigations into their activity, selectivity, and recyclability in the cyclopropanation of styrene and other terminal olefins. Additionally, these polymer supported Ru-salen-Py_2 catalysts generated superior yields and selectivities compared to other leading solid supported asymmetric cyclopropanation catalysts.

6.2 Experimental procedures

6.2.1 General remarks

All chemicals were purified prior to use and stored in a nitrogen glove box, and all reactions were initiated in the glove box. Dichloromethane (DCM) was distilled over calcium hydride. Tetrahydrofuran (THF) and toluene were distilled over sodium. Hexane

(<50 ppm water) was further dried over columns of activated copper oxide and alumina.[33] Styrene was washed to remove inhibitors (5% NaOH, water, and brine), dried over magnesium sulfate, distilled over calcium hydride, and stored at -23°C in the glove box prior to use. Divinylbenzene was washed to remove inhibitors (5% NaOH, water, and brine) and dried over sodium sulfate immediately prior to use. Tridecane was dried over calcium hydride, vacuum distilled, and stored in the glove box. Ethyldiazoacetate (EDA) was degassed via three freeze-pump-thaw cycles and stored in the glove box at -23°C.

6.2.2 Instrumentation

Cross-polarization magic angle spinning (CP-MAS) solid-state NMR spectra were measured using a Bruker DSX 300-MHz spectrometer. Samples were packed in 7-mm zirconia rotors and spun at 6.6 kHz. Solid state ^{13}C CP-MAS spectra were recorded using 3000 scans, a 90° pulse length of 4 μs, and recycle times of 4 s. Solid state ^{29}Si CP-MAS were recorded using 5000 scans, a 90° pulse length of 5 μs, and recycle times of 5 s. Conversions of ethyldiazoacetate (EDA), product yields (via calibration curves from pure samples), and *trans*/*cis* product ratios were calculated using capillary gas-phase chromatography on a Shimadzu GC 2010 equipped with a FID detector and a SHRX5 column (15 m × 0.25 mm × 0.25 μm). The oven profile heated from 50°C to 250°C at 10°C/min. When using styrene as the olefin, enantiomeric excesses of the *trans* cyclopropyl products were measured on a Shimadzu GC 2010 equipped with a FID detector and a Beta DEX 225 column (30 m × 0.25 mm × 0.25 μm). The oven profile heated from 100°C to 140°C at 0.5°C/min. *Cis* cyclopropyl product *ee*'s were measured on a Shimadzu 14A GC with a FID detector and a Astec Chiraldex γ-TA column (40 m × 0.25 mm × 0.12 μm) using the same oven profile as the *trans* products. When using other

olefins, similar analytic methods were used as previously reported.[11] A Netzsch Thermoanalyzer STA 409 was used for thermogravimetric analysis (TGA) and differential scanning calorimetry (DSC) with a heating rate of 10°C/min in air. Elemental analyses were performed by Columbia Analytics Lab (Tucson, AZ, USA) or Galbraith Laboratories, Inc. (Knoxville, TN, USA).

6.2.3 Synthesis of insoluble polymer resin supported Ru(II)-salen bis-pyridine catalysts (4a) and (4b)

An insoluble polymer resin was synthesized by combining divinylbenzene (521 mg, 4 mmol, inhibitors removed and freshly dried), styryl-salen[29, 30, 32, 34] (593 mg for **4a**, 681 mg for **4b**, 1 mmol), and AIBN (44 mg, 0.27 mmol) in chlorobenzene (2.2 g). The reaction was stirred under argon (80°C, 48 hrs). The solid polymer resin was recovered via filtration and washed with copious methanol, hexane, DCM, THF, and ether. The resin was ground to a powder with a mortar and pestle, filtered again, and dried under high vacuum (room temperature, 12 hrs). The salen polymer resin was then metallated with ruthenium using a slightly modified procedure from literature.[11] Inside a glove box, *n*-butyllithium (1.6 M in hexane, 170 mg, 0.4 mmol) was added to a mixture of polymer resin (containing 0.2 mmol of salen) and THF (1.44 g) cooled to -23°C. The mixture was stirred and allowed to warm to room temperature (6 hrs). A mixture of $[Ru(Cy)_2Cl_2]_2$ (61 mg, 0.1 mmol), THF (2.1 g), and pyridine (127 mg, 1.6 mmol) was added to the lithiated polymer mixture and stirred at room temperature inside the glove box (48 hrs). The metallated Ru-salen polymer resin was recovered via filtration and washed with copious THF, methanol, DCM, toluene, hexane, and ether. The resulting dark brown solid was dried under high vacuum at room temperature overnight and stored in the glove box.

6.2.4 Synthesis of SBA-15 supported Ru(II)-salen bis-pyridine catalyst (8)

SBA-15 was synthesized according to published procedures,[35, 36] dried under high vacuum (250°C, 3 hrs), and stored in a nitrogen glove box. A silane-modified salen species **5** was synthesized using procedures developed within our research group.[28] The salen was post-grafted to the SBA-15 support by refluxing silane-modified salen **5** (290 mg) and SBA-15 (1.7 g) in anhydrous toluene (16 g) under argon (24 hrs). The resulting solid was recovered via filtration and washed with copious toluene, DCM, hexane, and ether. The salen-functionalized SBA **6** was dried under high vacuum at room temperature (12 hrs). Unreacted SBA surface hydroxyl groups were then capped by stirring salen-functionalized SBA-15 **6** (500 mg) and hexamethyldisilazane (HMDS, 500 mg) in hexane (10 g) under argon at room temperature (48 hrs). The capped salen-modified SBA-15 **7** was recovered via filtration, washed with hexane, toluene, DCM, hexane, and ether, and dried overnight at room temperature under high vacuum. The capped, salen-functionalized SBA-15 was then metallated with ruthenium similar to the procedure described above. Inside a glove box, *n*-butyllithium (1.6 M in hexane, 54 mg, 0.13 mmol) was added to a mixture of capped, salen-modified SBA-15 **7** (494 mg, 0.064 mmol salen ligand) and THF (460 mg) cooled to -23°C. The mixture was stirred and allowed to warm to room temperature (6 hrs). A mixture of $[Ru(Cy)_2Cl_2]_2$ (20 mg, 0.032 mmol), THF (690 mg), and pyridine (40 mg, 0.51 mmol) was added to the lithiated SBA-15 mixture and stirred at room temperature inside the glove box (48 hrs). The metallated Ru-salen SBA-15 **8** was recovered via filtration and washed with copious THF, methanol, DCM, toluene, hexane, and ether. The resulting dark brown solid was dried under high vacuum at room temperature overnight and stored in the glove box.

6.2.5 General procedure for cyclopropanation reactions

All cyclopropanation reactions were carried out inside a nitrogen glove box. Prior to reaction, the mass of the empty flask and stir bar was recorded. Ru-salen catalyst (0.01 mmol, 0.02 eq), DCM (1 mL), and styrene (260 mg, 2.5 mmol, 5 eq) were added to the 10 mL pear shaped flask. A solution of DCM (2.5 mL), tridecane (92.2 mg, 1 eq), and EDA (65 mg, 1 eq, 88 wt% in DCM by ^{1}H NMR) was added drop wise over a 20 minute period to the catalyst solution to initiate the reaction. Samples (20 μL) were periodically removed and filtered with acetone (1 mL) through silica gel and a cotton plug to remove the catalyst. The samples were analyzed via GC with reference to the tridecane internal standard. Upon completion, the reaction mixture was diluted with THF (3 mL). The catalyst was allowed to settle gravimetrically and the solution was removed via pipette. This procedure was repeated once with THF and twice more with ethyl ether. For the recycling experiments using the pyridine treatment, pyridine (300 μL) was added to each wash cycle. The catalyst was dried under vacuum and returned to the glovebox. All recycle experiments were scaled to the mass of recovered catalyst due to losses during each cycle from sampling and washing (typically 13% loss per cycle).

6.3 Results and discussion

6.3.1 Ruthenium(II)-salen bis-pyridine polymer resin catalysts (4a, 4b): Synthesis and characterization

Borrowing from previous work developed in our research group, styrene modified mono-functionalized, unsymmetrical, chiral salen monomers (**2a**, **2b**) were synthesized.[29, 30, 32, 34] These styrene modified salen compounds were utilized in the synthesis of polymer

and silica supported materials. Mono-functionalized, unsymmetric salen ligands were preferred (in comparison to bi-functionalized, symmetric, bis-styryl modified salen ligands[37]) due to the greater degree of flexibility and increased distance from the polymer support imparted on the pendant catalyst site. In the proposed bimetallic transition state of the Co-salen catalyzed hydrolytic kinetic resolution (HKR) mechanism, this flexibility greatly affected the catalyst performance.[28, 38] In the mono-metallic mechanism of the Ru-salen cyclopropanation reaction, this flexibility could be less important. However, the linker does impact the steric hindrance of the polymer backbone near the catalytic active site, which can be important for polymer supported catalysts in general. Insoluble, cross-linked, salen functionalized polymer resins (**3a**, **3b**) were synthesized in high yield by reaction of the styryl-salen monomers with divinylbenzene (Scheme 6.2). Ruthenium(II)-salen bis-pyridine polymer resin catalysts (**4a**, **4b**) were then synthesized following modified published procedures[11] by initial treatment with *n*-butyllithium to deprotonate the phenolic protons of the salen ligand, followed by metallation with dichloro(*p*-cymene)ruthenium(II) dimer in the presence of excess pyridine. Elemental analysis indicated a ruthenium loading of 0.35 mmol/g at a 5.9:1 N:Ru ratio and 51% metallation efficiency for **4a**, and 0.37 mmol/g ruthenium at a 5.7:1 N:Ru ratio and 53.5% metallation efficiency for **4b**. Moderate metallation efficiencies are common when working with solid supports and likely resulted from reacting stoichiometric equivalents of *n*-butyllithium (2:1) and ruthenium dimer (0.5:1) to the solid supported salen. This metallation procedure was sufficient for small molecule Ru-salen complexes,[11] but was likely hindered by transport issues with the support. Extended reaction times at ambient temperature were utilized to maximize the metallation efficiency.

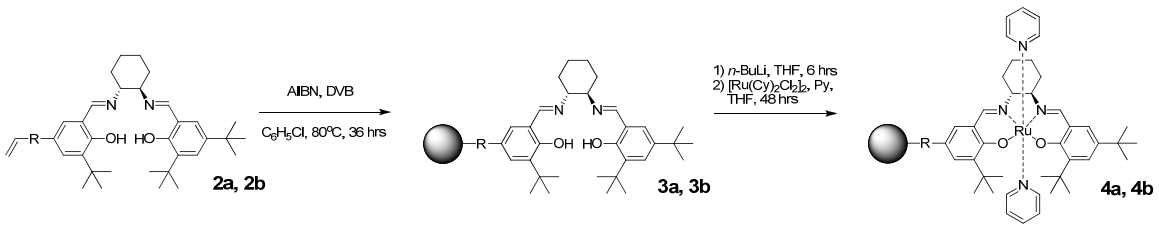

Scheme 6.2 - Synthesis of polymer resin supported Ru(II)-salen bis-pyridine catalysts. (a: R = -Ph-, b: R = -Ph-CH_2-O-$(CH_2)_2$-O-CH_2-).

The successful formation of the Ru(II)-salen-Py_2 complex was evidenced by FT-IR analysis (Figure 6.3). The characteristic imine stretch appeared at 1628 cm^{-1} for **3b**. Upon complexation with ruthenium, there was a sharp decrease in intensity of this band as it shifted towards lower frequencies at 1600 cm^{-1} resulting from a shift of electron density from the imine towards ruthenium.[39] Additional support for the formation of the Ru-salen complex was seen in the shift of the carbon-oxygen stretch of the phenolic oxygen. The non-metallated complex displayed a moderate peak at 1270 cm^{-1}, characteristic of the $\nu_{C\text{-}O}$ stretch.[40] Upon complexation, this band shifted towards higher frequencies at 1322 cm^{-1}. Additionally, the $\nu_{Ru\text{-}O \text{ and } }\nu_{Ru\text{-}N}$ bands appeared at 539 and 470 cm^{-1}, respectively in **4b**.[41] These frequency shifts and new bands support coordination of ruthenium to the nitrogen and oxygen of the salen ligand and formation of the Ru(II)-salen-Py_2 complex.

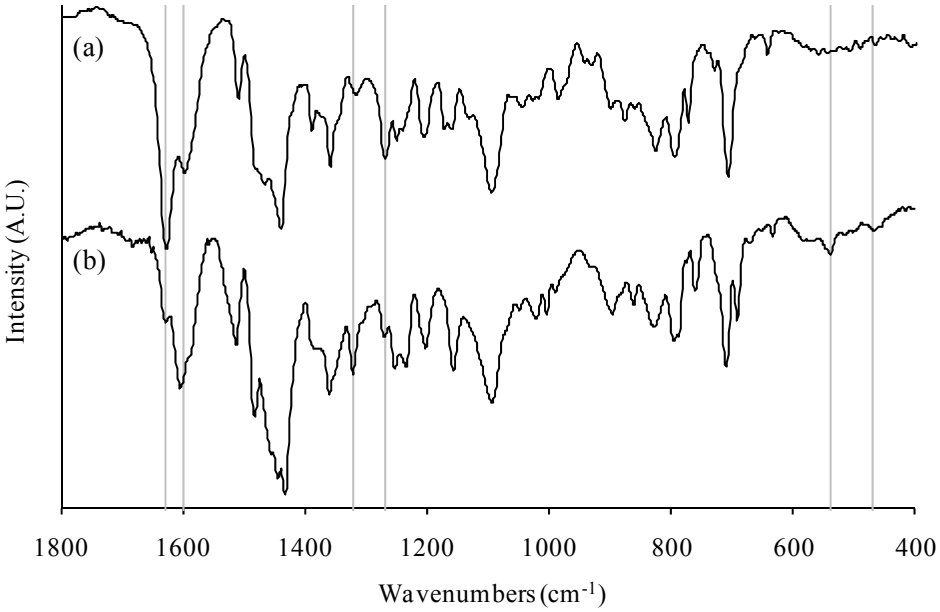

Figure 6.3 - FT-IR spectra of (a) non-metallated H_2salen polymer resin **3b** and (b) metallated Ru(II)-salen-Py_2 polymer resin **4b**.

6.3.2 SBA-15 supported Ru-salen catalyst (8): Synthesis and characterization

A ruthenium-salen bis-pyridine catalyst was also grafted from the surface of SBA-15 mesoporous silica (Scheme 6.3). A trimethoxysilane modified, chiral salen **5** was synthesized via thiol coupling of mercaptopropyltrimethoxysilane (MPTMS) with styryl-salen **2a** at 46% isolated yield.[28] Compound **5** was immobilized on 60 Å mesoporous SBA-15 silica by condensation with surface hydroxyl groups forming material **6**. Unreacted silanol groups were capped with hexamethyldisilazane (HMDS) to form material **7** prior to the metallation procedure with *n*-butyllithium and ruthenium dimer. Thermogravimetric analysis (TGA) indicated an organic content of 5.0% and 6.3% for **6** and **7**, respectively. These data equated to a loading of 0.075 mmol salen/g dry silica for **6**. Elemental analysis of **8** indicated a ruthenium loading of 0.031 mmol/g and a N:Ru ratio of 6.2, equating to a 48% metallation efficiency. This moderate metallation

efficiency was, again, likely a result of using a stoichiometric amount of *n*-butyllithium and ruthenium dimer in combination with the solid support.

Grafting of salen species on the silica surface was supported by cross-polarization magic-angle spinning (CP MAS) ^{13}C and ^{29}Si NMR spectra for material **7**. Carbon resonances appeared in the aliphatic region δ = 20 – 50 ppm (Si-*C*H_2, *C*Me_3, *C*H_2, cyclohexyl-*C*H_2, cyclohexyl-*C*H, S-*C*H_2, Ph-*C*H_2), aromatic region δ = 120 – 140 ppm, and imine region δ = 160 ppm (*C*=N) (Figure 6.4). In addition to framework silicon Q^2, Q^3, and Q^4 resonances (δ = -94 to -116 ppm), resonances corresponding to condensation of one to three methoxy groups of compound **5** (δ = -45 to -57 ppm) appeared in the ^{29}Si NMR spectrum (Figure 6.5). Presence of trimethylsilyl capping groups of material **7** were evident as the sharp peaks centered at δ = 0.7 ppm ((*C*H_3)$_3$Si) in the ^{13}C spectrum and δ = 13 ppm (Me_3*Si*-O) in the ^{29}Si spectrum.

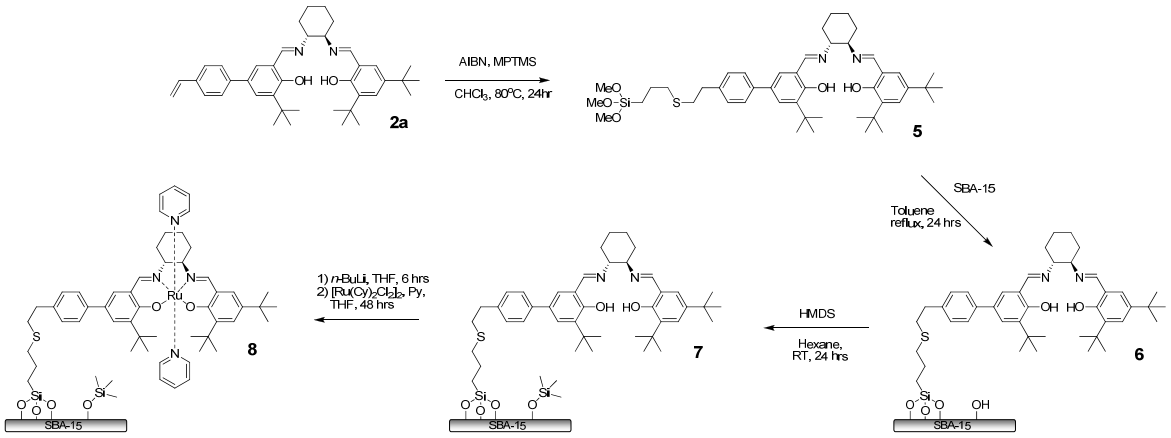

Scheme 6.3 - Synthesis of SBA-15 supported Ru(II)-salen bis-pyridine catalyst.

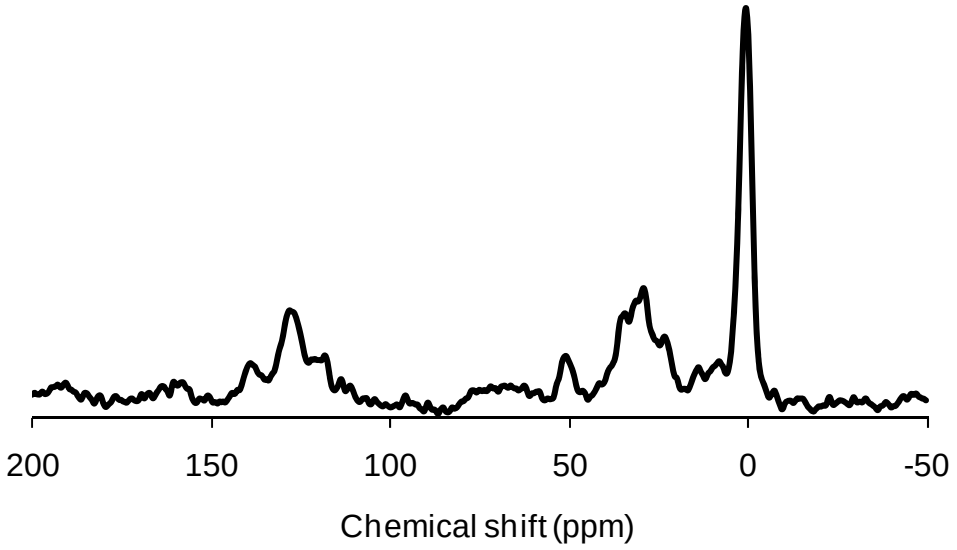

Figure 6.4 - CP MAS ^{13}C solid state NMR for **8**.

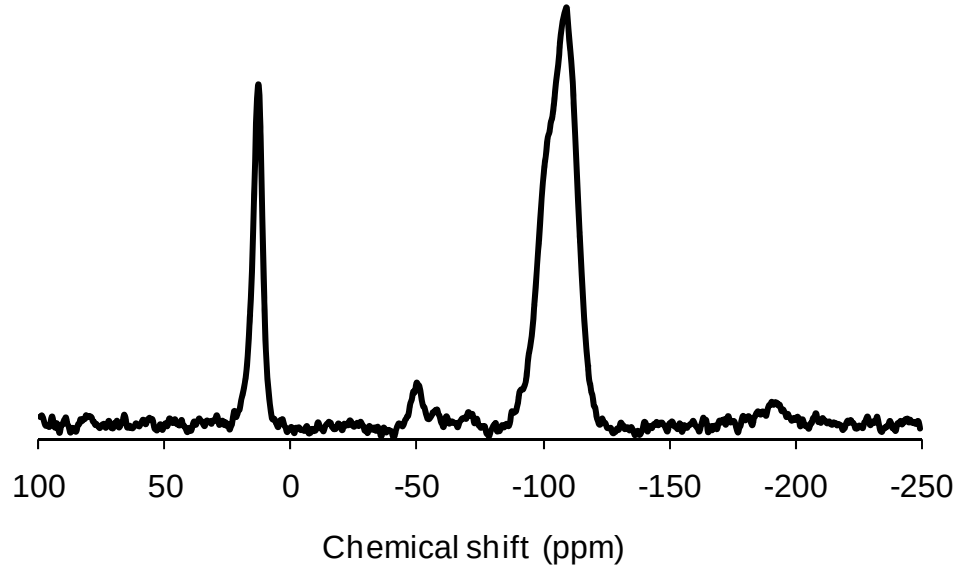

Figure 6.5 - CP MAS ^{29}Si solid state NMR for **8**.

FT-IR analysis confirmed the presence of organic species in **6-8** by the appearance of aliphatic ν_{C-H} stretch at 2967 cm^{-1} and imine $\nu_{C=N}$ stretch centered at 1635 cm^{-1} (Figure 6.6). As expected, the strongest peak in the FT-IR spectra for materials **6-8** corresponded to the ν_{Si-O} stretch from 1000 – 1280 cm^{-1} resulting from the SBA-15 silica support. A strong ν_{O-H} stretch appeared in material **6** from 3200 to 3700 cm^{-1} confirming

the presence of surface silanol groups and the inability to react all silanols with bulky compound **5**. This peak diminished but did not disappear in material **7** after the capping step with HMDS possibly due to inaccessible, uncapped silanols and/or the phenolic hydroxyl groups in the salen ligand. In conjunction, a sharp peak appeared at 850 cm^{-1}, corresponding to the ν_{Si-C} stretch in the trimethylsilyl capping groups. Upon metallation with ruthenium, no ν_{O-H} stretch was observed indicating formation of the ruthenium-salen complex.

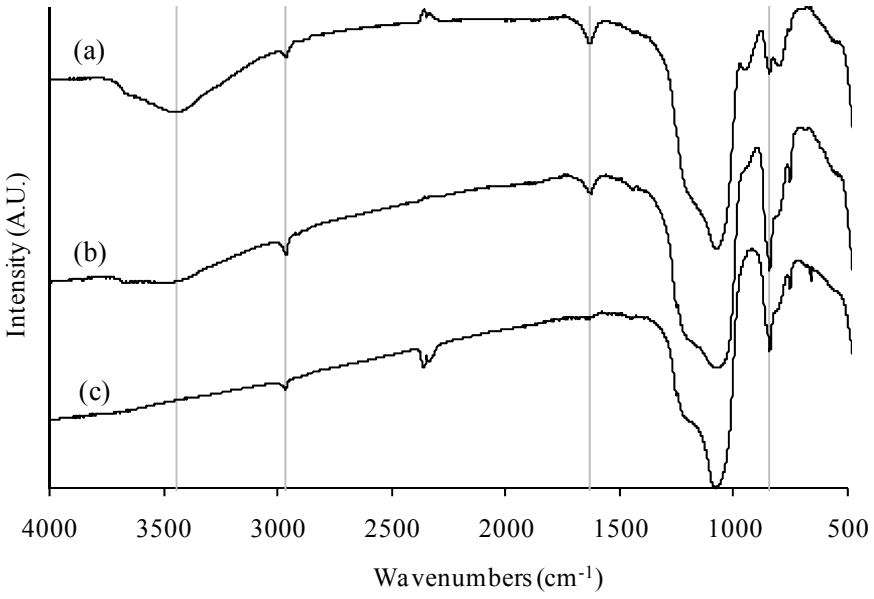

Figure 6.6 - FT-IR spectra of (a) SBA-H_2salen **6**, (b) SBA-H_2salen capped **7**, and (c) SBA-Ru-salen-Py_2 capped **8**.

6.3.3 Catalytic results and discussion: Recycling without pyridine treatment

All cyclopropanation reactions were evaluated in terms of yields, diastereoselectivities (*trans*/*cis* product ratio), and enantioselectivities (Table 6.1). Initial reactions using catalysts **4a**, **4b**, and **8** appeared promising (Table 6.1, entries 2, 5, 8). Yields were similar (≥95%), but selectivities of these catalysts suffered slightly in

comparison to the homogeneous Ru-salen reported previously.[11] Formation of dimeric side products diethyl maleate and diethyl fumarate was not detected via GC when using styrene as the olefin reactant. The polymer resin catalysts appeared more active than the silica based catalyst by reaching ≥95% yield in five hours versus 24 hrs. Catalyst **4b** achieved higher selectivities in all areas (10.6 *trans*/*cis* ratio, 94% *trans ee*, 91% *cis ee*, entry 5) compared to **4a** (8.8 *trans*/*cis* ratio, 87% *trans ee*, 77% *cis ee*, entry 2), slightly less than that of the homogeneous catalyst (entry 1). Repeated synthesis of these catalysts demonstrated similar results, suggesting the difference in selectivities resulted from the different linkers between the salen unit and polymer backbone. Related work using polymer brush supported Co-salen catalysts for the HKR of epoxides demonstrated a dramatic difference in activity between the rigid styryl and flexible ethylene glycyl linkers.[32] However, this observation was likely a consequence of the bimetallic mechanism of Co-salen catalyzed HKR. Ru-salen catalyzed cyclopropanation of olefins follows a monometallic mechanism, and therefore, the length/flexibility of the linker should not have as significant an impact on the rates. This seems to be the case, as catalysts **4a** and **4b** appear to be equally active. Due to the shorter linker of **4a** compared to **4b**, the closer proximity of the polymer backbone to the Ru-salen active site may be increasing the probability of steric interference during the cyclopropanation mechanism, thus causing the slight drop in selectivity. The longer, flexible linker of **4b** may lessen the steric hindrance, thereby producing higher selectivities.[32]

Table 6.1 - Results summary for the cyclopropanation of styrene with various catalysts.

Entry	Catalyst	Mol % catalyst	Solvent	Cycle number	Time [h]	Yield [%] [a]	*trans*/*cis* ratio	*trans ee* [%] [b,c]	*cis ee* [%] [c,d]
1	**1**[11]	1	DCM	1	3	95	10.8	99	96
2	**4a**	2	DCM	1	4	95	8.8	87	77
3	**4a**	2	DCM	2	8	80	8.9	88	80
4	**4a**	2	THF	1	4	91	10.4	84	73
5	**4b**	2	DCM	1	5	99	10.6	94	91
6	**4b**	2	DCM	2	8	94	10.9	95	92
7	**4b**	2	DCM	3	11	93	9.1	95	91
8	**8**	2	DCM	1	24	95	9.8	89	80
9	**8**	2	DCM	2	74	49	7.7	80	56
10	**8**	2	THF	1	24	79	12.1	79	67
11	**8**	2	THF	2	24	17	10.0	77	62

[a] Determined via GC calibration. [b] Enantioselectivity towards the (1*R*,2*R*) product. [c] Determined via chiral GC. [d] Enantioselectivity towards the (1*R*,2*S*) product.

SBA-15 supported catalyst **8** required longer reaction times to reach high yields than the polymer resin catalysts, but similar selectivities were achieved (9.8 *trans*/*cis* ratio, 89% *trans ee*, 80% *cis ee*, entry 8). Unfortunately, *ee*'s were only slightly better than those resulting from catalyst **4a** and less than those of **4b**. The decreased selectivities for **8** may have resulted from steric hindrance with the silica surface. However, a more likely explanation may result from the nature on the silica support itself. In the case of the SBA-15 supported catalyst, it proved impossible to react all surface silanol groups of bare SBA-15 with excess methoxysilane-modified salen **5** due to the bulky nature of the compound. Consequently, all silanol groups were capped to form material **6** prior to the metallation procedure in order to prevent reaction with *n*-butyllithium and subsequent immobilization of surface bound, non-chiral, ruthenium species. If any of the silanols or siloxane bridges present in the mesopores of SBA-15 survived the capping step, then they could create adverse interactions with the Ru-salen catalyst, potentially explaining the decreased *ee*'s, as seen experimentally.

It should be noted that extensive studies were performed trying to replicate previous metallation procedures,[42] which used triethylamine instead of a stronger deprotonating agents such lithium diisopropylamide used previously[11] or *n*-butyllithium in this work. However, the proposed Ru-salen could never be isolated using homogeneous or heterogeneous salens under a variety of conditions. For the supported salens, filtration with DCM always removed the brownish/red color associated with the ruthenium, resulting in no color change to the parent material. In both cases, no active cyclopropanation catalyst was ever isolated. For this reason, the stronger deprotonating agent was used.

Recycle studies using catalysts **4a**, **4b**, and **8** displayed very similar diastereoselectivities and enantioselectivities as the initial runs, but decreased rates were observed, leading to longer reaction times (Table 6.1, entries 3, 6, 7, 9). Catalyst **4b** required over twice as long to reach 95% yield in the third run (11 hr) versus the first run (5 hr) (Figure 6.7). These data suggest a fractional loss of active Ru-salen species with each successive cycle, possibly due to leaching of ruthenium during the washing steps between cycles or catalyst poisoning. Studies using THF as a solvent instead of DCM resulted in lower yields and *ee*'s but curiously higher diastereoselectivities (entries 4, 10). Recycle studies using THF solvent displayed similar losses in catalytic activity as using DCM (entry 11).

6.3.4 Evaluating recyclability with kinetic data

In order to fully understand catalytic activities, kinetic data was collected rather than analyzing single point yields at long times, a common problem in catalysis and chemistry literature. Reporting single point yields at long times can be misleading, as this

practice can mask the true kinetics, activity, recyclability, and deactivation. The yields reported in this paper are not collected at long times. Instead kinetics were collected for most reactions and yields were reported at the corresponding times. Figure 6.7 displays representative data for the deactivation of polymer resin catalyst **4b**. An analogous comparison for catalyst **4a** appears in Figure 6.8. Using kinetic data, instead of single point yields, a clearer picture of catalyst deactivation can be observed between the first and third cycle for catalyst **4b**.

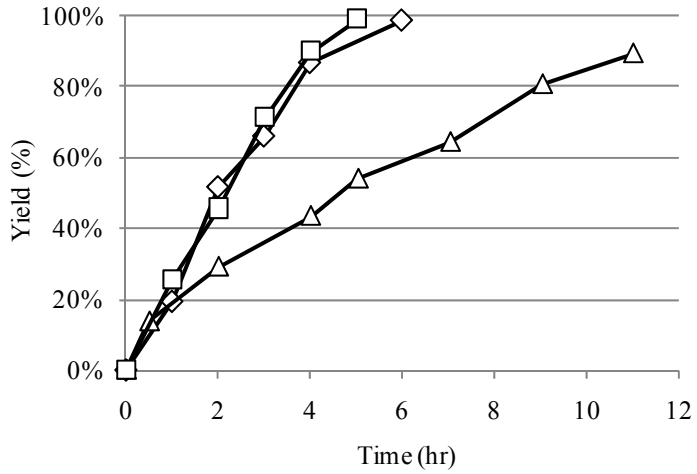

Figure 6.7 - Yield of cyclopropyl products versus time using catalyst **4b**: (□) first cycle, (△) third cycle, and (◇) third cycle with pyridine treatment between all previous cycles.

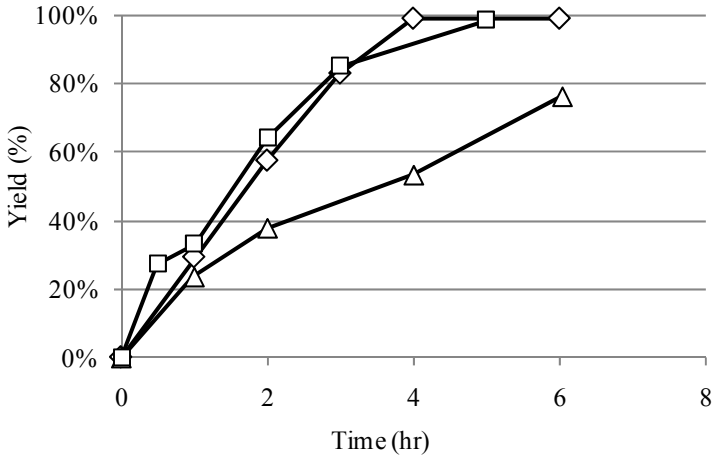

Figure 6.8 - Yield of cyclopropyl products versus time using catalyst **4a**: (□) first cycle, (△) second cycle without pyridine treatment, and (◇) third cycle with pyridine treatment used during all previous washing steps.

6.3.5 Catalytic results and discussion: Recycling with pyridine treatment

Catalyst deactivation proved to be an initial hurdle during this work. However, it was observed this could be minimized by the addition of pyridine during the washing steps between cycles. Addition of pyridine (300 μL) to each washing step proved to have a positive effect on catalyst stability over several cycles as seen by overlapping kinetics between the first cycle and third cycle with pyridine treatment (Figure 6.7 and 6.8). As a result, all recycle experiments were repeated using the pyridine treatment between cycles (Table 6.2). At slightly longer times (6 hr), very high yields (≥97%) could be achieved for both polymer resin catalysts over the three cycles tested and likely longer without any apparent deactivation (Table 6.2, entries 1-6). Initial cycles gave similar results as shown in Table 6.1, and subsequent cycles showed marginally better selectivities (entries 1-2, 4-5). This marginal increase may result from removal of any residual, non-chiral ruthenium species unremoved during the filtration steps following the metallation procedure. Catalysts **4a** and **4b** displayed very consistent yields and selectivities over three cycles, with catalyst **4b** approaching the performance of the homogeneous Ru-salen except for overall activity (entry 5).

The addition of excess pyridine during the washing steps is thought to stabilize the ruthenium center during the washing procedure. The Ru(II)-salen bis-pyridine complex must dissociate a pyridine ligand prior to entering the catalytic cycle. This vacant coordination site permits formation of the ruthenium carbene intermediate prior to carbene addition across the carbon-carbon double bond of the olefin. After complete consumption of the EDA and ruthenium carbene by excess styrene, a vacant coordination site reappears on the ruthenium center. Addition of excess pyridine shifts the equilibrium

towards binding two pyridine ligands, thus stabilizing the Ru-salen complex, and inhibiting leaching of ruthenium metal from the ligand. Anecdotal support for this hypothesis was seen in the solvent wash color after each reaction. The color from the fourth wash (after removing the yellow colored product during the first three washes) displayed an orange tint, indicative of leached ruthenium. The solvent from the fourth wash that included the pyridine treatment appeared colorless.

Table 6.2 - Results summary for the cyclopropanation of styrene with various catalysts by modified recycling method.

Entry	Catalyst	Mol % catalyst	Solvent	Cycle #	Time [h]	Yield [%][a]	*trans*/*cis* ratio	*trans ee* [%] [b,c]	*cis ee* [%] [c,d]
1	**4a**	2	DCM	1	6	97	9.1	90	82
2	**4a**	2	DCM	2	6	97	9.4	93	88
3	**4a**	2	DCM	3	6	99	8.9	91	86
4	**4b**	2	DCM	1	6	97	10.7	94	90
5	**4b**	2	DCM	2	6	99	10.9	96	95
6	**4b**	2	DCM	3	6	99	10.6	96	93
7	**8**	1	DCM	1	24	27	7.5	81	56
8	**8**	1	DCM	2	24	20	7.7	85	50
9	**8**	1	DCM	3	48	15	6.3	80	35
10	**8**	1	THF	1	24	18	8.0	73	42
11	**8**	1	THF	2	24	15	7.0	75	45
12	**8**	1	THF	3	48	11	5.2	69	32

[a] Determined via GC calibration. [b] Enantioselectivity towards the (1*R*,2*R*) product. [c] Determined via chiral GC. [d] Enantioselectivity towards the (1*R*,2*S*) product.

Attempts to assess changes to the Ru-salen catalysts upon recycling via FT-IR analysis proved inconclusive owing to overlapping peaks from pyridine (1633 and 1598 cm^{-1}) and the imine peaks of interest (1631 and 1607 cm^{-1}, Figure 6.9).[27] No apparent differences between the fresh and spent catalysts were observed in the ν_{C-O} stretching region (commonly 1275 cm^{-1} for non-metallated and 1310 cm^{-1} for the metallated ruthenium Schiff base complexes).[39-41, 43] In addition, the ν_{Ru-N} and ν_{Ru-O} stretches (450 cm^{-1} and 530 cm^{-1}, respectively) were only minutely visible, due to the low ruthenium loadings on the solid supports compared to analogous studies of homogeneous small

molecule complexes. A band at 1730 cm^{-1} did appear, presumably the carbonyl stretch from the ester group in unremoved product.

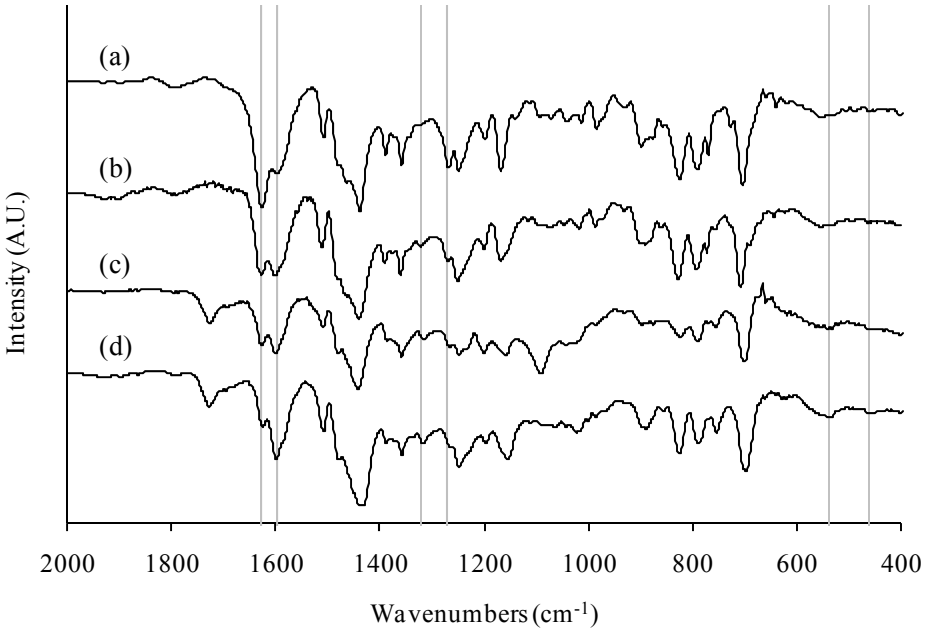

Figure 6.9 - FT-IR spectra for (a) non-metallated salen polymer resin **3a**, (b) metallated Ru(II)-salen bispyridine polymer resin catalyst **4a**, (c) spent catalyst after two cycles without pyridine wash, and (d) spent catalyst after three cycles with pyridine wash.

Catalyst **8** showed less consistent results over three cycles and its selectivities were moderate in comparison to the polymer resins, indicating such a sensitive catalyst may not be as suitable for immobilization on silicas or other inorganic oxides, where potentially negative interactions with surface hydroxyl groups or siloxane bridges may be present. This result appears in agreement with siliceous mesocellular foam (MCF) supported Cu-Box and Cu-PyBox investigations in which the authors theorize capping of surface hydroxyl groups to be paramount to activity and stability of the cyclopropanation catalyst.[44, 45]

6.3.6 Comparison to other supported asymmetric cyclopropanation catalysts

The Ru-salen polymer resin catalysts (**4a**, **4b**) compare extremely favorably against the best supported copper bis(oxazoline) catalysts to date (Table 6.3).[20] While the supported Ru-salen and Cu-Box catalysts exhibit comparable activities and enantioselectivities, Ru-salen catalysts exhibit extremely high yields and are about four times more diastereoselective to the *trans* products than the Cu-Box systems (Table 6.3, entries 3 – 6). Use of Ru-salen catalysts equates to about a 30% increase in atom efficiency versus the best Cu-AzaBox catalyst (Table 6.3, entry 4). Additionally, use of Ru-salen catalysts requires no activation step, unlike the Cu-Box systems which require addition of phenylhydrazine prior to reaction. Supported Ru-salen catalysts also supersede Ru-porphyrin and Ru-PyBox catalysts (Table 6.3, entries 7, 8) in terms of yields and enantioselectivities, but are comparable in diastereoselectivity.

Table 6.3 - Summary of best results from immobilized asymmetric catalysts for the cyclopropanation of styrene with EDA.

Entry	Catalyst	Support	Mol % catalyst	Cycle #[a]	Time [h]	Yield [%]	*trans/cis* ratio	*trans ee* [%]	*cis ee* [%]
1	Ru-salen **4a**	Copolymer	2	3	6	97	9.4	93	88
2	Ru-salen **4b**	Copolymer	2	3	6	99	10.9	96	95
3	Cu-Box[46]	Copolymer	2	5	3	61[b]	2.4	94	92
4	Cu-AzaBox[47]	Polystyrene	1	3	24	94	2.8	99	90
5	Cu-AzaBox[48]	Silica	1	8	7	87	1.9	93	91
6	Cu-Box[49]	Ionic liquid	1	3	20	34	2.6	92	88
7	Ru-porphyrin[25]	Copolymer	0.1	10	24	77[b]	11.5	82	8
8	Ru-PyBox[21]	Copolymer	6	5	n/a	70	9.0	89	64

[a] This chart displays data from the best single run of all cycles. [b] Isolated yield.

6.3.7 Cyclopropanation with olefins other than styrene

After successful cyclopropanation studies using styrene, the utility of supported Ru-salen catalysts on a range of electronically diverse terminal olefins was investigated.

These studies examined the most active and selective catalyst **4b** at 2 mol% catalyst (Table 6.4). Generally, the more activated olefins resulted in higher yields of cyclopropanated products. The differences between the product yields and ethyldiazoacetate (EDA) conversions resulted from formation of dimeric side products diethyl maleate and diethyl fumarate and minor amounts of trimer side product, presumably triethyl cyclopropane-1,2,3-tricarboxylate. Cyclopropanation of pentene resulted in very low yields (5%) of product at moderate enantioselectivity. Improved yields and selectivities of products were observed using ethylvinylether (EVE). In contrast to studies using the homogeneous catalyst, the use of solvent instead of neat olefin resulted in significant improvements to the *ee*'s and moderate increases in yield and diastereoselectivity. This difference likely resulted from positive solvent swelling effects of DCM on the polymer resin, reducing steric hindrance near the active site. The homogeneous Ru-salen catalyst would not experience these issues, explaining why no difference was observed between neat and solvated reactions.[11] As a result of this observation, all studies using different olefins were performed using solvent. Contrary to the case with homogeneous Ru-salen where very minimal *cis* products were observed (100 *trans*/*cis* ratio),[11] appreciable amounts of *cis* products from the cyclopropanation of methyl methacrylate (MMA) were observed using catalyst **4b** (10.1 *trans*/*cis* ratio). Consistently, a reversal in enantioselectivity of the MMA cyclopropanation products was observed using chiral GC, showing 7.5% *trans ee* (1*S*,2*S*) and 26% *cis ee* (1*S*,2*R*). Cyclopropanation of *trans* piperylene generated the highest product yields of the olefins studied with moderate enantioselectivities and low diastereoselectivity (Table 6.4, entry 5).

Table 6.4 - Results summary for the cyclopropanation of various terminal olefins with catalyst **4b**.

Entry	Olefin	Solvent	Time [h]	Conversion [%]	Yield [%][a]	*trans*/*cis* ratio	*trans ee* [%] [b,c]	*cis ee* [%] [c,d]
1	Pentene	DCM	39	93	5.0	2.7	54	34
2	EVE	Neat	24	75	7.5	2.1	36	33
3	EVE	DCM	48	85	13	2.3	50	80
4	MMA	DCM	52	100	36	10.1	-7.5	-26
5	Piperylene	DCM	48	100	48	1.6	55	55
6	Styrene	DCM	6	100	97	10.7	94	90

[a] Determined via GC calibration. [b] Enantioselectivity towards the (1*R*,2*R*) product. [c] Determined via chiral GC. [d] Enantioselectivity towards the (1*R*,2*S*) product.

6.4. Conclusions

This work demonstrates the first report of covalently grafted Ru-salen complexes on solid supports. These catalysts were observed to be highly active, selective, and recyclable for use in the asymmetric cyclopropanation of olefins useful in the pharmaceutical and agro-chemical industries. Two polymer resin and one SBA-15 supported Ru(II)-salen bis-pyridine catalyst were synthesized and tested in the cyclopropanation of styrene. All three generated the desired products in high yield and *trans* selectivity with moderate to high enantioselectivities. Polymer resin catalyst **4b** was observed to generate products with the highest selectivities and yield, an observation potentially occurring from lessened steric hindrance due to the lengthened linker between the Ru-salen active site and polymer support. Fractional losses in activity were observed upon recycle of these catalysts while product selectivities were unchanged. However, addition of pyridine during the washing steps between cycles was observed to retain the polymer resin catalysts' high activities after three cycles, presumably by stabilizing the complex between cycles and preventing leaching of ruthenium. Moderate enantioselectivities were observed using the SBA-15 supported catalyst **8**, possibly due to adverse reactions with the silica surface. Additional studies with other terminal olefins

demonstrated better catalyst performance for the more activated olefins, consistent with previous reports. In contrast to the homogeneous case, the use of solvent resulted in increased yields and selectivities, presumably by making the active site more accessible and less hindered inside the swollen polymer resin. These solid supported analogues of homogeneous Ru-salen catalysts show promise in the facile recycling of these expensive catalysts for repeated processes. Additionally, polymer resin supported Ru-salen catalysts **4a** and **4b** generated superior selectivities and yields versus other leading solid supported, asymmetric cyclopropanation catalysts.

6.5 Acknowledgements

The authors acknowledge financial support of this work by the DOE-BES through Catalysis Science contract DE-FG02-03ER15459. We also thank Dr. Carsten Sievers for assistance obtaining solid state NMR spectra.

6.6 References

1. Donaldson, W.A., *Tetrahedron* **2001**, 57, 8589.
2. Salaun, J., *Chem. Rev.* **1989**, 89, 1247.
3. Lopez, O., Fernandez-Bolanos, J.G., and Gil, M.V., *Green Chem.* **2005**, 7, 431.
4. Doyle, M.P. and Forbes, D.C., *Chem. Rev.* **1998**, 98, 911.
5. Doyle, M.P. and Protopopova, M.N., *Tetrahedron* **1998**, 54, 7919.
6. Lebel, H., Marcoux, J.F., Molinaro, C., and Charette, A.B., *Chem. Rev.* **2003**, 103, 977.
7. Pellissier, H., *Tetrahedron* **2008**, 64, 7041.
8. Maas, G., *Chem. Soc. Rev.* **2004**, 33, 183.
9. Katsuki, T., *Adv. Synth. Catal.* **2002**, 344, 131.
10. Katsuki, T., *Synlett* **2003**, 281.
11. Miller, J.A., Jin, W.C., and Nguyen, S.T., *Angew. Chem., Int. Ed.* **2002**, 41, 2953.
12. Miller, J.A., Hennessy, E.J., Marshall, W.J., Scialdone, M.A., and Nguyen, S.T., *J. Org. Chem.* **2003**, 68, 7884.
13. Miller, J.A., Gross, B.A., Zhuravel, M.A., Jin, W.C., and Nguyen, S.T., *Angew. Chem., Int. Ed.* **2005**, 44, 3885.
14. Li, G.Y., Zhang, J., Chan, P.W.H., Xu, Z.J., Zhu, N.Y., and Che, C.M., *Organometallics* **2006**, 25, 1676.

15. Suematsu, H., Kanchiku, S., Uchida, T., and Katsuki, T., *J. Am. Chem. Soc.* **2008**, 130, 10327.
16. Cornejo, A., Fraile, J.M., Garcia, J.I., Gil, M.J., Martinez-Merino, V., Mayoral, J.A., and Salvatella, L., *Organometallics* **2005**, 24, 3448.
17. Iwakura, I., Ikeno, T., and Yamada, T., *Org. Lett.* **2004**, 6, 949.
18. Song, C.E. and Lee, S.G., *Chem. Rev.* **2002**, 102, 3495.
19. Brase, S., Lauterwasser, F., and Ziegert, R.E., *Adv. Synth. Catal.* **2003**, 345, 869.
20. Fraile, J.M., Garcia, J.I., and Mayoral, J.A., *Coord. Chem. Rev.* **2008**, 252, 624.
21. Cornejo, A., Fraile, J.M., Garcia, J.I., Gil, M.J., Luis, S.V., Martinez-Merino, V., and Mayoral, J.A., *J. Org. Chem.* **2005**, 70, 5536.
22. Cornejo, A., Fraile, J.M., Garcia, J.I., Garcia-Verdugo, E., Gil, M.J., Legarreta, G., Luis, S.V., Martinez-Merino, V., and Mayoral, J.A., *Org. Lett.* **2002**, 4, 3927.
23. Cornejo, A., Fraile, J.M., Garcia, J.I., Gil, M.J., Martinez-Merino, V., and Mayoral, J.A., *Tetrahedron* **2005**, 61, 12107.
24. Cornejo, A., Fraile, J.M., Garcia, J.I., Gil, M.J., Luis, S.V., Martinez-Merino, V., and Mayoral, J.A., *C. R. Chim.* **2004**, 7, 161.
25. Ferrand, Y., Le Maux, P., and Simonneaux, G., *Tetrahedron: Asymmetry* **2005**, 16, 3829.
26. Zhang, J.L., Liu, Y.L., and Che, C.M., *Chem. Commun.* **2002**, 2906.
27. Syukri, S., Sun, W., and Kühn, F.E., *Tetrahedron Lett.* **2007**, 48, 1613.
28. Gill, C.S., Venkatasubbaiah, K., Phan, N.T.S., Weck, M., and Jones, C.W., *Chem. Eur. J.* **2008**, 14, 7306.
29. Holbach, M. and Weck, M., *J. Org. Chem.* **2006**, 71, 1825.
30. Zheng, X.L., Jones, C.W., and Weck, M., *Chem. Eur. J.* **2006**, 12, 576.
31. Zheng, X.L., Jones, C.W., and Weck, M., *J. Am. Chem. Soc.* **2007**, 129, 1105.
32. Zheng, X.L., Jones, C.W., and Weck, M., *Adv. Synth. Catal.* **2008**, 350, 255.
33. Pangborn, A.B., Giardello, M.A., Grubbs, R.H., Rosen, R.K., and Timmers, F.J., *Organometallics* **1996**, 15, 1518.
34. Holbach, M., Zheng, X.L., Burd, C., Jones, C.W., and Weck, M., *J. Org. Chem.* **2006**, 71, 2903.
35. Zhao, D.Y., Huo, Q.S., Feng, J.L., Chmelka, B.F., and Stucky, G.D., *J. Am. Chem. Soc.* **1998**, 120, 6024.
36. Hicks, J.C. and Jones, C.W., *Langmuir* **2006**, 22, 2676.
37. Heckel, A. and Seebach, D., *Helv. Chim. Acta* **2002**, 85, 913.
38. Madhavan, N., Jones, C.W., and Weck, M., *Acc. Chem. Res.* **2008**, 41, 1153.
39. Kannan, S. and Ramesh, R., *Polyhedron* **2006**, 25, 3095.
40. Kumar, K.N., Venkatachalam, G., Ramesh, R., and Liu, Y., *Polyhedron* **2008**, 27, 157.
41. Refat, M.S., Ei-Korashy, S.A., Kumar, D.N., and Ahmed, A.S., *Spectrochim. Acta, Part A* **2008**, 70, 898.
42. Liang, J.L., Yu, X.Q., and Che, C.M., *Chem. Commun.* **2002**, 124.
43. Mishra, L., Prajapati, R., and Pandey, K.K., *Spectrochim. Acta, Part A* **2008**, 70, 79.
44. Lee, S.S., Hadinoto, S., and Ying, J.Y., *Adv. Synth. Catal.* **2006**, 348, 1248.
45. Lee, S.S. and Ying, J.Y., *J. Mol. Catal. A: Chem.* **2006**, 256, 219.
46. Mandoli, A., Orlandi, S., Pini, D., and Salvadori, P., *Chem. Commun.* **2003**, 2466.

47. Werner, H., Herrerias, C.I., Glos, M., Gissibl, A., Fraile, J.M., Perez, I., Mayoral, J.A., and Reiser, O., *Adv. Synth. Catal.* **2006**, 348, 125.
48. Lim, J.H., Riduan, S.N., Lee, S.S., and Ying, J.Y., *Adv. Synth. Catal.* **2008**, 350, 1295.
49. Fraile, J.M., Garcia, J.I., Herrerias, C.I., Mayoral, J.A., Gmough, S., and Vaultier, M., *Green Chem.* **2004**, 6, 93.

CHAPTER 7

SUMMARY AND FUTURE WORK

7.1 Summary

As stated in the introduction, the main theme of this thesis work was development of novel hybrid organic/inorganic catalysts and catalyst supports for the advancement of the field of supported catalysis. Within this broad approach were four objectives: (1) identification of novel catalyst supports and architectures for supported hybrid organic/inorganic catalysts, (2) understanding the effects of the covalent linker on catalytic performance, (3) intelligent design of supported catalysts based on mechanistic knowledge, and (4) demonstration of novel techniques of supporting homogeneous catalysts. Insights gained during the course of this thesis work are now summarized for these goals.

7.1.1 Identification of novel catalyst supports

In the field of supported catalysis, a number of useful solid supports exist, each with their own advantages and disadvantages. As this field progresses, researchers are constantly searching for new supports. This thesis work touches on two very novel catalyst supports: magnetic nanoparticles and polymer brushes. MNPs are promising catalyst supports for a number of reasons: high surface areas, high thermal stability, capacity for surface modifications, and the ability to dispersed in solution and recovered magnetically. Although this work did not pioneer the idea of MNP supports, it has demonstrated several interesting applications for them as catalyst supports. Chapter 2 illustrated use of MNP supported base catalysts. These were used in conjunction with polymer resin supported acid catalysts to promote cascade acid/base catalyzed reactions in one-pot. The concept of one-pot acid/base catalyzed reactions has been demonstrated previously using other supported catalysts. The novelty of this system was the ability to

individually recover the acid and base catalysts via magnetic separation, a feat not easily accomplished using non-magnetic supports. Using this methodology, one might envision building a library of catalysts for use in one-pot multi-step syntheses, in which two or more catalysts could be used and individually recovered later.

The MNP supports were also utilized in other unique ways. Chapter 3 demonstrated use of silica coated MNP as supports for sulfonic acids. Prior to publication of this work, no acid functionalized MNP catalysts existed in the literature. This work hypothesized traditional methods for supporting sulfonic acids on silicas may not be possible with MNPs due to conflicting chemistries. It then demonstrated how to resolve the problem by first coating the MNPs with protective layers of amorphous silica. This innovation could permit use of any silica based surface modification chemistries on silica coated MNPs that may not be possible on bare nanoparticles, thus expanding the utility of MNPs as catalyst supports.

Chapter 5 demonstrated use of ATRP initiator functionalized MNP as supports for the growth of polymer brushes bearing pendant catalyst sites. Reports of silica based polymer brushes appeared only recently with even fewer examples of MNP based polymer brushes existing. These polymer brush systems offered unique opportunities for exploration in search of novel catalyst supports. Soluble and insoluble polymer supported catalysts are quite common in the literature. The soluble polymer catalysts tend to be more difficult to recover but more active, since they are less restricted by diffusion limitations present in insoluble polymer matrices. Polymer brush catalysts (PBCs) offer a unique way to support otherwise soluble polymers on solid supports. This architecture permits easy accessibility of the pendant active sites and simple recovery due to the insoluble support. When MNPs are used as the support, the catalyst can be recovered magnetically. Silica based PBCs are more difficult to recover (via centrifugation), because they can easily clog filters, making their washing/recycling procedures laborious. Chapters 4 and 5 demonstrate organic and organometallic PBCs supported on silica and

MNPs. These novel catalysts were shown to be recoverable and recyclable and offered the ability to synthesize supported catalysts with high, local catalyst concentrations.

7.1.2 Understanding linker effects of catalyst performance

The covalent linker between the active catalyst and solid support can have significant impacts on catalyst performance. When designing a covalently grafted catalyst, one must contemplate the appropriate choice of linker based on length, flexibility, functional groups, and electronics. These variables become important in terms of accessibility and steric hinderance from the support. In general, longer linkers help to minimize steric intereference with rigid, solid supports. Steric intereference and accessibility become more complicated with polymer supports due to their non-ordered nature, making generalizations difficult. In the case of the Co-salen catalyzed HKR of epichlorohydrin in Chapter 4, the choice of linker was critically important to catalytic activities. This observation resulted from the bimetallic mechanism of Co-salen catalyzed HKR. It was confirmed that longer, flexible linkers generated increased activities in the polymer brush supported Co-salen catalysts, likely due to increased site-site interactions resulting from the extra translational and rotational degrees of freedom imparted by the flexible linker. In contrast, the Ru-salen catalyzed cyclopropanation of olefins follows a monometallic mechanism. In Chapter 6, it was observed that Ru-salen polymer resin catalysts containing short, rigid linkers and longer, flexible linkers exhibited equal activities. While linker properties may be less important in non-cooperative catalytic systems, a small but growing number of reactions require cooperative catalysis. Consequently, linker optimization of supported catalysts may lead to significant improvements for these reactions. A combination of theoretical and experimental studies may useful in this pursuit.

The use of linkers containing varying functional groups and electronic properties can also impact catalyst performance and stability. Non-hydrolizable linkers are generally

preferred to maximize catalyst stability and recyclability, as esters, amides, and ethers are susceptible to cleavage under reaction conditions, especially in the presence of acids or bases. This may be the reason for the decreasing activity of the piperazine based MPBC described in Chapter 5. The ester group of the ATRP initiator was likely hydrolized by the piperazine base catalyst in the presence of water generated in the reaction. Possible synthetic methods for creating non-hydrolizable ATRP initiator silanes to prevent catalyst decomposition are outlined in the suggestions for future work.

Linker electronics also played an important role in the supported sulfonic acids in Chapter 3. A direct correlation between the electron withdrawing capacity of the functional linkers and activity of the acid catalyst was observed. This observation resulted from the linker electronics influencing the electron density in the sulfonic acid, thereby affecting the Brønsted acidity of the catalyst. By changing the linker electronics using different functional groups, one may tune the electronic properties of supported catalysts. This could be accomplished with acid/base catalysts or by affecting the Lewis acidity of ligands in organometallic catalysts.

7.1.3 Design of supported catalysts based on mechanistic knowledge

Mechanistic insights of catalytic processes can be useful in designing new adaptations of existing catalysts. Although these insights are generally difficult to uncover, experimental evidence has indicated the Co-salen catalyzed HKR of epoxides follows a bimetallic mechanism. As mentioned above, the judicial selection of linkers resulted in a six-fold increase in the turnover frequency (TOF) of the polymer brush catalysts in Chapter 4. This promising result spurred further work into synthesizing dual salen functionalized styryl monomers. The polymer brushes used in this thesis work were synthesized from mono-salen styryl monomers. By copolymerizing these monomers with styrene, it was impossible to control the distance between salen sites along the polymer chain. This distance can be controlled and manipulated by synthesizing two salen units on

one styryl monomer. New polymeric, dual salen catalysts developed by colleague, Dr. Krishnan Venkatasubbaiah, and assisted by this author showed a five-fold increase in TOF over the best PBC developed in this thesis work. This example highlights the need for detailed mechanistic knowledge in order to develop enhanced activity from existing catalysts.

7.1.4 Demonstration of novel techniques for supporting homogeneous catalysts

As promising new homogeneous catalysts are developed, their commercial application may be hindered due to the known difficulties of recycling homogeneous catalysts. This becomes especially important for expensive precious metal or chiral catalysts. The highly active and selective homogeneous ruthenium-salen catalyst was first reported in 2002, and no reports of efforts to immobilize the catalyst on solid supports existed. Chapter 6 illustrates the first report of covalently graftinged Ru-salen catalysts for the asymmetric cyclopropanation of olefins. The catalyst was immobilized on SBA-15 silica and polymer resins. Metallation of the ligand with ruthenium was initially problematic, especially on silica, and successful experimental procedures were outlined. The polymer resin supported catalysts showed high degrees on activity and selectivity, approaching that of the homogeneous complex, and compared very favorably against the best existing supported, asymmetric cyclopropanation catalysts. Kinetic data also demonstrated the polymer resin catalysts were fully recyclable over the three cycles tested with no loss in activity. This work expands the possibilities for synthesizing chiral cyclopropyl chemicals useful in the pharmaceutical and agro-chemical industries.

7.1.5 Concluding remarks

Supported catalysts offer a unique combination of high activity, selectivity, and recyclability for use in the fine chemical and pharmaceutical industries. They effectively combine the advantages of both homogenous and heterogeneous catalysis via

immobilization of homogeneous catalysts on heterogeneous supports. This thesis work has strived to advance this field through (1) identification of novel catalyst supports and architectures for supported hybrid organic/inorganic catalysts, (2) understanding the effects of the covalent linker on catalytic performance, (3) intelligent design of supported catalysts based on mechanistic knowledge, and (4) demonstration of novel techniques of supporting homogeneous catalysts. Five studies were performed in pursuit of these goals utilizing organic and organometallic catalysts supported on silicas, magnetic nanoparticles, and polymers. This work offered new advancements and opportunities for supported catalysis, warranting further investigation for application of these catalysts to the fine chemical and pharmaceutical industries.

7.2 Suggestions for future work

Polymer brush materials have been recently appearing in the literature. As such, there is opportunity to explore these materials as catalyst supports. They offer several advantageous characteristics for supported catalysts. Due to the solid, heterogeneous support such as silica or magnetic nanoparticles, polymer brush catalysts (PBCs) can be easily recovered via filtration, centrifugation, or magnetically. The polymer chains grafted from the surface mimic soluble or insoluble linear polymers. These polymers can be constructed to carry pendant catalyst sites. Using polymers, there is a multitude of options on how to construct these brushes. Homopolymers, copolymers, and block polymers are all possible. A number of mono- or multifunctional polymer brush catalysts can be generated through creative manipulation of the synthesis conditions.

7.2.1 Mono-functional polymer brush catalysts

Mono-functionalized polymer brush catalysts can be prepared via ATRP with functionalized monomers to form homopolymers or copolymers with styrene. A variety of organic and organometallic catalysts are possible (Figure 7.1). Vinylpyridine or other

amine modified styryl monomers could be used make basic PBCs **1**. Thiol styrene based polymer brushes **2** could be oxidized to form a sulfonic acids or reacted to attach other functional groups via thiol coupling. Sodium vinylbenezenesulfonate based polymer brushes **3** could be hydrolyzed to form sulfonic acids or ion exchanged to support homogeneous organometallic catalysts through electrostatic interactions. Polymer brush **4** could be further functionalized based on any number of functional units and coupling methods. Additionally, materials **1** and **2** could be used to coordinate metal catalysts or be used as metal scavengers. Furthermore, these PBCs could be supported on silica or magnetic nanoparticles, depending on the desired use.

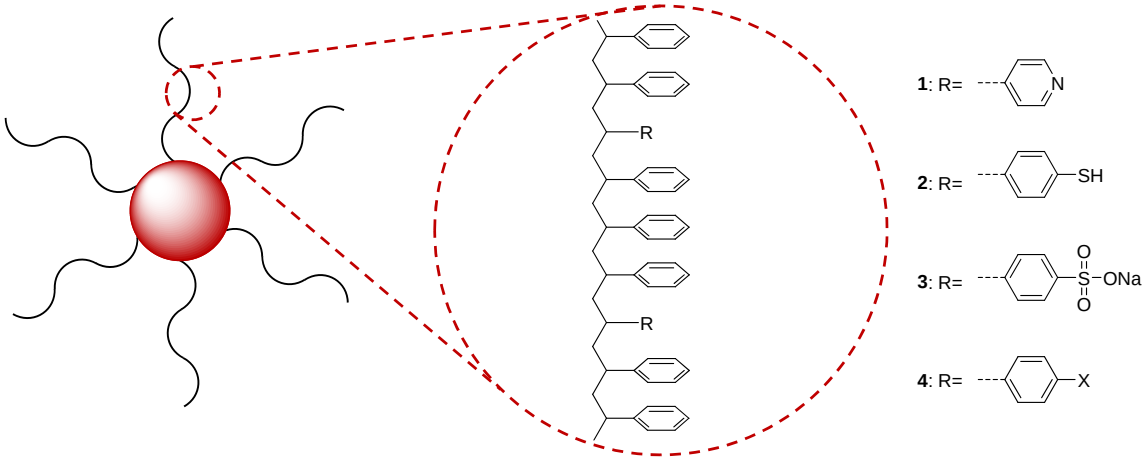

Figure 7.1 - Mono-functionalized polymer brush materials.

7.2.2 Multi-functional polymer brush catalysts

In addition to mono-functional PBCs, copolymers of functionalized styrenes (either random or block) can be synthesized to from multi-functional PBCs (Figure 7.2). These multifunctional catalysts could be useful for running cascade reactions in one pot with one catalyst. While combinations of acids and bases may prove difficult, other combinations of acids or bases with metals or other functional groups could be prepared.

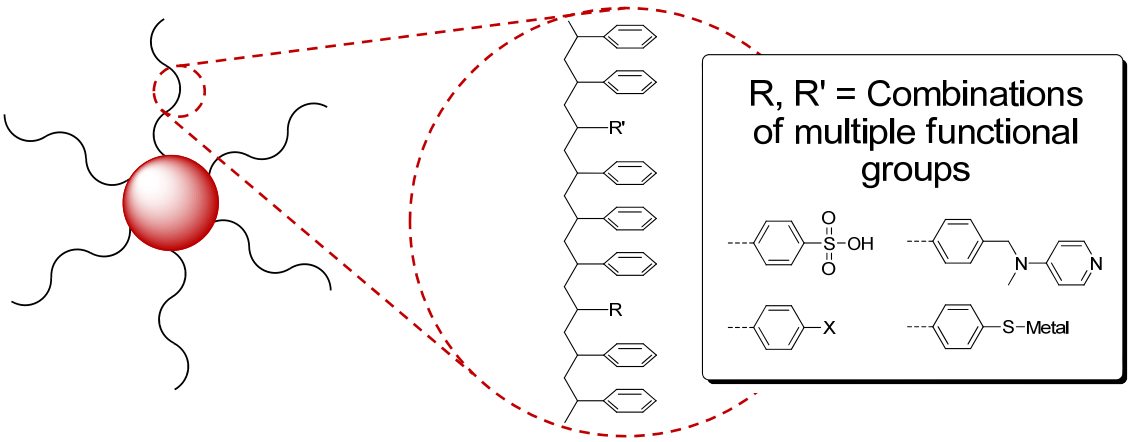

Figure 7.2 - Multi-functional polymer brush catalysts.

7.2.3 Synthesis of non-hydrolizable ATRP initiator silanes

Since the proposed mono- or multi-functional polymer brush catalysts may contain acid or base sites, a non-hydrolizable linker between the polymer and heterogeneous support should be developed. Previously used ATRP initiators incorporated ester[1] or amide[2] groups. In the presence of acid or base and suitable nucleophiles, these esters or amides can be easily hydrolyzed, breaking the covalent bond between the polymer and support. This would have detrimental effects of the catalyst in terms of stability and recyclability. Furthermore, one could not claim a "heterogeneous" catalyst if active species are being leached into the reaction media. Consequently, a stable, non-hydrolizable ATRP initiator silane must be developed. According to a recent review by Matyjaszewski, "Generally, alkyl halides RX with either inductive or resonance stabilizing substituents are efficient initiators for ATRP."[3] To this end, a series of novel ATRP initiator silanes with inductive and/or resonance stabilization are proposed (Scheme 7.1). A radical generated from abstraction of bromine by a copper(I) bromide catalyst can be resonance stabilized by the phenyl group in compounds **2** and **6** and by the carbonyl group in compound **4**. Additionally, inductive stabilization of the

radical is provided by the two methyl groups beta to the bromine in compounds **2**, **4**, and **8**.

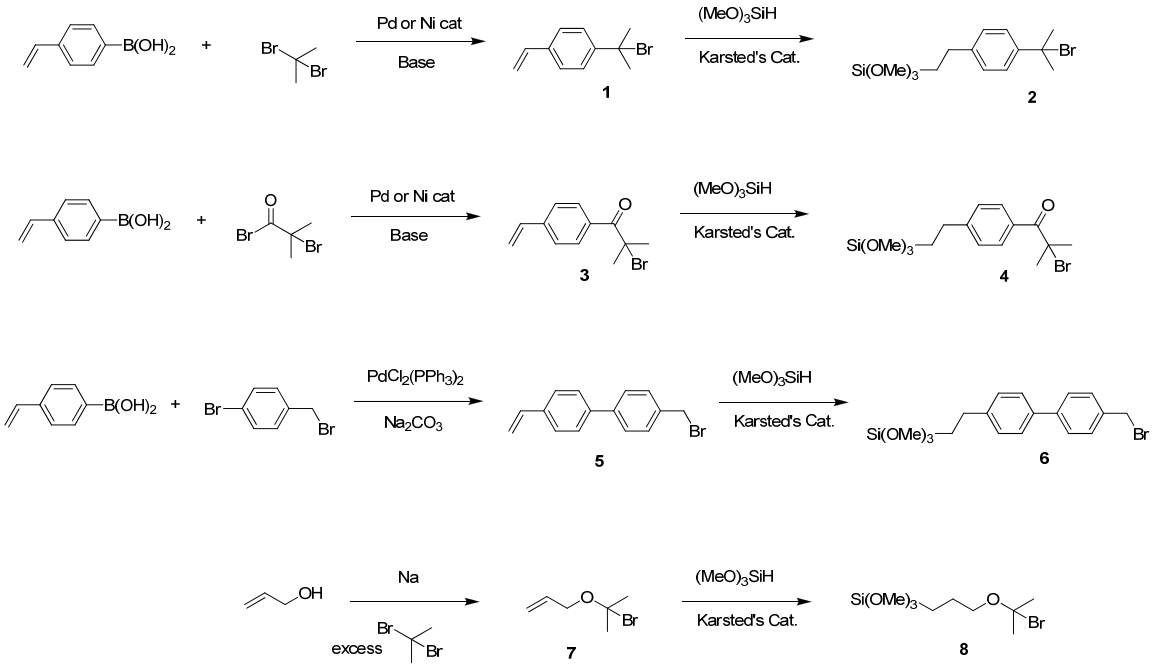

Scheme 7.1 - Synthesis of novel ATRP initiator silanes.

Each of these novel silanes may be synthesized in two steps. Compound **1** may be synthesized via a Suzuki-like coupling between 4-vinylphenylboronic acid and excess 2,2-dibromo-2-propanol. Successful coupling between aryl boronic acids and alkyl bromides in high yields by nickel catalysts have recently appeared, giving promise to this strategy.[4] The product can then be reacted with trimethoxysilane (TMS) using Karsted's catalyst to generate compound **2**. A similar strategy may be employed to generate compound **4** starting with 2-bromo-2-methylpropanoyl bromide. Compound **6** can be synthesized via a true Suzuki coupling followed by addition of TMS. Compound **8** can be synthesized first by reaction of sodium to vinylalcohol followed by addition of excess 2,2-dibromo-2-propanol. Product **7** can then be reacted with TMS to form compound **8**. Another strategy might employ reaction of chloromethylstyrene with TMS to generate a chlorine based ATRP initiator silane.

Using these strategies, ester groups are avoided, and the resulting ATRP initiators **2**, **4**, and **6** should be stable under acidic or basic conditions. The ether linkage in compound **8** may be less stable and hydrolyze under these conditions. It is hoped these new ATRP initiator silanes will aid the stability and recyclability of novel polymer brush catalysts.

7.2.4 Continuous magnetic nanoparticle flow reactors

All MNP supported catalysts currently appearing in the literature are used in batch reactions. An interesting project could develop flow reactors for MNP catalysts with continuous catalyst recycling. Because MNPs can be dispersed in solution and have totally external surface areas, reactions should be rate limited since only bulk diffusion is present. As a result, MNP supported catalysts may be advantageous in cases where diffusion limited traditional catalysts are currently used, such as zeolites or other microporous materials. Designing a packed bed reactor for MNPs would be foolish since the resulting pressure drop would be drastic. This design also overlooks the best attribute of MNPs: magnetic separations. Slurry reactors would also be insufficient in this case, as the gravitational forces would likely be insufficient to retain the MNPs inside the reactor. Consequently, a new MNP flow reactor is proposed (Figure 7.3).

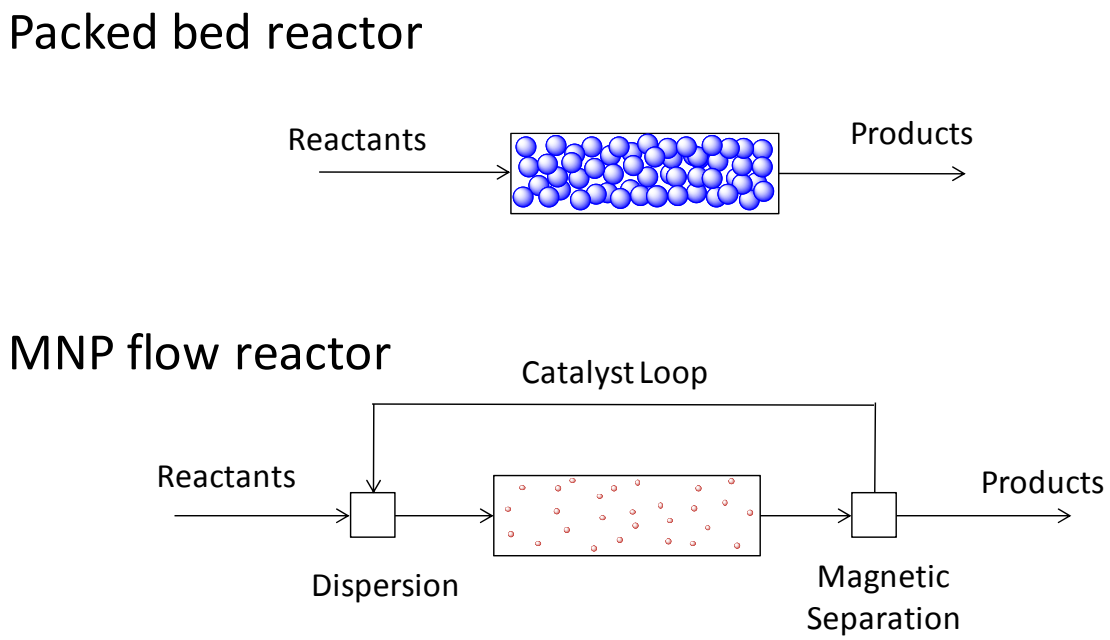

Figure 7.3 - Packed bed reactors versus magnetic nanoparticle flow reactors.

In the MNP flow reactor, a solvent loop containing the MNP catalyst is dispersed with reactants. This combined stream flows through the reactor where the reaction occurs. Upon exiting the reactor, the MNPs are recovered magnetically and the catalyst is recycled through a solvent loop. The advantage to this system is essentially zero pressure drop across the reactor. Design of the magnetic separator would present the biggest challenge, possibly through use of alternating electromagnets. Regardless, this type of reactor is envisioned as one solution to the problem that plagues implementation of homogeneous catalysts in industrial processes: difficult recovery and reuse. A variation on this system could use MNPs as scavengers to recover homogeneous catalysts from solution. The catalyst could be later desorbed and recycled. Despite their advantages offered by MNP supported catalysts, one would likely have to find niche operations where their use is warranted on an industrial scale.

7.3 References

1. Marsh, A., Khan, A., Garcia, M., and Haddleton, D.M., *Chem. Commun.* **2000**, 2083.
2. Sun, Y.B., Ding, X.B., Zheng, Z.H., Cheng, X., Hu, X.H., and Peng, Y.X., *Eur. Poly. J.* **2007**, 43, 762.
3. Coessens, V., Pintauer, T., and Matyjaszewski, K., *Prog. Poly. Sci.* **2001**, 26, 337.
4. Gonzalez-Bobes, F. and Fu, G.C., *J. Am. Chem. Soc.* **2006**, 128, 5360.

VITA

CHRISTOPHER STEPHEN GILL

Christopher Stephen Gill was born November 1, 1980 in Olmsted Falls, Ohio (a suburb of Cleveland, OH) to David and Karin Gill. He has one elder sister, Maggie Gill. The family lived briefly in Ohio and Rochester, MI (suburb of Detroit, MI) prior to relocating to Franklin, TN due to David's transfer with the opening of the Saturn auto manufacturing plant in Spring Hill, TN by General Motors. Chris began second grade in Tennessee and graduated fifth of over 450 students from Franklin High School in 1999. He attended Tennessee Technological University in Cookeville, TN where he earned his B.S. degree in Chemical Engineering in 2004 with a 3.97 GPA. Chris was also active in his fraternity, Phi Gamma Delta, and worked in a papermill as a co-op engineer at Bowater Newsprint, Inc. in Calhoun, TN in 2002 and 2003. He attended Georgia Institute of Technology beginning in 2004 and earned his Ph.D. from the Department of Chemical & Biomolecular Engineering in 2009. Post-graduation, Chris will begin working in the Advanced Hydrocarbon Processing research group at ConocoPhillips in Bartlesville, OK. Chris became engaged to Brooke Anne Mullis on July 4, 2008, and their wedding is scheduled for November 7, 2009 at Frost Chapel at Berry College in Rome, GA.